

國立臺灣大學工學院土木工程學系



碩士論文

Department of Civil Engineering

College of Engineering

National Taiwan University

Master Thesis

地盤反應與土壤液化之數值模擬研究

Numerical Modeling of Site Response and

Soil Liquefaction

張暉承

Chang, Wei-Chen

指導教授：郭安妮 教授

Major Professor: Kwok, On-Lei

中華民國 103 年 7 月

July. 2014

國立臺灣大學碩士學位論文
口試委員會審定書

地盤反應與土壤液化之數值模擬研究
Numerical Modeling of Site Response and
Soil Liquefaction

本論文係張暉承君 (R01521124) 在國立臺灣大學土木工程學系碩士班完成之碩士學位論文，於民國 103 年 7 月 9 日承下列考試委員審查通過及口試及格，特此證明

口試委員：

郭 安 妮

(指導教授)

翁 作 新

葛 宇 甯

郭安妮

翁作新

葛宇甯

系主任

呂 良 正

呂良正

(簽名)

致謝



這篇論文的完成表示著碩士生涯的結束，碩一的時候常常想著要完成一篇論文實在是太困難了，但隨著不斷的努力及許許多多人的幫助下，終於把論文生了出來！

要感謝的人有很多，首先要謝謝家人的支持陪伴及鼓勵，讓我完成這兩年的碩士學業，特別是給我許多幫助的姐姐，如果沒有妳的鼓勵、吐槽及大力幫忙，我可能考不上研究所就當兵去了～再來要感謝我的指導教授—郭安妮老師，老師總是細心並耐心的解說我不懂的部分，花了很多的時間在指導學生身上，在課業的部分外，也給了我很多新的觀點、想法與啟發，而在論文的部分老師更是幫了我許多忙，真的十分感謝老師！另外也要謝謝研究所的同學們～雖然和大家不是很熟，但還是受到了許多人的幫忙，如果少了你們的幫忙，這兩年一定會過得更加辛苦，謝謝你們！也要謝謝大學的同學還有高中的同學們～在適當的時機一起約出去走走玩玩散散心，適時的紓解壓力真的是十分重要，感謝啦！

雖然完成了此論文，但我知道自身的能力還是有許多不足的地方，在這個階段結束後，我會更加努力的提升自我能力！這兩年內真的學到許多東西，並且受到很多人的幫忙，要感謝的人太多，有些我沒有在這邊提到的朋友抱歉啦！在此感謝所有幫助過我的人，謝謝大家！

中文摘要



當地震發生時，不同的地址狀況會使傳達的地震波產生改變，並產生放大或縮小的作用，而當地震波經過土層及岩盤時，波的性質會因為經過不同的土層而有所改變，可能改變的性質有頻率、振幅等等。在地震工程中，我們可以利用地盤反應分析理論來求得不同土層在震波之影響下會有甚麼樣的改變及反應。

地盤反應分析可分為時間域及頻率域來求解，在頻率域中之土壤行為可假設為線性及擬線性，而在時間域中只能進行總應力分析，也就是無法考慮孔隙水壓之狀況；在時間域的土壤行為可假設為線性及非線性，並可做有效應力之分析，得到孔隙水壓之激發狀況。頻率域之分析是較為常見的分析方式，因為其所需之參數及步驟相較簡單，然而近年來有效應力的分析越來越多人關注，因為已發展了有效應力分析的基本參數選取及步驟，其相關研究也越來越多，但是有效應力分析在實際案例上的應用還是很少，對於參數上的選定及孔隙水壓之模型的適用性還有待釐清，本研究的目標是回顧近期有效應力動態分析之數值模擬並把總應力及有效應力之結果進行比對及討論，希望能釐清不同的參數對於有效應力分析結果之影響，並建立有效應力分析參數選取之準則或建議。本研究中進行的數值模擬包括一系列的簡易假想地址、動態三軸試驗及大型振動台試驗。而使用的數值模擬軟體有 DEEPSOIL 及 OpenSees。

為了比較總應力及有效應力分析之結果差異，首先會進行不同假想地址之模擬比較，其中的土壤材料包含了砂土及黏土；接下來是對砂土進行動態三軸試驗之數值模擬比較，而最後是模擬大型振動台試驗；所有的數值分析都會將有效應力分析及總應力分析之結果做比較及討論。

模擬結果得到：當較小振幅時，任何分析分法的結果都十分接近。當振幅較大時，有效應力分析之結果開始與總應力分析有差異。在黏土層中所激發之孔隙

水壓比砂土層來的小。用單一元素作模擬時，其結果和實驗室的數據相近。在 DEEPSOIL 中有模擬到類似液化的情形發生，而其孔隙水壓比也有達到 1。



關鍵字：DEEPSOIL、OpenSees、有限元素分析、地盤反應分析、有效應力分析

ABSTRACT



In the discipline of geotechnical earthquake engineering, theoretical site response analyses can be performed to evaluate how geologic deposit responds, in terms of particle motion and pore water pressure generation, when it is subjected to earthquake shaking.

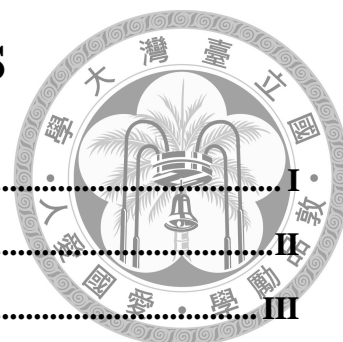
Site response analyses can be classified according to their solution domain, the type of soil model employed, and whether pore water pressure response is considered. In common practice, frequency-domain total-stress site response analyses are often performed because parameter selection and code usage are relatively simple. Time-domain total stress site response analyses have become more popular because benchmarking studies had been performed to set up the proper parameter selection procedures and evaluate the differences between the ground motions predicted from frequency-domain and time-domain total stress analyses. On the other hand, effective-stress time-domain site response analyses are rarely performed because the parameter selection protocols for the soil material model and pore water pressure generation scheme are not available. The objective of this research is to review the currently available computer programs for effective-stress dynamic analyses and to compare the solutions from total stress and effective stress dynamic analyses. In this research, a series of numerical simulations had been run for simple hypothetical site conditions, cyclic triaxial tests and shaking table tests. From the simulation results, it is observed that the acceleration and pore pressure response predictions from different effective stress models are generally similar when the input motion level is low. However, at large input motion, the pore pressure response predictions from different effective stress models can be very different, even if the acceleration response

predictions are similar. In addition, the pore pressure prediction model from OpenSees (compared to that in DEEPSOIL) seems to have a better performance as it is able to reproduce the shaking table test data on liquefied sand.



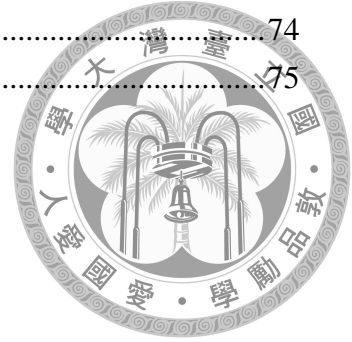
Keywords: DEEPSOIL, OpenSees, effective stress, site response analysis, site effect

TABLE OF CONTENTS



論文口試委員審定書	I
致謝.....	II
中文摘要.....	III
ABSTRACT.....	V
TABLE OF CONTENTS.....	VII
LIST OF FIGURES	IX
LIST OF TABLES.....	XII
CHAPTER 1 INTRODUCTION.....	1
1.1 MOTIVATION.....	1
1.2 OBJECTIVE	2
1.3 ORGANIZATION OF THESIS	2
CHAPTER 2 LITERATURE REVIEW.....	3
2.1 SITE RESPONSE ANALYSIS.....	3
2.1.1 <i>Overview of site response modeling.....</i>	<i>3</i>
2.1.2 <i>Theoretical Site Response Modeling.....</i>	<i>3</i>
2.1.3 <i>Previous research related to effective stress dynamic analysis.....</i>	<i>15</i>
2.2 LABORATORY & PHYSICAL TESTS WITH DYNAMIC LOADING.....	17
CHAPTER 3 NUMERICAL MODELING	30
3.1 INTRODUCTION	30
3.2 NUMERICAL MODELING OF SIMPLE HYPOTHETICAL SITES.....	30
3.2.1 <i>Site condition and analysis model.....</i>	<i>30</i>
3.2.2 <i>Input motion.....</i>	<i>32</i>
3.2.3 <i>Simulation results.....</i>	<i>32</i>
3.3 NUMERICAL MODELING OF CYCLIC TRIAXIAL TEST	34
3.3.1 <i>Soil properties and analysis model</i>	<i>34</i>
3.3.2 <i>Simulation results.....</i>	<i>35</i>
3.4 NUMERICAL MODELING OF SHAKING TABLE TESTS	35
3.4.1 <i>Site condition and analysis model.....</i>	<i>35</i>
3.4.2 <i>Simulation results.....</i>	<i>36</i>
CHAPTER 4 CONCLUSION AND RECOMMENDATION FOR FUTURE RESEARCH 74	

4.1 CONCLUSIONS.....74
4.2 RECOMMENDATIONS FOR FUTURE RESEARCH.....75



List of Figures

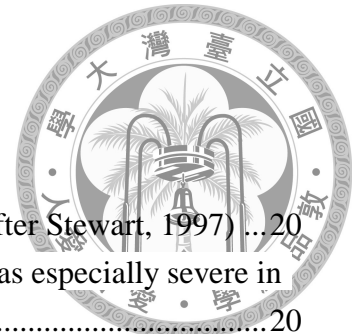


Figure 2-1 San Francisco Bay area and surrounding region. (After Stewart, 1997) ...20

Figure 2-2 Seismograms (upper right) show that the shaking was especially severe in the soft mud. (After Stewart, 1997) 20

Figure 2-3 Equivalent linear iterative procedure a) Modulus reduction curve, b) Damping curve. (After Hashash et al, 2010) 21

Figure 2-4 Backbone curve. (After Tuladhar, 2009)..... 21

Figure 2-5 Masing rules. (After Ebrahimian, 2013) 22

Figure 2-6 Definition of damping. (After Bartlett, 2011) 22

Figure 2-7 Effective damping for one, two and four modes Rayleigh formulation (After Hashash et al, 2010)..... 23

Figure 2-8 Comparison of different fitting procedures (After Hashash et al, 2010) ... 23

Figure 2-9 Dissipated energy per unit volume for a soil sample is defined as the area bound by the stress-strain loop (After Hashash et al, 2010)..... 24

Figure 2-10 The schematic of constitutive model response showing shear stress, effective confinement, and shear strain relationship (After Yang et al, 2003) 24

Figure 2-11 Conical yield surface in principal stress space and deviatoric plane (after Prevost 1985, Parra 1996, Yang 2000)..... 25

Figure 2-12 Cylindrical Von Mises yield surfaces for clay (after Prevost 1985, Lacy 1986, Parra 1996 and Yang 2000)..... 25

Figure 2-13 Hyperbolic backbone curve for soil nonlinear shear stress-strain response and piecewise-linear representation in multi-surface plasticity (after Prevost 1985 and Parra1996). 25

Figure 2-14 Schematic drawings of the biaxial laminar shear box. (After Ueng et al, 2006) 26

Figure 2-15 Picture of the empty laminar shear box. (After Ueng et al, 2006) 26

Figure 2-16 Locations of instrumentation on the frames. (After Ueng et al, 2006) 27

Figure 2-17 Locations of piezometers and accelerometers inside the specimen. (After Ueng et al, 2006)..... 27

Figure 2-18 Liquefaction of shaking table tests (Vietnam sand, F30). (After Ueng et al, 2006) 28

Figure 2-19 Acceleration history of shaking table tests (Vietnam sand, F30). (After Ueng et al, 2006)..... 29

Figure 3-1 Six simple hypothetical sites..... 38

Figure 3-2 Four-node element in Opensees, DOF = 2.	38
Figure 3-3 Nine-node element in Opensees, node 1, 2, 3, 4 are DOF = 3, node 5, 6, 7, 8, 9 are DOF = 2.	38
Figure 3-4 Vs versus SPT-N ₆₀ for (a) all Soils, (b) sands, and (c) clays (Hasaneebi and Ulusay 2007).	39
Figure 3-5 Normalized shear modulus curve and damping ratio curve for sand layer (Red curves: target values from Seed and Idriss; Blue curves: fitted curves that are actually used in analyses).	40
Figure 3-6 Acceleration history of case (a) with weak input motion.	41
Figure 3-7 Acceleration history of case (a) with strong input motion.	42
Figure 3-8 Pore water pressure ratio of case (a) with weak input motion.	43
Figure 3-9 Pore water pressure ratio of case (a) with strong input motion.	44
Figure 3-10 Acceleration history of case (b) with weak input motion.	45
Figure 3-11 Acceleration history of case (b) with strong input motion.	46
Figure 3-12 Pore water pressure ratio of case (b) with weak input motion.	47
Figure 3-13 Pore water pressure ratio of case (b) with strong input motion.	48
Figure 3-14 Acceleration history of case (c) with weak input motion.	49
Figure 3-15 Acceleration history of case (c) with strong input motion.	50
Figure 3-16 Pore water pressure ratio of case (c) with weak input motion.	51
Figure 3-17 Pore water pressure ratio of case (c) with strong input motion.	52
Figure 3-18 Acceleration history of case (d) with weak input motion.	53
Figure 3-19 Acceleration history of case (d) with strong input motion.	54
Figure 3-20 Pore water pressure ratio of case (d) with weak input motion.	55
Figure 3-21 Pore water pressure ratio of case (d) with strong input motion.	56
Figure 3-22 Acceleration history of case (e) with weak input motion.	57
Figure 3-23 Acceleration history of case (e) with strong input motion.	58
Figure 3-24 Pore water pressure ratio of case (e) with weak input motion.	59
Figure 3-25 Pore water pressure ratio of case (e) with strong input motion.	60
Figure 3-26 Acceleration history of case (f) with weak input motion.	61
Figure 3-27 Acceleration history of case (f) with strong input motion.	62
Figure 3-28 Pore water pressure ratio of case (f) with weak input motion.	63
Figure 3-29 Pore water pressure ratio of case (f) with strong input motion.	64
Figure 3-30 Normalized shear modulus data for Vietnam sand (Wang, 2004).	65
Figure 3-31 Damping ratio curve of Vietnam sand (Wang, 2004).	65
Figure 3-32 Shear modulus curve of Vietnam sand in numerical analysis.	66
Figure 3-33 Damping ratio curve of Vietnam sand in numerical analysis.	66
Figure 3-34 Acceleration history of shaking table test case 1 (weak motion).	67
Figure 3-35 Acceleration history of shaking table test case 4 (strong motion).	68

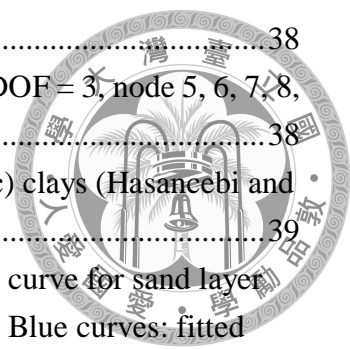
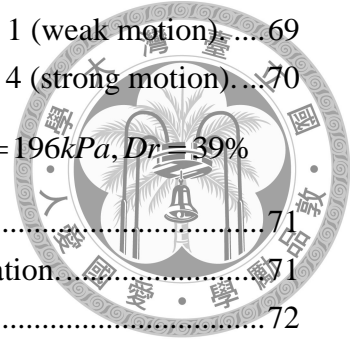


Figure 3-36 Pore water pressure ratio of shaking table test case 1 (weak motion).....	69
Figure 3-37 Pore water pressure ratio of shaking table test case 4 (strong motion)....	70
Figure 3-38 Deviator stress and axial strain of triaxial test, $\sigma'_v = 196kPa, Dr = 39\%$ (Jiang, 2000).	71
Figure 3-39 Deviator stress and axial strain of Opensees simulation.....	71
Figure 3-40 Pore water pressure of OpenSsees simulation.	72



List of Tables

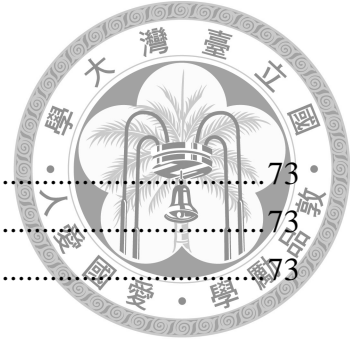


Table 3-1 Soil properties of simple hypothetical cases.....73

Table 3-2 Soil properties of shaking table tests73

Table 3-3 Soil properties of cyclic triaxial test73

Chapter 1 Introduction

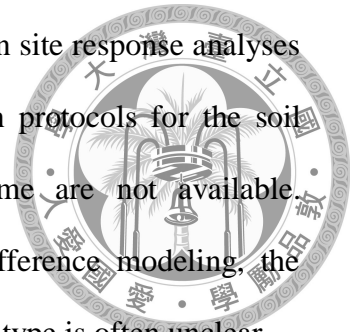


1.1 Motivation

Effect of ground condition on earthquake motion had been observed in past earthquakes. When earthquake waves propagate through soil and rock layers, characteristics of the waves, such as frequency content and amplitude would be changed. In the discipline of geotechnical earthquake engineering, theoretical site response analyses can be performed to evaluate how geologic deposit responds, in terms of particle motion and pore water pressure generation, when it is subjected to earthquake shaking.

Site response analyses can be classified according to their solution domain, the type of soil model employed, and whether pore water pressure response is considered. In terms of solution domain, site response analyses can either be solved in frequency domain or time domain. In frequency-domain analysis, the soil property is assumed to be linear or equivalent-linear. Moreover, only total stress is evaluated in frequency-domain analysis. For time-domain analyses, soil property can be linear or nonlinear. Soil stress can be evaluated in terms of total stress or effective stress. For effective stress analyses, pore water pressure response during the dynamic loading would be modeled. In common practice, frequency-domain total-stress site response analyses are often performed because parameter selection and code usage are relatively simple. Time-domain total stress site response analyses have become more popular because benchmarking studies (e.g. Stewart et al., 2008) had been performed to set up the proper parameter selection procedures and evaluate the differences between the ground motions predicted from frequency-domain and time-domain total

stress analyses. On the other hand, effective-stress time-domain site response analyses are rarely performed in practice because parameter selection protocols for the soil material model and pore water pressure generation scheme are not available. Moreover, for analyses that involve finite element/finite difference modeling, the proper way to set up the analysis domain and to select element type is often unclear.



1.2 Objective

The objective of this research is to review the currently available computer programs for effective-stress dynamic analyses and to compare the solutions from total stress and effective stress dynamic analyses. Through this study, it is expected that the impact of different parameters on the predictions from effective-stress analyses can be better understood. In this research, a series of numerical simulations had been run for simple hypothetical site conditions, cyclic triaxial tests and shaking table tests.

1.3 Organization of thesis

This thesis is divided into four chapters. In the first chapter, background and objective of this research are presented. In Chapter Two, different types of ground response modeling schemes and previous numerical studies on simulating shaking table and centrifuge tests are reviewed. In Chapter Three, the effective-stress dynamic analyses performed in this study, as well as analysis results and discussion, are presented. Lastly, conclusion and recommendations for future research are given in Chapter Four.

Chapter 2 Literature Review



2.1 Site Response Analysis

2.1.1 Overview of site response modeling

Seismic waves can be affected by local geological conditions. This phenomenon is commonly known as the site effect, Importance of site effect had been observed in past earthquakes, e.g. during the Loma Prieta Earthquake of October 17, 1989. The location of the earthquake epicenter for this earthquake is shown in Figure 2-1. As shown in Figure 2-2, the ground shaking is much stronger in area with soft sediments than in area comprising of bedrock.

Different soil types can have different impacts on earthquake motion. The purpose of theoretical site response analysis is to evaluate how the earthquake wave alters as it passes through different soil layers. Site response analysis can be divided into two main categories: (1) frequency domain and (2) time domain, which will be discussed in the following section.

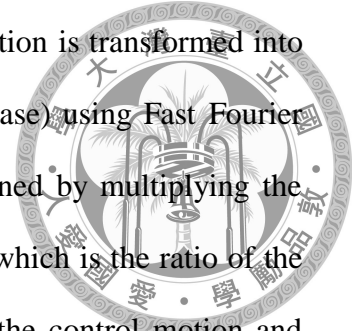
2.1.2 Theoretical Site Response Modeling

The solution of theoretical site effect modeling can be evaluated in either frequency domain or time domain. In the following subsections, these two types of modeling will be described.

Frequency Domain Site Response Analysis

In frequency domain analyses, a control input motion (in terms of acceleration time

history) is known and specified at a particular depth. This motion is transformed into the frequency domain (in terms of Fourier amplitude and phase) using Fast Fourier transform. At the depth of interest, the motion can be obtained by multiplying the control motion to the frequency-dependent transfer function, which is the ratio of the amplitudes of the motions at the two depths (i.e., depth of the control motion and depth of interest). The transfer function depends on the difference in soil properties (e.g. soil density, shear modulus and damping). The motion at the depth of interest (in terms of acceleration time history) can then be calculated by using the Inverse Fast Fourier Transform.



Throughout the frequency domain site response analysis, the soil properties (shear modulus and damping ratio) are assumed to be linear and constant. However, soil behaves nonlinearly in reality and different levels of shear strain would be induced during an earthquake. In order to better represent the soil behavior, an equivalent-linear approach can be used. The equivalent linear site response analysis was an iterative procedure to determine the shear modulus and damping ratio at different strain level. The first step of the analysis is to assign an initial shear modulus and damping ratio. Using these values, the shear strain induced in the soil column would be calculated. Then the shear modulus and damping ratio would be updated based on the new shear strain. This process would be repeated until the shear modulus and damping ratio that are compatible with the average shear strain level of the earthquake are found. A schematic diagram of the equivalent linear procedure is shown in Figure 2-3.

Time domain Site Response Analysis

In time domain site response analyses, the governing equation is solved at each time

step. Soil properties can be assumed to be either linear or non-linear. For linear analysis, the soil property is constant throughout the earthquake; while for nonlinear analysis, soil property may change (possibly) at each time step and according to the shear strain level. In general, the parameter selection procedure for time domain analysis is more complex than that for frequency-domain analysis because the users have to specify the parameters for the stress-strain model (backbone curve), unloading and reloading schemes (e.g. Masing rules), damping formulation and damping ratio (in terms of hysteretic damping and viscous damping), pore water pressure generation and dissipation models.

There are many computer programs that are readily available for performing site response analysis, for example, SHAKE (Idriss and Sun, 1992), DEEPSOIL (Hashash, 2012), OpenSees (McKenna and Fenves, 2014), etc.. In this research, DEEPSOIL and OpenSees are used. In DEEPSOIL, frequency domain equivalent-linear analysis and time domain nonlinear analyses (both total stress analysis and effective stress analysis) are available. For OpenSees, time domain nonlinear analyses (both total stress analysis and effective stress analysis) are available. In the following subsections, key components of DEEPSOIL and OpenSees are introduced.

DEEPSOIL

DEEPSOIL is a bundled program which allows the users to perform both frequency domain and time domain site response analyses. For frequency domain analysis, the materials can be either linear or equivalent linear. For time domain analysis, the materials can be linear or nonlinear. In addition, either total stress analysis or effective stress analysis can be performed. The theoretical background of DEEPSOIL will be described in the following subsections.

Backbone curve

The backbone curve represents the relationship between shear stress and shear strain.

The equation of backbone curve in DEEPSOIL can be described as follow:

$$\tau = \frac{G_{\max} \gamma}{1 + \text{Beta} \left(\frac{\gamma}{\gamma_r} \right)^s} \quad (2-1)$$

$$\gamma_r = \text{REF.strain} \left(\frac{\sigma_v'}{\text{REF.stress}} \right)^b \quad (2-2)$$

where τ is the shear stress, γ is the shear strain, G_{\max} is the initial shear modulus, Beta and s are the fitting parameters, and γ_r is the reference strain. In DEEPSOIL, the backbone curve is made pressure-dependent by making γ_r to be dependent on the effective vertical stress σ_v' . REF.strain and REF.stress are the reference strain and reference stress for computing γ_r which correspond to the vertical stress at 1 atm.

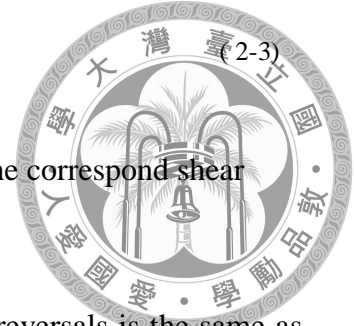
Unloading and Reloading Rules

The backbone curve only describes the shear stress and shear strain relationship under monotonic loading condition. A set of rules are needed to describe the behavior of soil when it is unloaded or reloaded. Masing rules are often used and their details are as follows:

1. The reloading curve can be obtained by scaling the backbone curve by a factor of 2. By rotating 180 degrees of the reloading curve, the unloading curve can be obtained. Mathematically, it can be represented by:

$$\frac{q_R + q_a}{2} = f\left(\frac{\varepsilon_s + \varepsilon_{sa}}{2}\right); \quad \frac{q_a + q_U}{2} = f\left(\frac{\varepsilon_{sa} + \varepsilon_s}{2}\right)$$

where q_a is the deviator stress of reflexes point and ε_{sa} is the correspond shear strain.



2. The initial tangent shear modulus G_{t0} after all the stress reversals is the same as the initial tangent shear modulus G_0 of the backbone curve.
3. When the unloading or reloading curve meets the backbone curve, the unloading or reloading curve will continues along the backbone curve.
4. When a stress-strain curve meets a curve from previous cycle, it will follow the previous curve.

Damping

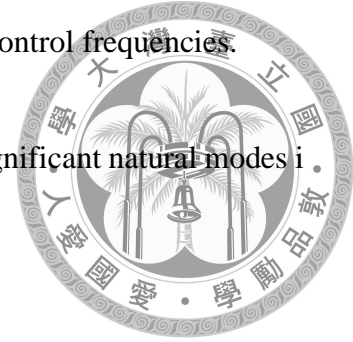
The hysteretic damping of soil can be evaluated based on the hysteresis loop as defined by the unloading and reloading rules. Figure 2-4 shows how hysteresis damping can be evaluated. When the shear strain is very small, hysteretic damping is practically zero which is not consistent with the data from laboratory tests. For this reason, viscous damping is usually used and added to hysteresis damping in the numerical model. The viscous damping formulation used in DEEPSOIL was originally proposed by Rayleigh and Lindsay (1945). The viscous damping matrix is related to the mass matrix and stiffness matrix, as follows:

$$[C] = a_0[M] + a_1[K] \quad (2-4)$$

where $[M]$ is the mass matrix, $[K]$ is the stiffness matrix and a_0 and a_1 are scalar

values selected to obtain the specific damping values for two control frequencies.

The scalar values of a_0 and a_1 can be computed using two significant natural modes i and j using the equation below:



$$\begin{bmatrix} \xi_i \\ \xi_j \end{bmatrix} = \frac{1}{4\pi} \begin{bmatrix} \frac{1}{f_i} & f_i \\ \frac{1}{f_j} & f_j \end{bmatrix} \quad (2-5)$$

where ξ_i and ξ_j are the damping ratios corresponding to frequencies f_i and f_j .

The way to decide the natural frequency of the selected mode is commonly calculated as (Kramer 1996):

$$f_n = (2n-1) \frac{\bar{V}_s}{4H} \quad (2-6)$$

where n is the mode number and f_n is the natural frequency of the corresponding mode. Figure 2-7 presents a comparison of the effective damping obtained using one-mode, two-mode and four-mode solutions.

Once the target modulus reduction and damping curves (which may be determined from laboratory testing or published literature) are chosen for a soil layer, the parameters for the background curves and damping must be determined. The selection can be achieved by different fitting procedures: (1) MR (Modulus Reduction) which aims to match the target and model modulus reduction curves; (2) MD (Damping) which aims to match the target and model damping curves; (3) MRD (Modulus Reduction and Damping) which aims to match the target and model modulus reduction and damping curves. The fitted curves obtained from these

procedures are compared in Figure 2-8.



Pore pressure generation and dissipation models

Pore pressure generation models can generally be categorized into two different categories: strain-based and energy-based models.

The strain-based model for cohesionless soil was developed by Matasovic et al. (1992), and the equation is as follows:

$$u_N = \frac{p \cdot f \cdot N_c \cdot F \cdot (\gamma_{ct} - \gamma_{tvp})^s}{1 + f \cdot N_c \cdot F \cdot (\gamma_{ct} - \gamma_{tvp})^s} \quad (2-7)$$

where u_N is the pore pressure after cycle N , N_c is the number of cycles, γ_{ct} is the cyclic shear strain, γ_{tvp} is the magnitude of the volumetric threshold shear strain, f is to simulate 1-D or 2-D effects of pore pressure generation, and p , F , and s are curve-fitting parameters. These parameters can be determined by a curve-fitting procedure with the use of cyclic undrained laboratory test data.

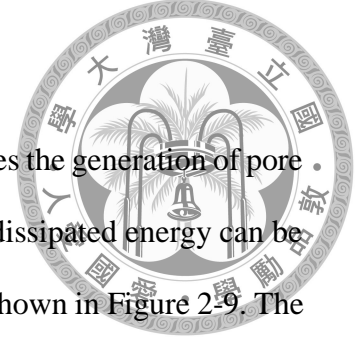
The equation below is the pore pressure generation model for cohesive soils which was developed by Matasovic and Vucetic (1995):

$$u_N = AN^{-3s(\gamma_c - \gamma_{tvp})^r} + BN^{-2s(\gamma_c - \gamma_{tvp})^r} + CN^{-s(\gamma_c - \gamma_{tvp})^r} + D \quad (2-8)$$

where γ_c is the amplitude of the cyclic shear strain, γ_{tvp} is the magnitude of the volumetric threshold shear strain, s and r are curve-fitting parameters correlated to plasticity index (PI) and overconsolidation ratio (OCR), and A , B , C , D are the

curve-fitting parameters.

The energy-based model is an empirical expression which relates the generation of pore pressure to the energy dissipated per unit volume of soil. The dissipated energy can be calculated by stress-strain curve as the area under the curve as shown in Figure 2-9. The equation of generally energy-based model is shown below:



$$r_u = \alpha W_N^\beta \quad (2-9)$$

where W_N is the energy dissipated of cycle N , α and β are curve-fitting parameters.

The energy-based model in DEEPSOIL is the GMP model developed by Green et al (2000) which can be described as:

$$r_u = \sqrt{\frac{W_s}{PEC}} \quad (2-10)$$

where W_s is the dissipated energy per unit volume of soil divided by the initial effective confining pressure, and the PEC is the “pseudo energy capacity”. The W_s can be calculated as:

$$W_s = \frac{1}{2\sigma'_{v0}} \sum_{i=1}^{n-1} (\tau_{i+1} + \tau_i) \cdot (\gamma_{i+1} - \gamma_i) \quad (2-11)$$

σ'_{v0} is the initial effective vertical stress, n is the number of load increments to trigger liquefaction, τ_i and τ_{i+1} are shear stresses at time step i and $i+1$, γ_i and γ_{i+1} are the shear strain at time step i and $i+1$. The purpose of Equation (2.11) is to compute the area bounded by the stress-strain loop and then normalized by σ'_{v0} . The model

parameter “*PEC*” is relate to relative density (D_r) and fines content (FC). This model is developed based on the database of laboratory data on non-plastic silt-sand mixtures ranging from clean sands to pure silts. The empirical relationship is defined by Equation (2.12)



$$\ln(PEC) = \begin{cases} FC < 35\% : \exp(c_3 \cdot D_r) + c_4 \\ FC \geq 35\% : c_1 FC^{c_2} + \exp(c_3 \cdot D_r) + c_4 \end{cases} \quad (2-12)$$

where $c_1 = -0.597$, $c_2 = 0.312$, $c_3 = 0.0139$, $c_4 = -1.021$.

Input Parameters of DEEPSOIL

1. The parameters of total stress analysis in DEEPSOIL include thickness of soil layer, unit weight, shear wave velocity, damping ratio, reference stress, reference strain and the parameters of pressure depend.
2. In effective stress analysis, there are some additional required parameters (in addition to the parameters needed for the total stress model) for the pore water pressure generation model: relative density, fine content, coefficient of consolidation and some curve fitting parameters of sand or clay model.

OpenSees

OpenSees is finite element method software which can be used for dynamic analysis. It utilizes a two-phase (solid and fluid) fully coupled finite element formulation to simulate both the motion of the solid and the pore pressure response. The constitutive model used in this study is based on the multi-surface plasticity by Yang (2000). The detail of this plasticity model will be described in the following subsections.

Cyclic mobility mechanism



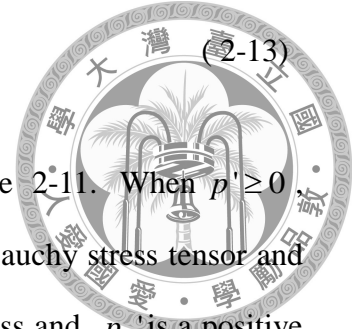
During a cyclic shear loading process, a saturated undrained cohesionless soil exhibits the following pattern of behavior:

1. At low shear strains, the soil skeleton experiences a tendency for contraction, leading to development of excess pore-pressure and reduction in effective confinement, this step is shown in Figure 2-10 (phase 0-1).
2. When the shear stress approaches the failure envelope, or more precisely the Phase Transformation (PT) envelope (Ishihara 1985, Iai 1991, Vaid and Thomas 1995, Vaid and Sivathayalan 1999), significant shear strain may develop without appreciable change in shear stress (the perfectly plastic phase 1-2 in Figure 2-10). Numerical versatility is achieved by defining the highly yield segment of stress strain response as a distinct phase (γ_y as shown in Figure 2-10, where $\gamma = \sqrt{2/3} e:e$ refers to octahedral shear strain, and $e =$ deviatoric strain tensor). This feature allows for direct control over the extent of shear strain accumulation.
3. A dilative tendency (phase 2-3 in Figure 2-10) increases effective confinement (consequently shear stiffness and strength), allowing the soil to resist increased levels of shear stress.

Yield Function

The yield function f is of the following form (Prevost 1985):

$$f = \frac{3}{2}(s - (p' + p_0)\alpha) : (s - (p' + p_0)\alpha) - M^2(p' + p_0)^2 = 0 \quad (2-13)$$



The shape of the yield function is illustrated in Figure 2-11. When $p' \geq 0$, $s = \sigma' - p'\delta$ is the deviatoric stress tensor (σ' is effective Cauchy stress tensor and δ is second-order identity tensor), p' is mean effective stress and p_0 is a positive constant to remain yield surface size remains finite at $p' = 0$; α is a second-order kinematic deviatoric tensor to define the coordinates of yield surface, M dictates the yield surface size and the “:” means doubly contracted scalar product of two tensors. For the multisurface plasticity, each surface is associated with a constant plastic modulus and the outmost surface is the failure surface. Yield surface is open in the positive direction of hydrostatic axis and it may use a cap yield function to close the open end. For clay, the yield function is assumed to follow the Von Mises shape and is shown in Figure 2-12. The Von Mises yield surface is a function of undrained shear strength.

Hardening Rule

A purely deviatoric kinematic hardening rule is employed for generate soil hysteretic response under cyclic loading. This rule dictates that all yield surfaces may translate in stress space within the failure envelope and is consistent with Masing criteria. In drained monotonic shear loading, the hardening zone is represented by some similar yield surfaces and the elastoplastic modulus can be defined by using a piecewise linear approximation of hyperbolic backbone curve. As we can see in Figure 2-13, f_m is yield surface, H_m is shear modulus, M_m is the size and $m = 1, 2, \dots, NYS$ (the total number of yield surfaces), H_m is defined as:

$$H_m = \frac{2(\tau_{m+1} - \tau_m)}{\gamma_{m+1} - \gamma_m} \quad (2-14)$$

where $H_{NYS} = 0$. The outermost surface is the envelope of peak shear strength (failure envelope), the size of which can be calculated as:

$$M_f = M_{NYS} = \frac{6 \sin \phi}{3 - \sin \phi} \quad (2-15)$$

where ϕ is friction angle.

Flow Rule

The non-associated flow rule (Parra 1996) is used for the sand model to control the soil contractive/dilative behavior during shear loading to achieve appropriate interaction between shear and volumetric responses. The non-associativity is limited to the volumetric component (P'') of the plastic flow tensor. And P'' is defined as (Prevost 1985, Parra 1996):

$$3P'' = \frac{1 - (\eta / \bar{\eta})^2}{1 + (\eta / \bar{\eta})^2} \Psi \quad (2-16)$$

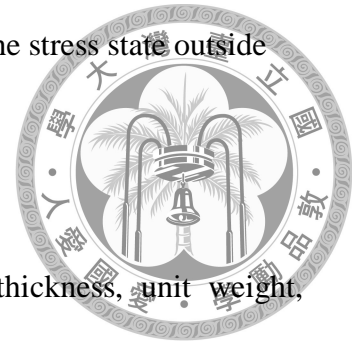
where $\eta = \sqrt{(3/2)s:s} / (p' + p_0')$ is effective stress ratio, $\bar{\eta}$ is material parameter defining the stress ratio of the PT surface, Ψ is a scalar-valued function for controlling the magnitudes of dilation and contraction, if $(1 - (\eta / \bar{\eta})^2)$ is positive, the stress state lies within PT surface, if it is negative, the stress state lies above the PT surface.

Depending on the relative location of the stress state with respect to the PT surface, different P'' were specified below as we can see in Figure 2-10:

1. Phase 0-1 is the contractive phase, the stress state inside the PT surface.
2. Phase 2-3 is the dilative phase during loading, the stress state lies outside the PT surface.



3. Phase 3-4 is the contractive phase during unloading and the stress state outside the PT surface.



Input Parameters of OpenSees

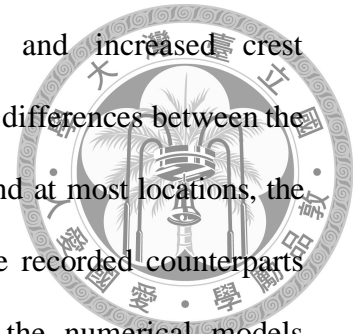
1. Properties of each layer and visco-elastic halfspace: thickness, unit weight, small-strain shear modulus, shear wave velocity, bulk modulus and the unit weight and shear wave velocity of halfspace.
2. Parameters of yield surfaces, modulus reduction at different strain or a hyperbolic backbone curve.
3. Parameters that control the contraction and dilatency response.
4. Frequencies of the Rayleigh damping formulation.

2.1.3 Previous research related to effective stress dynamic analysis

Fattah et al. (2012) performed effective stress dynamic analyses using OpenSees to analyze the site response of a homogeneous layer of a saturated natural soil deposit over impermeable bedrock. They found that the dynamic response of the solid displacement and pore pressure would be larger for elasto-plastic soil than for elastic soil. In addition, at low viscous coupling, the peak of the amplitude of excess pore water pressure decreases at each cycle due to the relatively little dissipation of the water. In contrast, at high viscous coupling, the excess pore water pressure builds up to the same peak value, and the amplitude of pore pressure is larger than that at low viscous coupling.

Yang et al. (2004) performed a series of numerical simulations for dynamic centrifuge testing to investigate the effect of foundation densification on the seismic performance of a zoned earth dam with a saturated sand foundation. The physical and

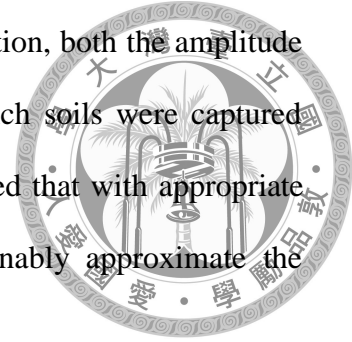
numerical models both indicated reduced deformations and increased crest accelerations with an increase in densified layer thickness. The differences between the computed and recorded dam displacements were under 50% and at most locations, the computed excess pore pressure and acceleration matched the recorded counterparts reasonably well. Regarding the liquefaction phenomenon, the numerical models captured the predominant liquefaction response mechanism as exhibited in the physical models, in terms of lateral spreading deformations and spiky acceleration response.



Jishnu et al. (2013) performed 1D and 2D ground response analysis and liquefaction analysis of alluvial soil deposits from Kanpur region along Indo-Gangetic plains. According to the simulation results, they found that the soil layers at greater depths (21 to 30 m) were prone to liquefaction. Post liquefaction settlement contributed by the deeper layers (21 to 30 m) was more than 50% of the total liquefaction settlement, which was due to the presence of loose to moderate dense soil in deeper region. Jishnu et al. also found that there was significant amount of amplification at greater depths.

Chang et al. (2008) performed nonlinear dynamic finite element analyses and compared the simulation results to the experimentally recorded dynamic response of an immersed tunnel in liquefiable soil. The models were shaken with a series of motions progressively from smaller amplitude to the design peak ground acceleration (PGA) of about 0.6g. The selection of parameters for the constitutive model was based on calibrations against laboratory cyclic simple shear tests performed for the tunnel project. The experimental records and the numerical simulations showed good agreement on overall model responses (e.g., accelerations and pore pressures

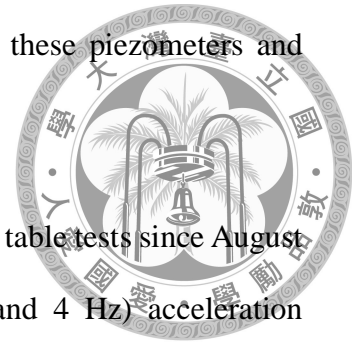
developed in the liquefiable sand) and the tube uplift. In addition, both the amplitude and rate of pore pressures dissipation in the liquefiable trench soils were captured satisfactorily by the numerical analyses. Chang et al. concluded that with appropriate calibrations, the finite element models were able to reasonably approximate the essential features of soil and tunnel responses.



2.2 Laboratory & Physical Tests with Dynamic Loading

Ueng et al. (2003 and 2006) studied the behavior of saturated sand by using a large flexible laminar shear box and subjecting it to two-dimensional shaking on the shaking table at National Center for Research on Earthquake Engineering. The shear box has 15 layers and each layer has two parallel frames. The inner frames can move in Y-direction and the outer frames can move in X-direction, so the soil specimen can move freely in horizontal plane, the schematic of shear box is shown in Figure 2-14. Figure 2-15 shows a picture of the empty shear box. The size of the inner frame is 1800 by 1800 mm and the outer frame is 1940 by 2340 mm. Each frame has 30 mm in thickness and 80 mm in height, except for the top layer which has 100 mm of height. In the experiments by Ueng et al. (2003 and 2006), a sand specimen of 1800 by 1800 by 1520 mm were placed into the shear box. The transducers for displacement and acceleration measurements were placed on the outside rigid walls, the outer frames for X-direction movement and the inner frames for Y-direction movement. The displacement of the frames was measured by linear displacement transducers (LDT). There were four velocity transducers placed on the outside rigid walls to measure the velocities of the shear box. This instrumentation is shown in Figure 2-16. Some piezometers were installed inside the box for pore pressure measurements at different depths. Piezo-resistive accelerometers were placed for measuring the accelerations within the

sand specimen in both X and Y-directions. The locations of these piezometers and accelerometers are shown in Figure 2-17.



Ueng et al. (2003 and 2006) performed a series of shaking table tests since August 2002. These tests used input motions with sinusoidal (2 and 4 Hz) acceleration histories, which amplitudes ranged from 0.03 to 0.15g in X or Y-directions, or both. They also used the record of Chi-Chi Earthquake as the input motion in the tests. Figure 2-18 shows the results for one of their shaking table tests which liquefaction had occurred. According to the measurements of the piezometer at depth of 553 mm, liquefaction may have occurred at 5 second. The measurements from the piezometer at depth of 749 mm did not show any sign of liquefaction. So the range of liquefaction was speculated to be between the depths of 553 mm and 749 mm. Figure 2-19 shows the acceleration histories at different depths.

Baydaa et al. (2011) performed three-dimensional finite element analysis to simulate the seismic pile-supported bridge structure reaction in liquefying ground. OpenSees, which is a finite element based numerical simulation platform, was used for the simulation. Their simulation results were compared to the data of shaking table tests. Baydaa et al. (2011) found that the three-dimensional numerical simulation can correctly predict the dynamic response of soil under earthquake loading, in terms of acceleration and pore pressure histories.

Ahmad and Radu (2004) performed both experimental and numerical studies to optimize the liquefaction remediation measures for the Fraser River Delta. In their research program, they performed laboratory soil tests, eight centrifuge experiments and numerical simulations. Nonlinear dynamic effective stress analyses were performed using the finite element code DYNAFLOW. This code considers the fully

coupled solid-fluid equations for porous media and implements a multi-yield plasticity soil constitutive model. In the process of numerical model calibration, they tried to identify the test conditions which could have induced significant differences between numerical predictions and experimental results. They found that the differences may be due to possible incomplete sand saturation in centrifuge models and possible discrepancy between the liquefaction resistance and soil stiffness of the soil samples in laboratory cyclic simple shear tests and that of the soil in centrifuge models. In addition, they found that the numerical model did not capture large negative acceleration peaks as observed in some of the centrifuge experiments.

Byrne et al. (2004) simulated dynamic centrifuge tests using effective stress numerical modeling. The centrifuge models were analyzed with a single column of elements. The effective stress analyses were carried out to obtain a measure of understanding of the importance of various aspects of the centrifuge testing, including the degree of saturation of the pore fluid and stress densification effect. By comparing the centrifuge testing and simulation results, Byrne et al. speculated that a lack of complete saturation as well as densification at depth arising from the application of the high acceleration field were largely responsible for the apparent limitation on liquefaction at depth observed in some centrifuge tests.



Figure 2-1 San Francisco Bay area and surrounding region. (After Stewart, 1997)

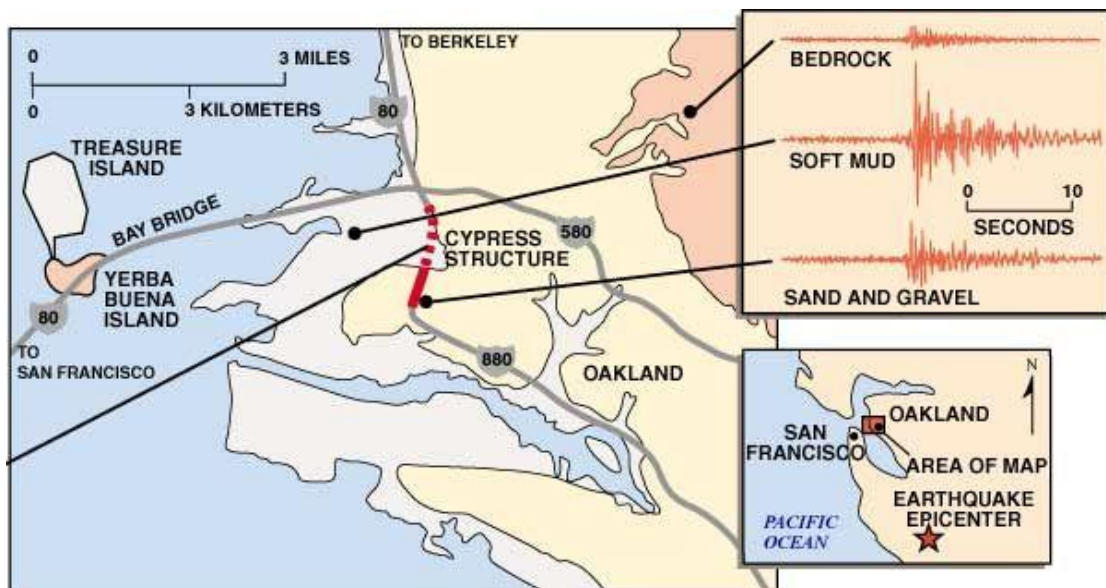


Figure 2-2 Seismograms (upper right) show that the shaking was especially severe in the soft mud. (After Stewart, 1997)

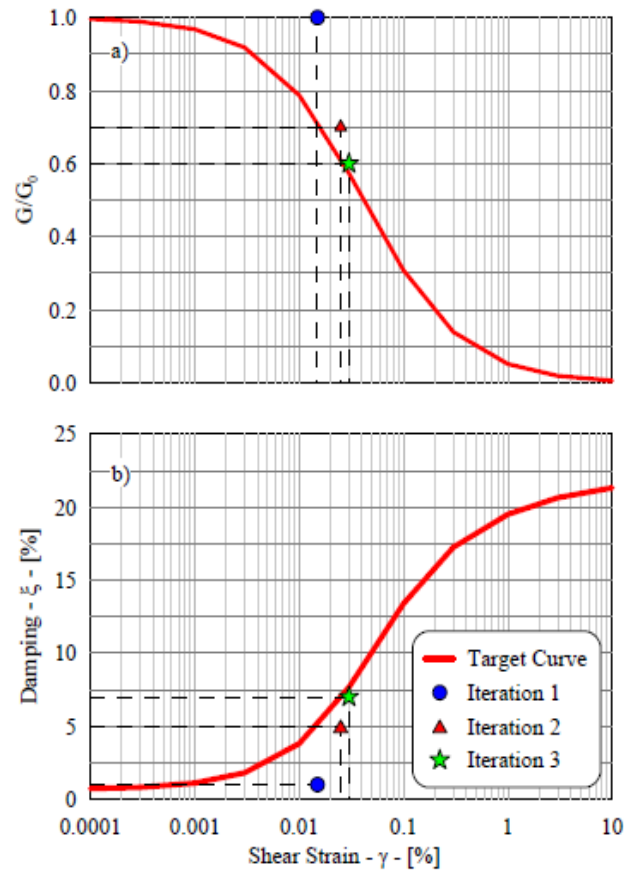


Figure 2-3 Equivalent linear iterative procedure a) Modulus reduction curve, b) Damping curve. (After Hashash et al, 2010)

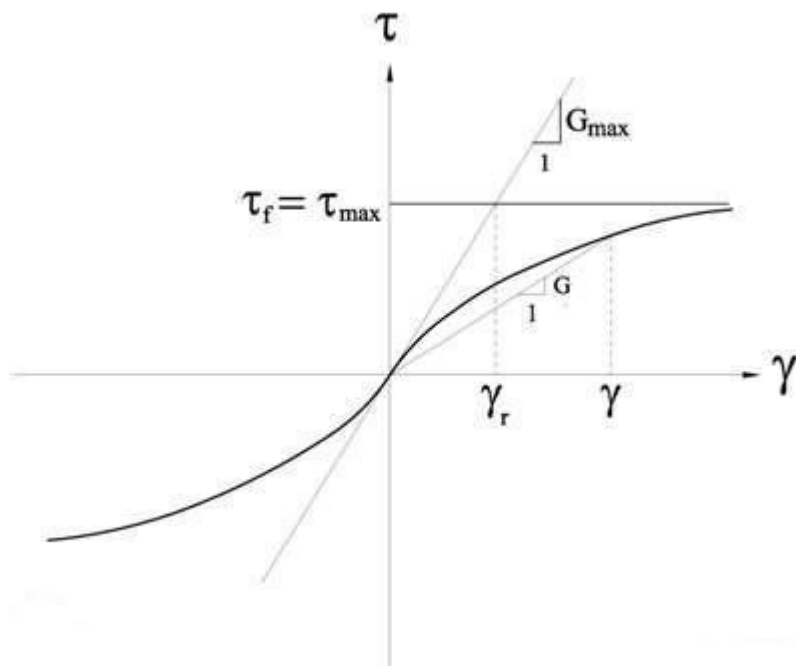


Figure 2-4 Backbone curve. (After Tuladhar, 2009)

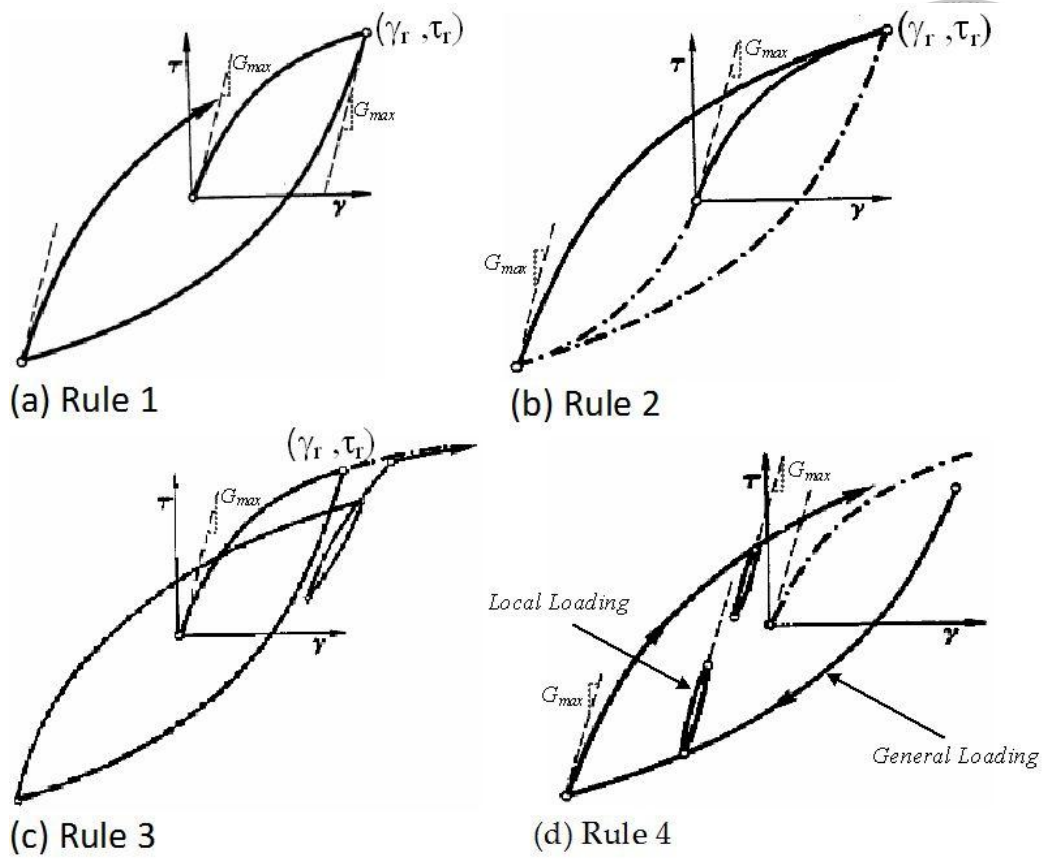


Figure 2-5 Masing rules. (After Ebrahimiyan, 2013)

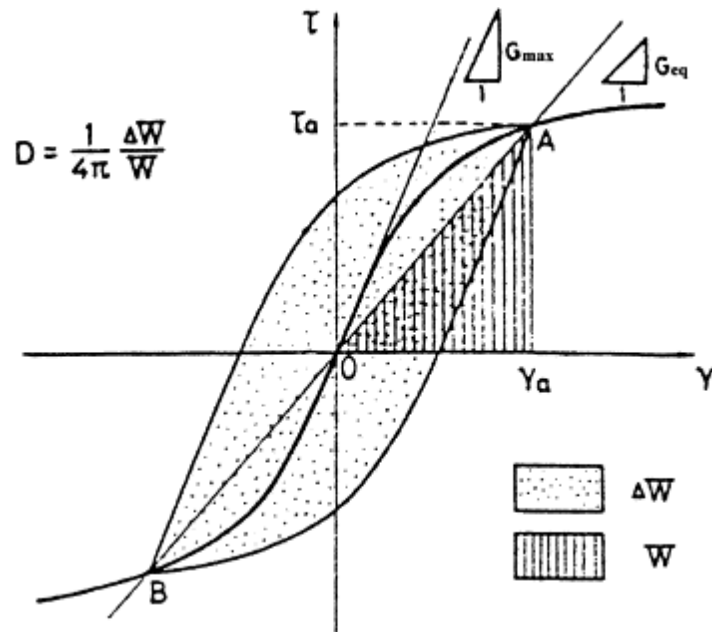


Figure 2-6 Definition of damping. (After Bartlett, 2011)

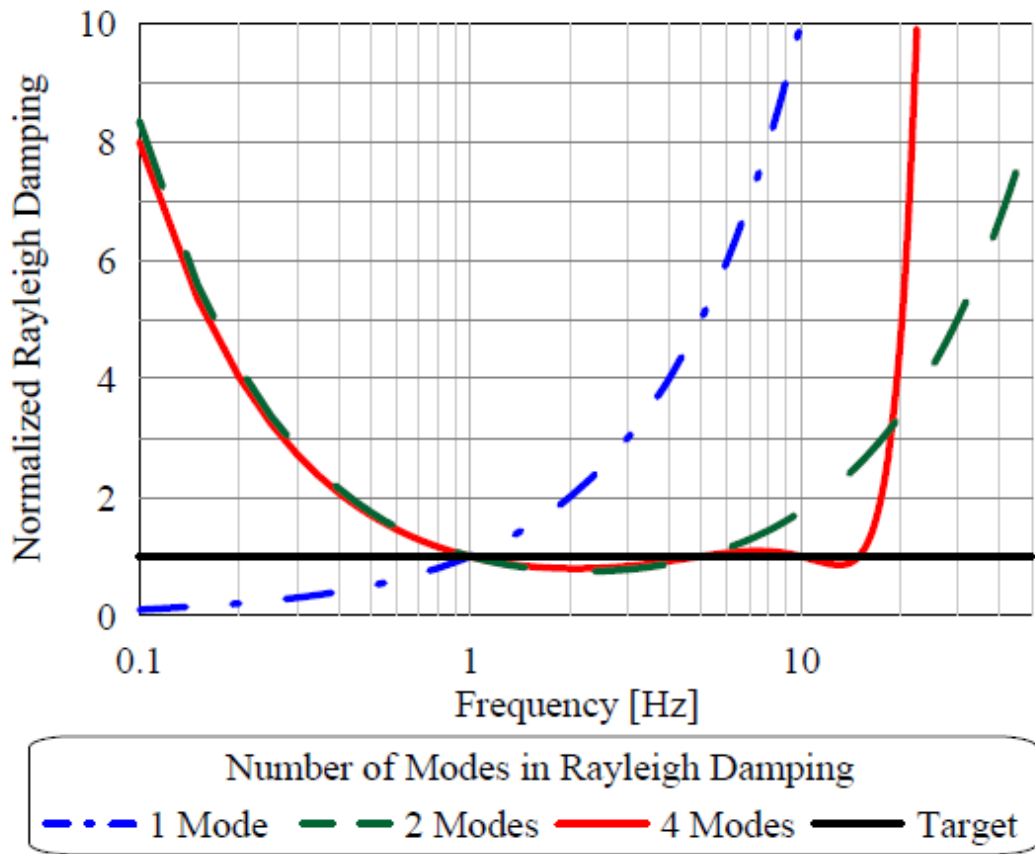


Figure 2-7 Effective damping for one, two and four modes Rayleigh formulation (After Hashash et al, 2010)

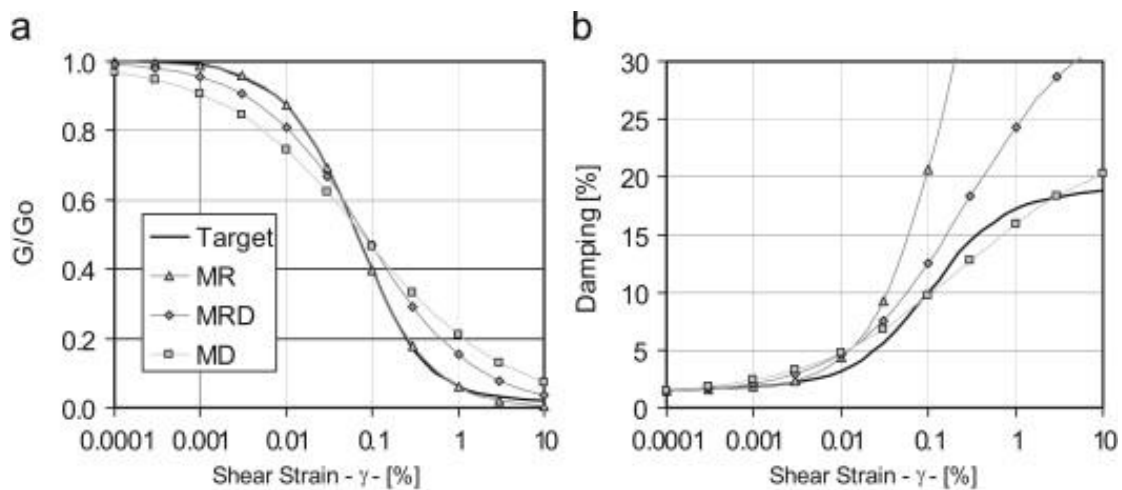


Figure 2-8 Comparison of different fitting procedures (After Hashash et al, 2010)

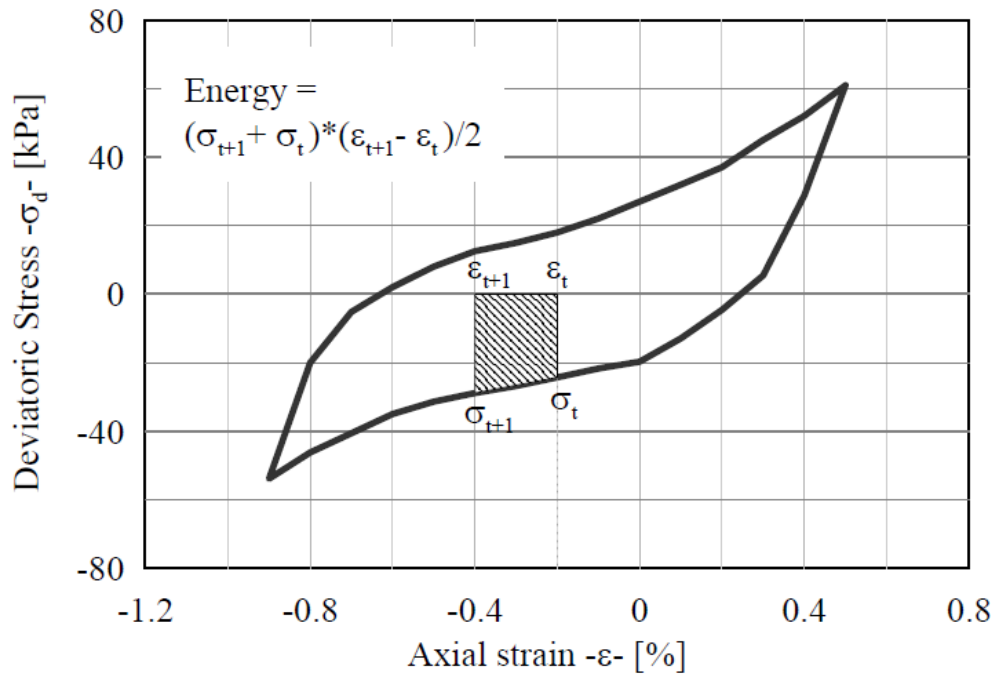


Figure 2-9 Dissipated energy per unit volume for a soil sample is defined as the area bound by the stress-strain loop (After Hashash et al, 2010)

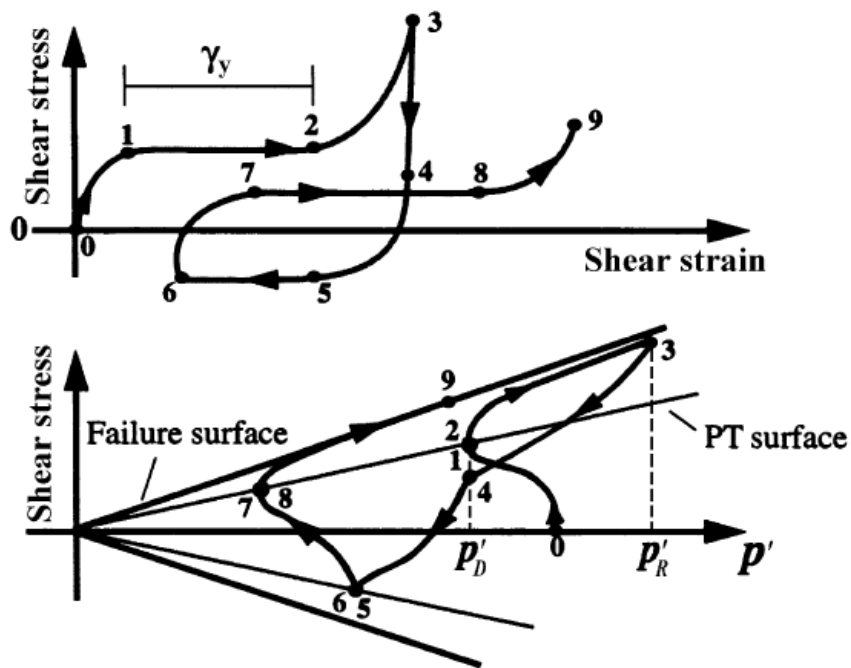


Figure 2-10 The schematic of constitutive model response showing shear stress, effective confinement, and shear strain relationship (After Yang et al, 2003)

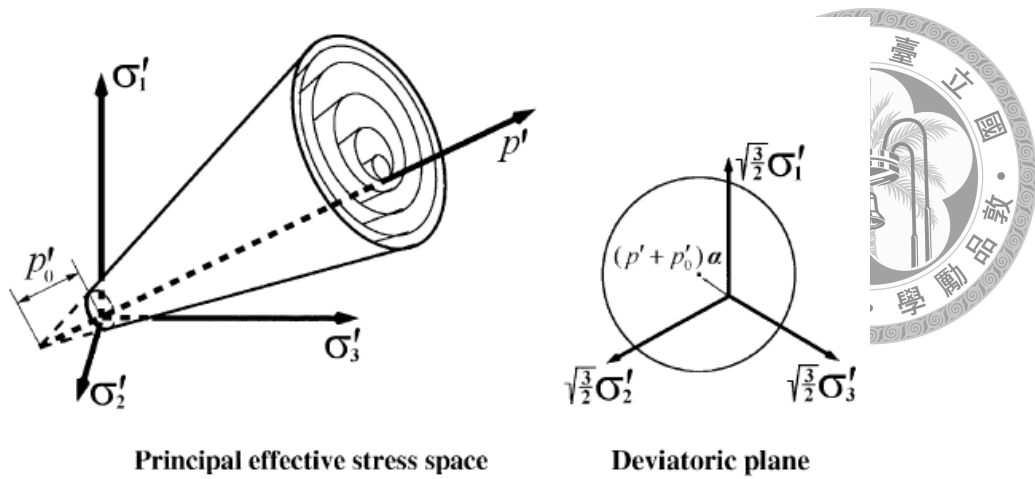


Figure 2-11 Conical yield surface in principal stress space and deviatoric plane (after Prevost 1985, Parra 1996, Yang 2000).

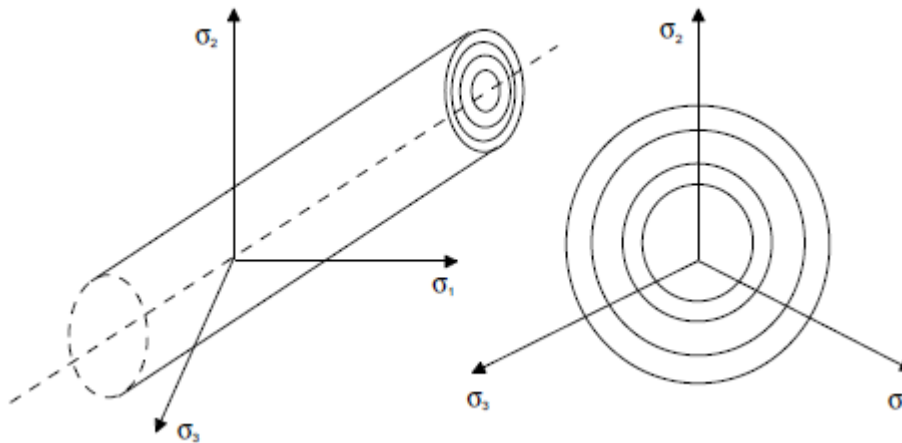


Figure 2-12 Cylindrical Von Mises yield surfaces for clay (after Prevost 1985, Lacy 1986, Parra 1996 and Yang 2000).

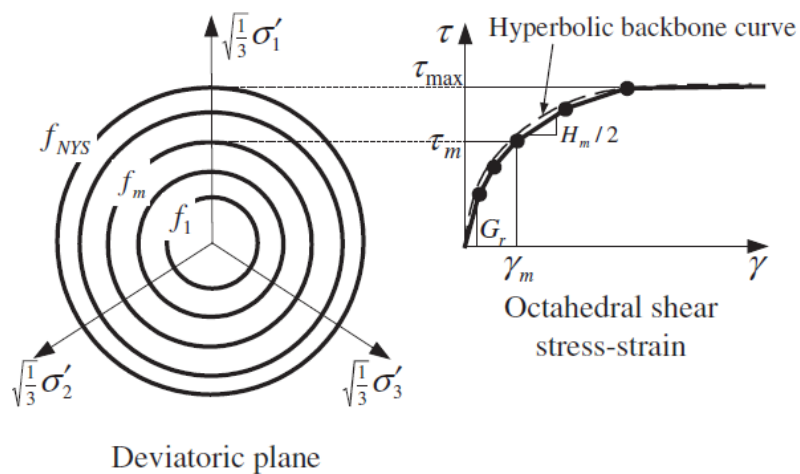


Figure 2-13 Hyperbolic backbone curve for soil nonlinear shear stress-strain response and piecewise-linear representation in multi-surface plasticity (after Prevost 1985 and Parra1996).

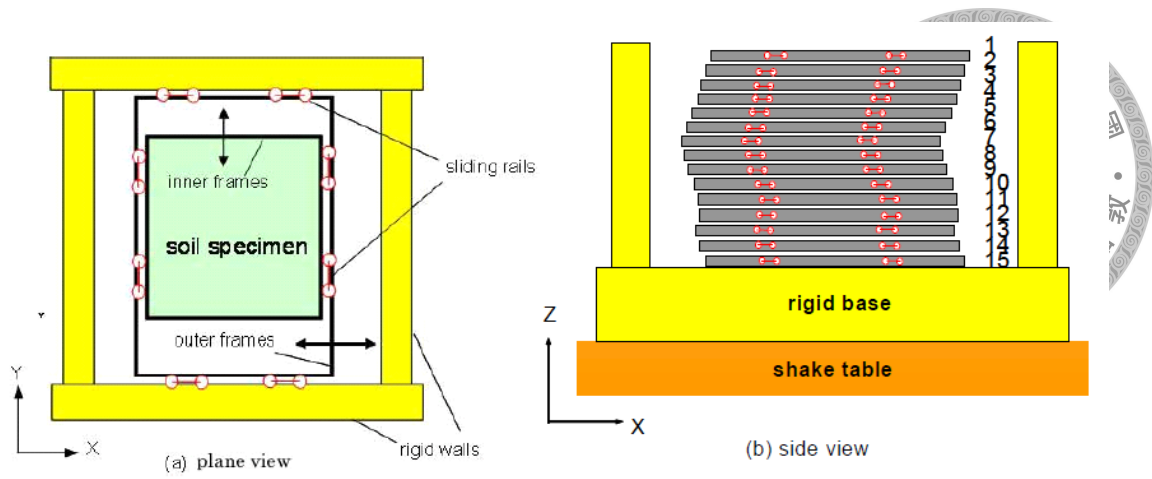
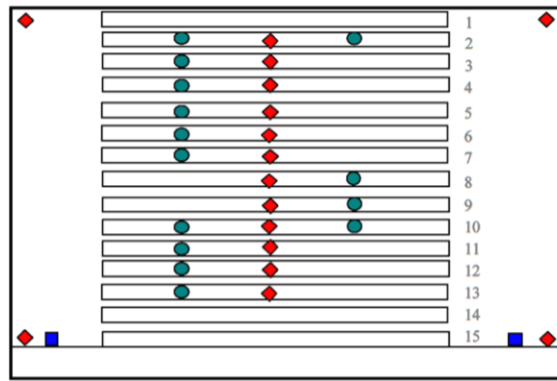


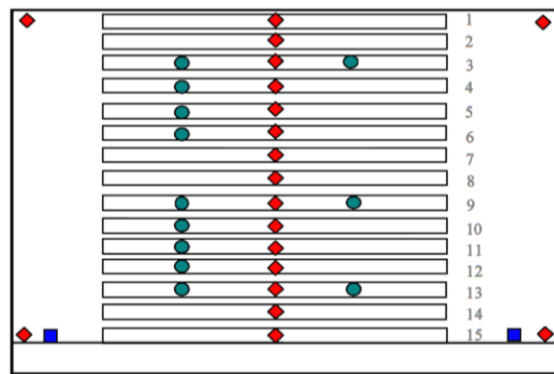
Figure 2-14 Schematic drawings of the biaxial laminar shear box. (After Ueng et al, 2006)



Figure 2-15 Picture of the empty laminar shear box. (After Ueng et al, 2006)



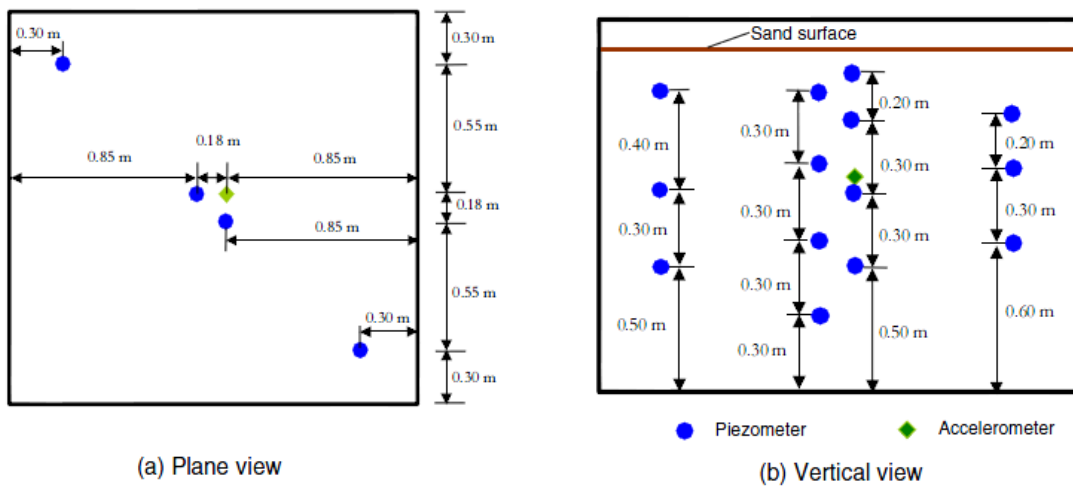
(a) Inner frame



(b) Outer frame

● LDT ■ velocity transducer ◆ accelerometer

Figure 2-16 Locations of instrumentation on the frames. (After Ueng et al, 2006)



(a) Plane view

(b) Vertical view

Figure 2-17 Locations of piezometers and accelerometers inside the specimen. (After Ueng et al, 2006)

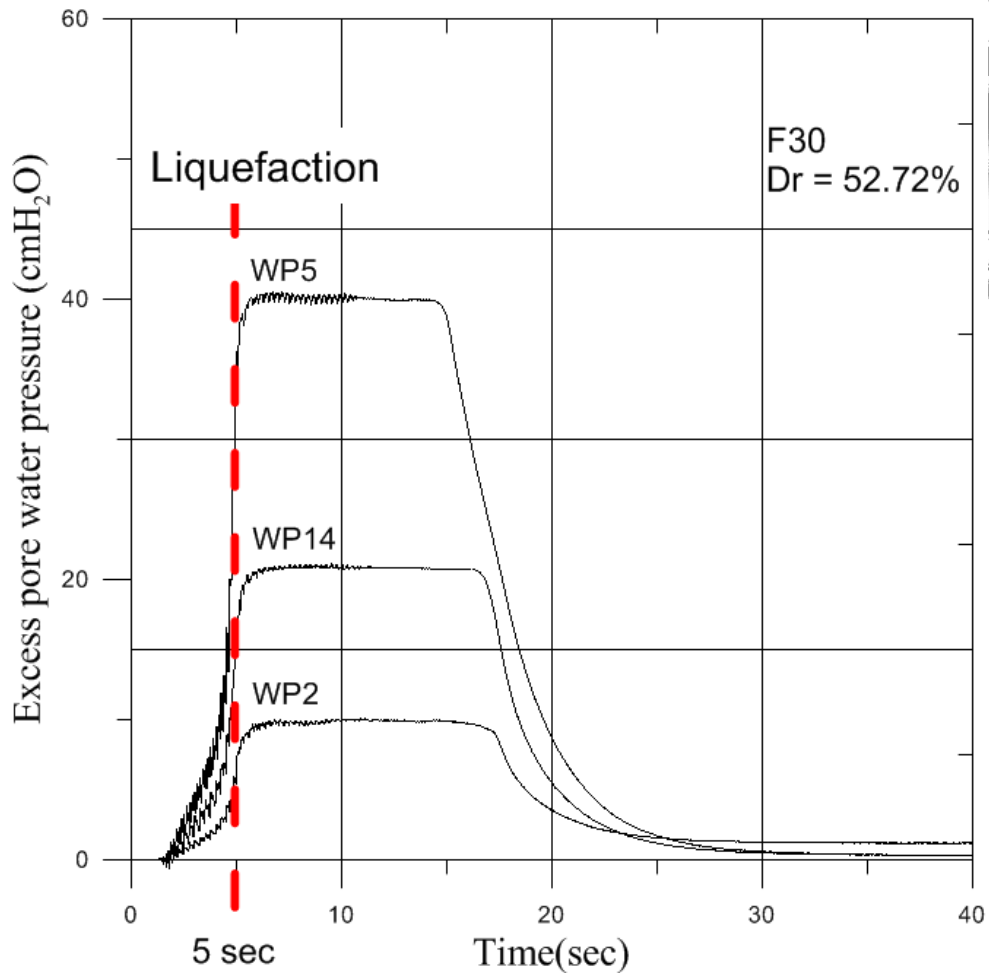


Figure 2-18 Liquefaction of shaking table tests (Vietnam sand, F30). (After Ueng et al, 2006)

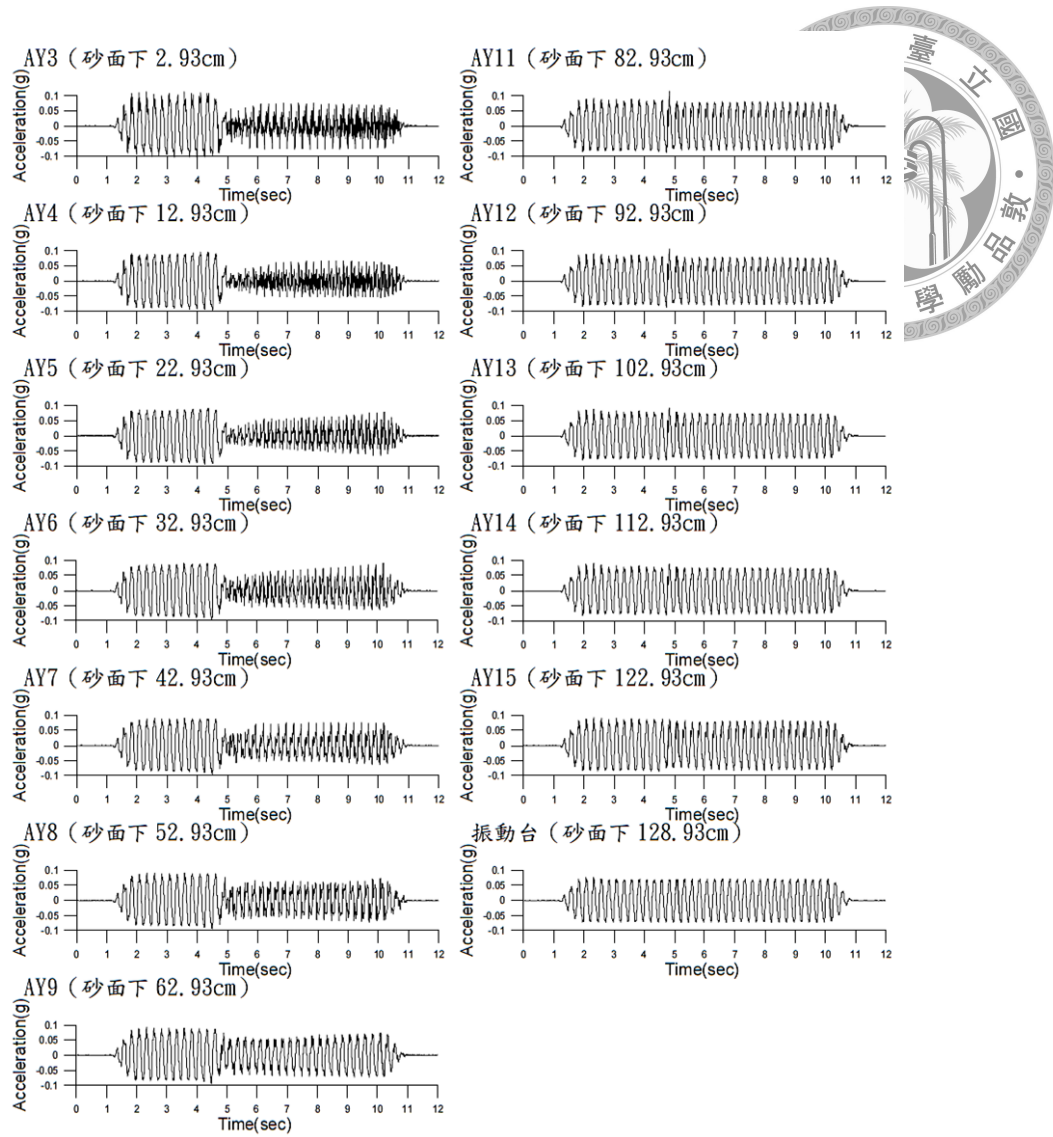


Figure 2-19 Acceleration history of shaking table tests (Vietnam sand, F30). (After Ueng et al, 2006)

Chapter 3 Numerical Modeling



3.1 Introduction

In order to evaluate the performance of effective-stress site response analyses, a series of numerical analyses were performed. Firstly, the site response of several hypothetical sites, which include simple layering of clays and sands, were analyzed. Secondly, numerical analyses were performed to model the cyclic triaxial tests on sand. Thirdly, simulations of shaking table tests were carried out. In all the analyses, results from effective stress analyses were compared to those from total stress analyses.

3.2 Numerical modeling of simple hypothetical sites

3.2.1 Site condition and analysis model

Six hypothetical sites are used. These sites are illustrated in Figure 3-1. The first two cases (a and b) are one-layer of clay and one-layer of sand, respectively, underlain by bedrock (which is modeled as elastic halfspace with unit weight of 23.54 kN/m^3 and shear wave velocity of 760 m/sec). Cases c and d are two-layer soil deposits which consist of clay and sand. Cases e and f are three-layer soil deposits, which contain interlayers and clay and sand. The purpose of using these simple hypothetical sites is to compare the particle motions as predicted by the total stress and effective stress site response analyses. Also, pore-water pressure response for different layering systems would be examined.

Frequency-domain total stress analysis (available in DEEPSOIL), time-domain total stress analysis (available in DEEPSOIL and OpenSees) and time-domain effective stress analysis (available in DEEPSOIL and OpenSees) were performed for the above six site conditions. In OpenSees, different element types were used for total stress and effective-stress analyses. A four-node element was used in total stress analysis. Each node has two degrees-of-freedom which are the displacements in vertical and horizontal directions. Figure 3-2 shows the schematics of the four node element. For effective-stress analysis, a nine-node element is used and is shown in Figure 3-3. The corner nodes have three degrees of freedom, two for vertical and horizontal directions and one for pore water pressure. The interior nodes have only two degrees of freedom for vertical and horizontal directions.

All hypothetical sites have total thickness of 30 meters. The sand layers in all the sites have the same soil properties, while the same also holds true for the clay layer. The soil properties and input motion will be introduced below.

Sand

The shear wave velocity (V_s) of sand was determined based on Hasancebi and Ulusay (2007) which correlates V_s with blow count (N-value). Figure 3-4 shows their correlation relationship. Assuming that the N-value for the sand layer is 10, the corresponding V_s value is about 200 m/s. The target normalized shear modulus curve and damping ratio curve were based on Seed and Idriss (1970). The curves that are actually used in the analyses are obtained by optimizing the fitting for both modulus reduction and damping curves (i.e. MRD method). The target and fitted curves are shown in Figure 3-5. For the effective stress analyses in DEEPSOIL, the GMP pore water pressure model is used for sand. The soil parameters are summarized in Table

3-1.

Clay



Based on Hasancebi and Ulusay (2007), the shear-wave velocity of clay with N_v value of 10 is about 180 m/s. The target normalized shear modulus curve and damping ratio curve were based on Vucetic and Dobry (1991). The fitted curves are obtained by MRD method. For effective stress analysis in DEEPSOIL, the pore water pressure model by Matasovic and Vucetic (1995) is used for clay. The soil parameters are summarized in Table 3-1.

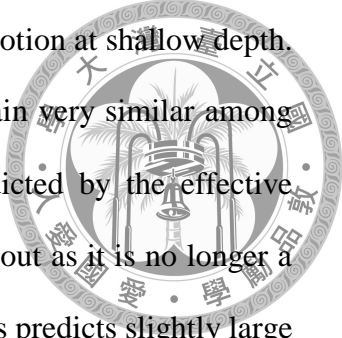
3.2.2 Input motion

There are two input motions used in these analyses, which are sinusoidal waves with amplitudes of 0.05g and 0.5g. Both input motions have frequency of 2 Hz and duration of 10 seconds.

3.2.3 Simulation results

Figure 3-6 to Figure 3-29 show the site response simulation results for simple hypothetical sites, in terms of acceleration histories and histories of excess pore pressure ratio at different depths. The following are the observations from the simulation results:

1. For site condition a (single layer of sand) with weak input motion, the amplitude of the motion increases with decreasing depth. This trend is predicted by all analysis types (frequency-domain, time domain total stress and effective stress analyses) and the predicted waveform is also very similar. For the case with



strong input motion, there is de-amplification of ground motion at shallow depth. As shown in Figure 3-7, the predicted waveforms are again very similar among most analysis types. However, the ground motion predicted by the effective stress analysis from DEEPSOIL seems to be “smoothed” out as it is no longer a sinusoidal wave. The effective stress analysis by OpenSees predicts slightly large motion at large depth (layer 15 to layer 8), and the predicted motion becomes “normal” at shallow depth. As for the modeling of excess pore water pressure ratio, OpenSees predicts large excess water pressure for both weak and strong input motions. Predictions from OpenSees is much larger than DEEPSOIL for the weak input motion case but similar to DEEPSOIL for the strong input motion case. It is also observed that the excess water pressure ratio in DEEPSOIL decreases with decreasing depth, which is not observed in the simulations from OpenSees.

2. For site condition b with single-layer of clay, the results are shown in Figure 3-10 to Figure 3-13. The predicted trend of ground motion (acceleration histories) with depth is generally similar to that for single-layer of sand. All the analysis types give nearly the same trend. As for the excess water pore pressure prediction, effective stress analyses from both DEEPSOIL and OpenSees give smaller excess pore pressure prediction for the clay case than that for the sand case (case a). In addition, the trend of the predicted excess pore water pressure is also quite different for DEEPSOIL and OpenSees.
3. The results for the two-layer cases (sand underlain by clay for case c and clay underlain by sand for case d) are shown in Figure 3-14 to Figure 3-21. The trends of the acceleration histories predicted by different analysis types tend to be

similar when weak input motion is used. For large input motion, the acceleration history predicted from effective stress analysis of DEEPSOIL is “smoothed” and the predicted motions from all analyses seem to have some fluctuations (noise). For the pore water pressure response, the predicted excess pore water pressure is always larger in sand layer than in clay layer. For clay layer, the pore pressure predictions from OpenSees have some unusual vibration although the amplitudes were small. For the strong input motion case, the predicted excess pore water pressure in sand layer was similar in OpenSees and DEEPSOIL (trend and amplitude).

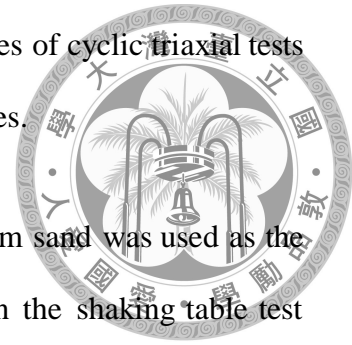
4. The results for the three-layer cases (sand-clay-sand layer system for case e and clay-sand-clay system for case f) are shown in Figure 3-22 to Figure 3-29. The predicted acceleration histories from different analysis types are generally similar when small input motion is used. However, as in the two-layer cases, the results from effective stress analysis of DEEPSOIL also have the “smoothed” phenomenon for the strong input motion case. In addition, for clay layers, the pore pressure predictions from OpenSees have some unusual vibration although the amplitudes are small. The pore pressure predictions are larger in sand layers than in the clay layers for all analysis types and input motions.

3.3 Numerical modeling of cyclic triaxial test

3.3.1 Soil properties and analysis model

In order to test the effective stress dynamic analysis model from OpenSees at an element level and to calibrate the soil parameters for use in the simulation of shaking

table test (which will be presented in next sub-section), a series of cyclic triaxial tests by Jiang (2000, written in Chinese) are modeled using Opensees.



For the cyclic triaxial tests performed by Jiang (2000), Vietnam sand was used as the tested material, which was the same as the materials used in the shaking table test (presented in the next sub-section). The cyclic triaxial test was performed using confining pressure of 196 kPa. Moreover, the relative density of the Vietnam sand was about 39%. The properties of Vietnam sand and the parameters of experiment in cyclic triaxial test are shown in Table 3-3. The cyclic deviator stress of this experiment is a sine wave with frequency of 20 Hz and the amplitude of 35.28 kPa.

3.3.2 Simulation results

Figure 3-38 shows the as-recorded deviator stress and axial strain of the cyclic triaxial experiment, while Figure 3-39 shows the simulation results of OpenSees. The simulation results are in general similar to the experimental data. However, there is a slight asymmetry of strain according to the simulation result. Figure 3-40 is the pore water pressure response predicted by OpenSees. It suggests that the pore water pressure keeps increasing as the number of cycle increases.

3.4 Numerical modeling of shaking table tests

3.4.1 Site condition and analysis model

Shaking table tests (Ueng et al. 2003 and 2006, both written in Chinese) were simulated using frequency-domain analyses, total-stress and effective-stress time-domain analyses from DEEPSOIL and OpenSees. .

Soil properties

The soil used in the shaking table tests was Vietnam sand. The soil properties are summarized in Table 3-2. The normalized shear modulus curve and damping ratio curve used in the simulation are based on Wang (2004, written in Chinese), whose experimental data were obtained by resonant column tests. These data are shown in Figure 3-30 and Figure 3-31, and the curve we decided to use in the analysis are shown in Figure 3-32 and Figure 3-33. The pore water pressure model used in DEEPSOIL was based on the GMP model.



Input motion

The input motions for the shaking table tests considered in this study have amplitudes of 0.03g and 0.1g. They are sinusoidal waves with frequency of 2 Hz and duration of 10 seconds.

3.4.2 Simulation results

The simulation results of shaking table test are shown in Figure 3-34 to Figure 3-37. As shown in Figure 3-34 (weak input motion case), the predicted acceleration histories are the same for all analysis types in general and are consistent with the measured data from the shaking table test. The predicted pore water pressure ratio is also in the vicinity of the recorded data. On the other hand, for the strong input motion case (Figure 3-35), different analysis types generally give similar predicted acceleration histories. According to Ueng et al. (2003 and 2006), liquefaction did actually occur for this case because the recorded acceleration data are different for accelerometers installed within the soil and on the frame. The pore pressure simulations from OpenSees seem to match pretty well with the recorded data, although the simulations

from DEEPSOIL underpredict the pore pressure significantly.



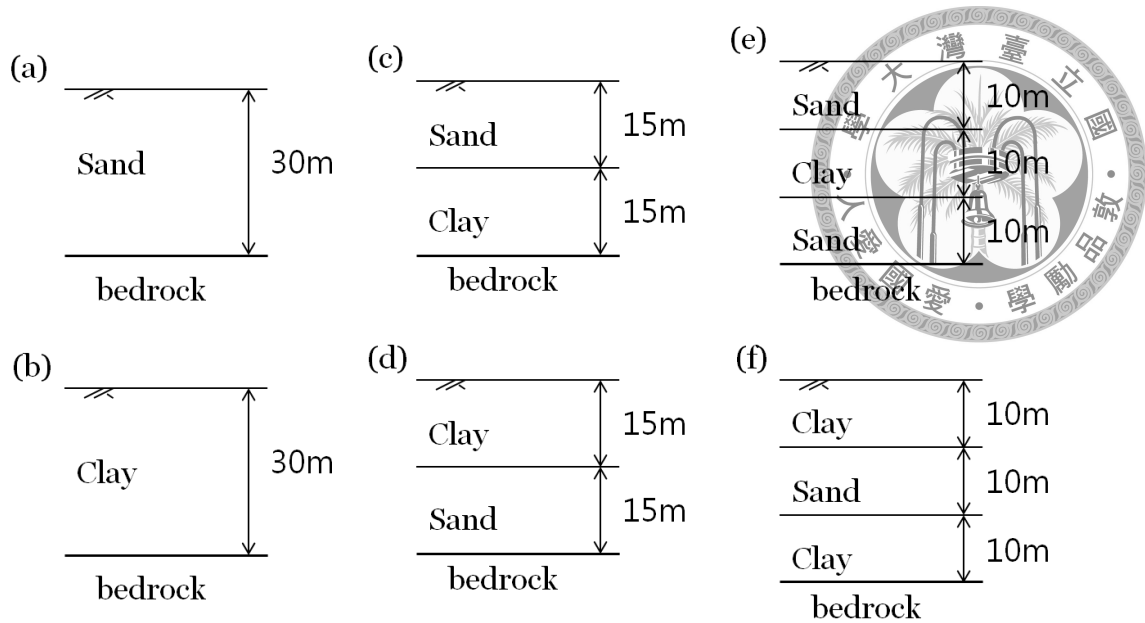


Figure 3-1 Six simple hypothetical sites.

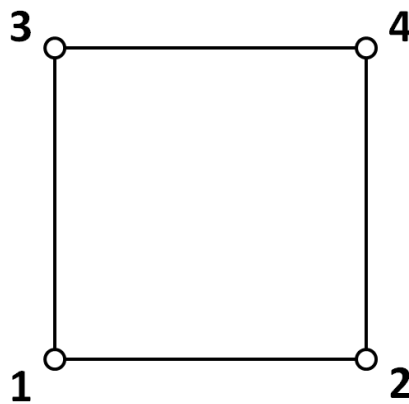


Figure 3-2 Four-node element in Opensees, DOF = 2.

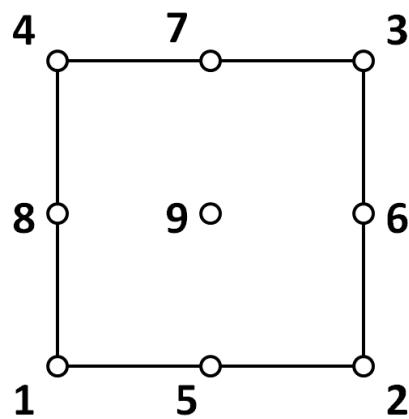


Figure 3-3 Nine-node element in Opensees, node 1, 2, 3, 4 are DOF = 3, node 5, 6, 7, 8, 9 are DOF = 2.

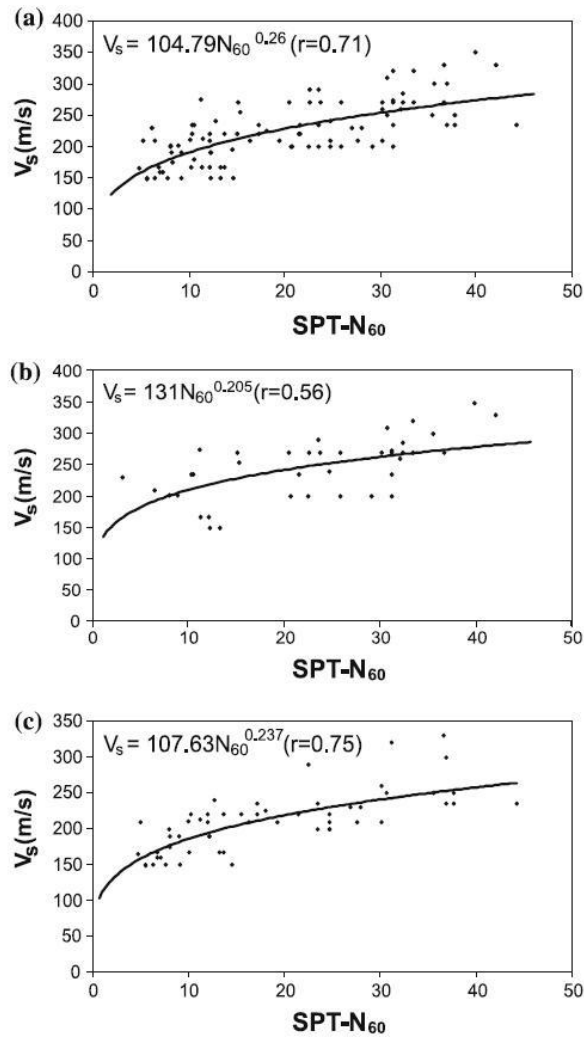


Figure 3-4 V_s versus $SPT-N_{60}$ for (a) all Soils, (b) sands, and (c) clays (Hasancebi and Ulusay 2007).

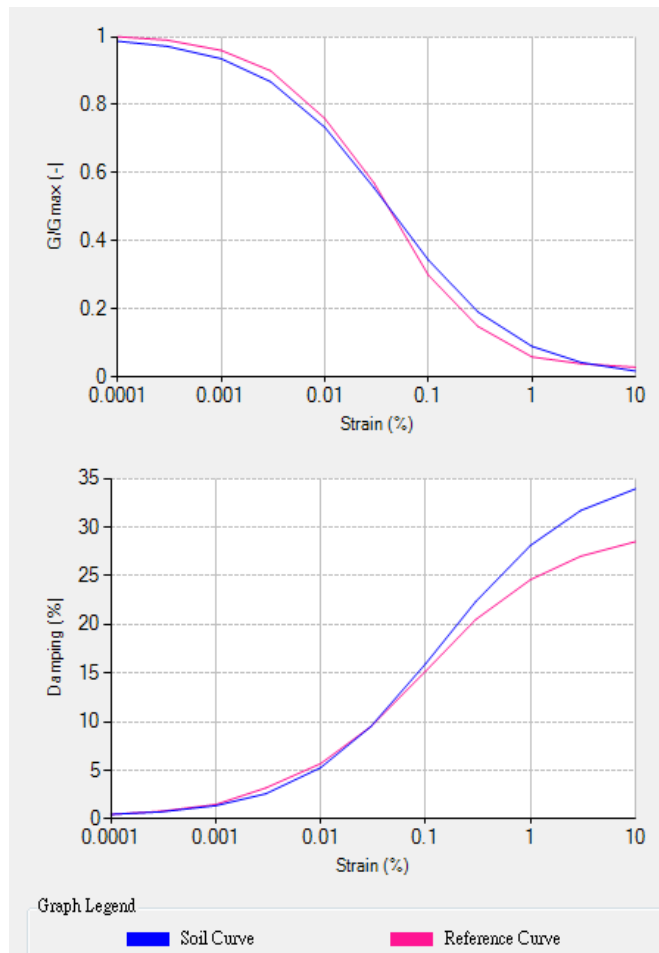


Figure 3-5 Normalized shear modulus curve and damping ratio curve for sand layer (Red curves: target values from Seed and Idriss; Blue curves: fitted curves that are actually used in analyses).

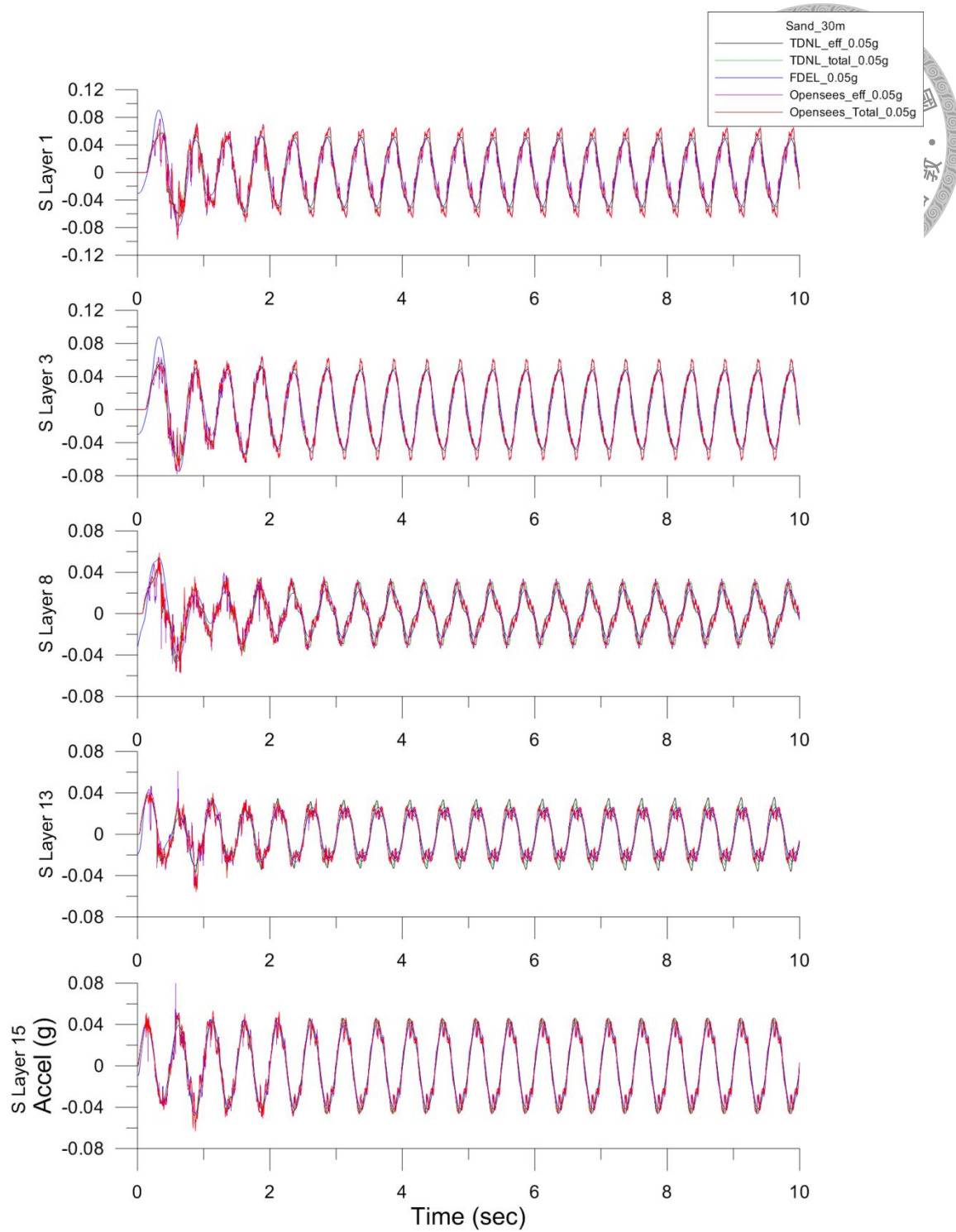


Figure 3-6 Acceleration history of case (a) with weak input motion.

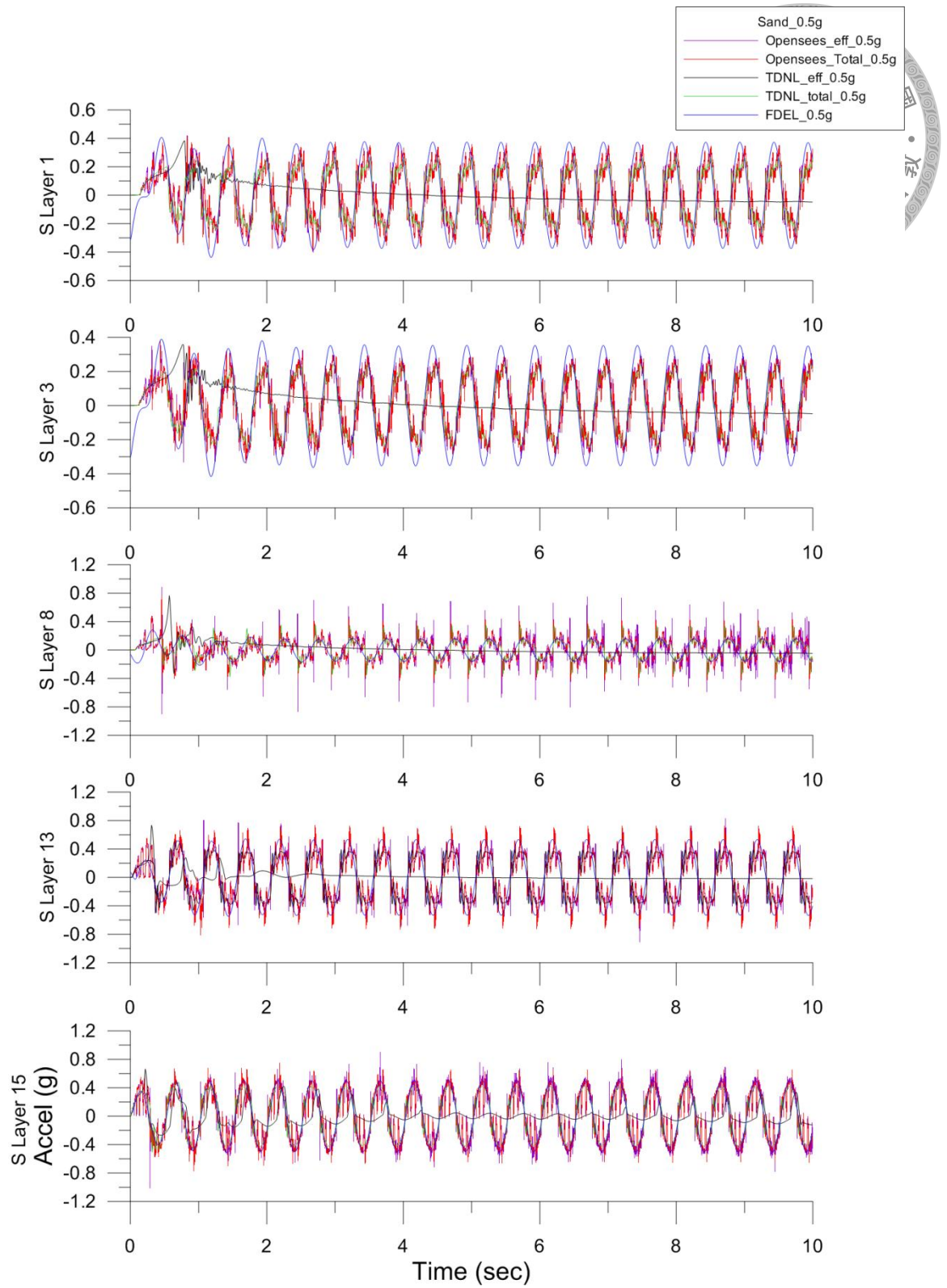


Figure 3-7 Acceleration history of case (a) with strong input motion.

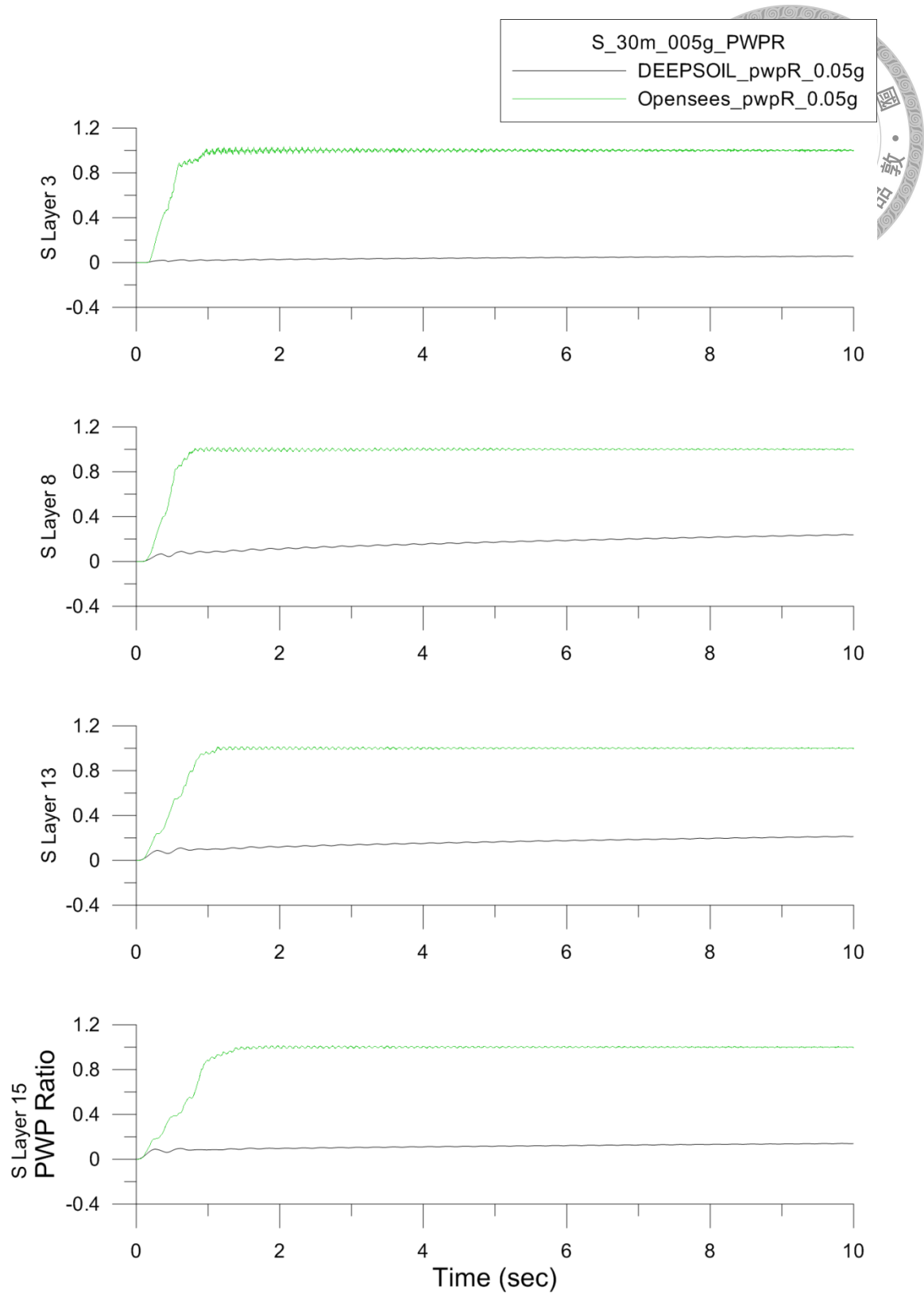


Figure 3-8 Pore water pressure ratio of case (a) with weak input motion.

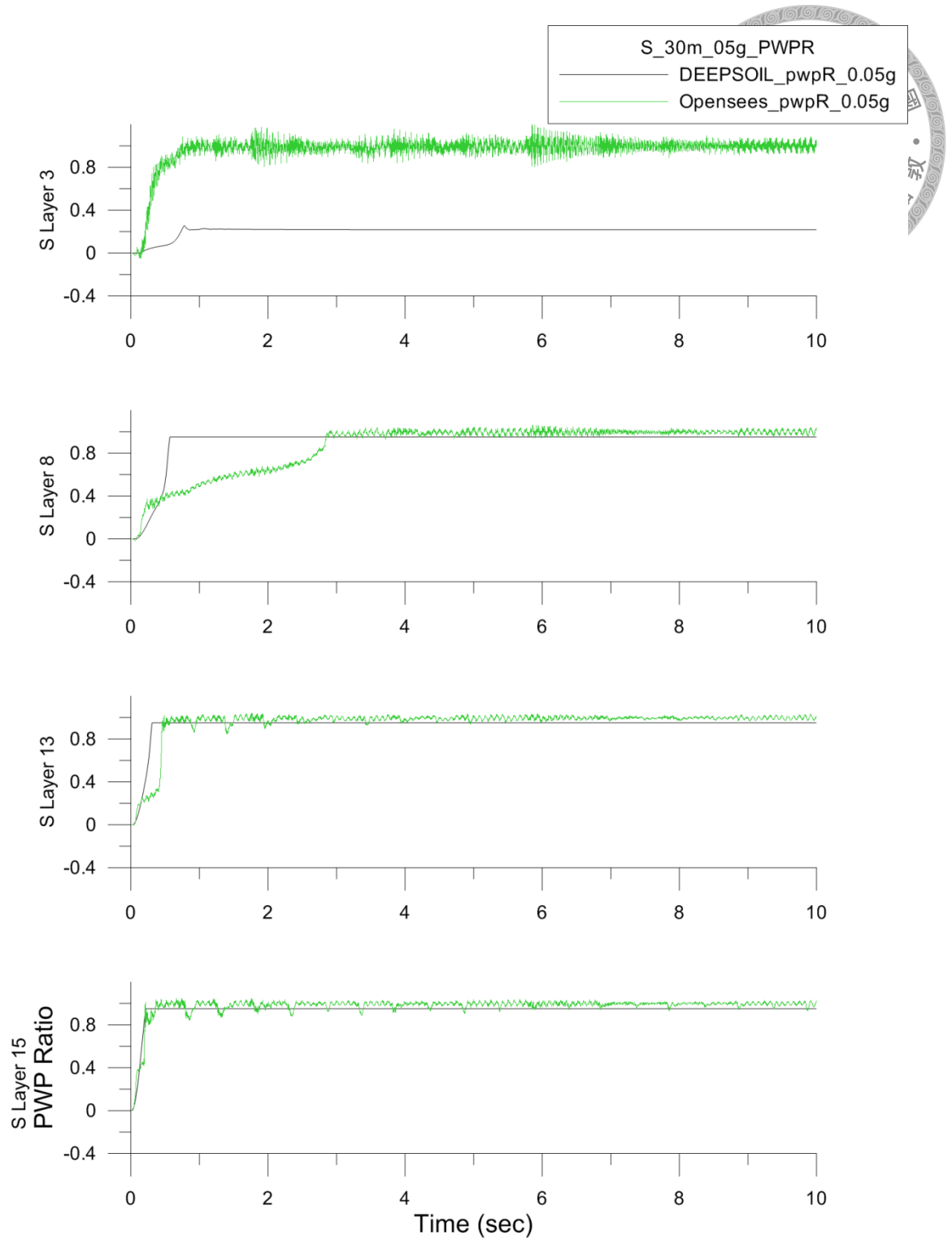


Figure 3-9 Pore water pressure ratio of case (a) with strong input motion.

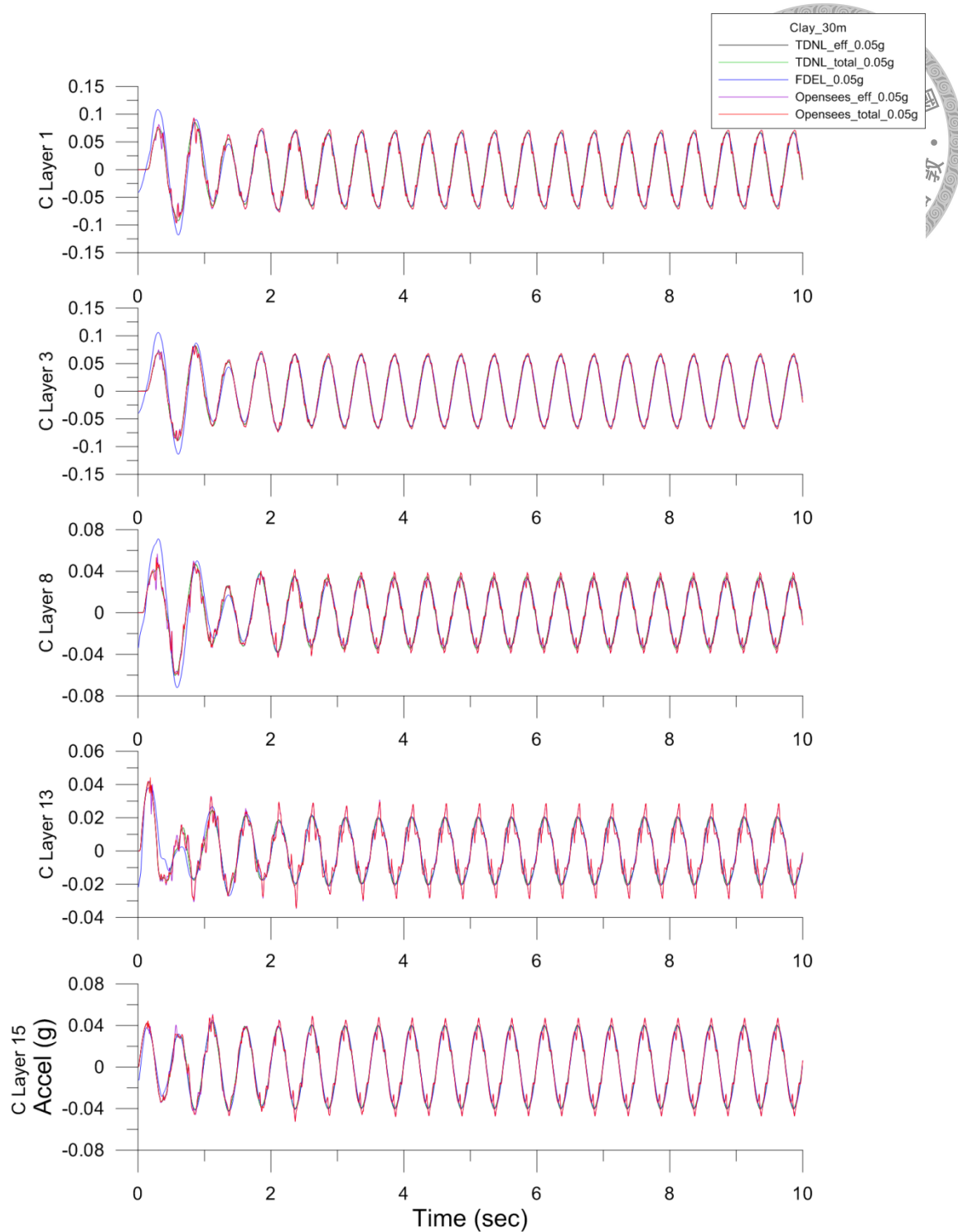


Figure 3-10 Acceleration history of case (b) with weak input motion.

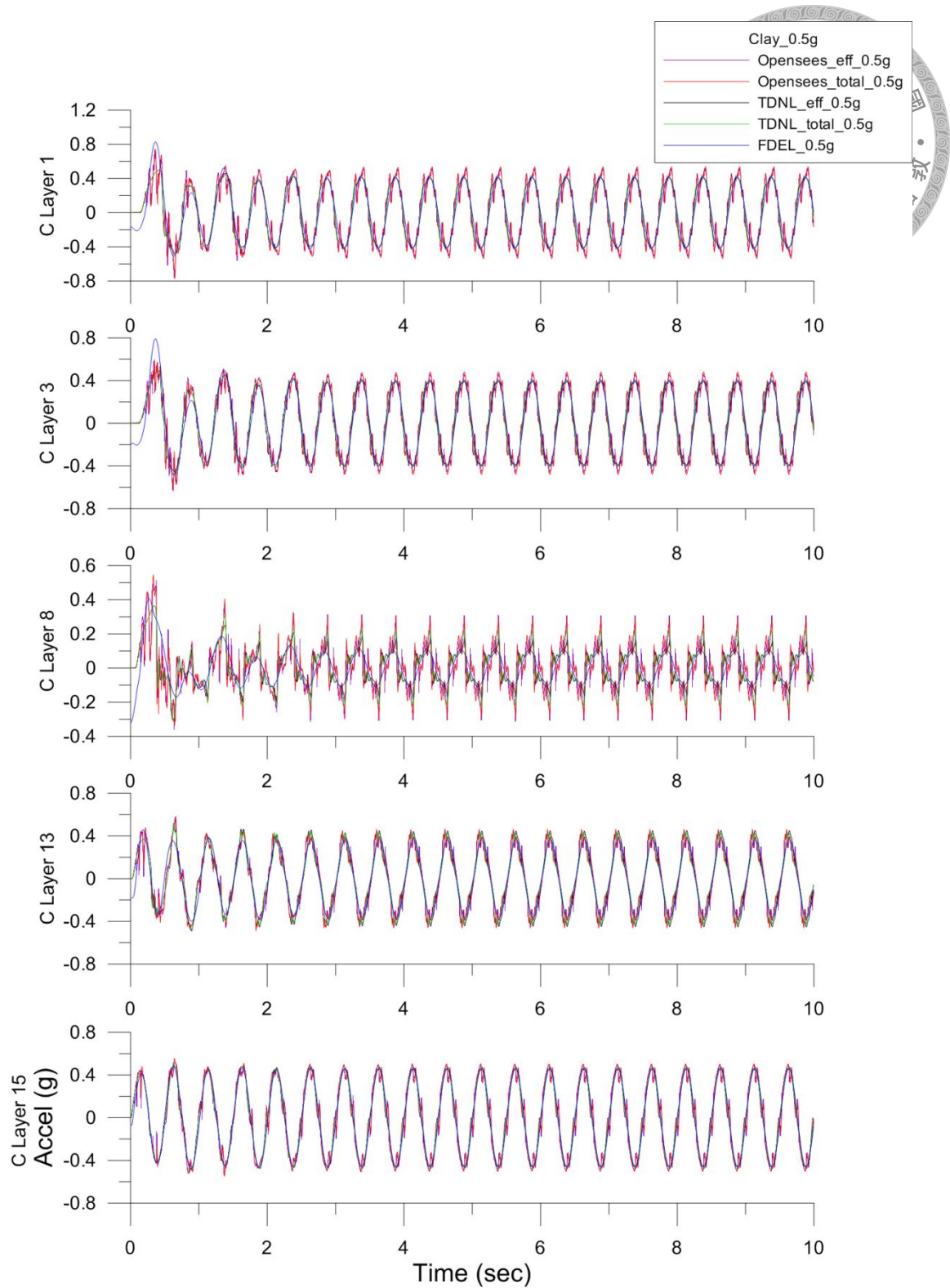


Figure 3-11 Acceleration history of case (b) with strong input motion.

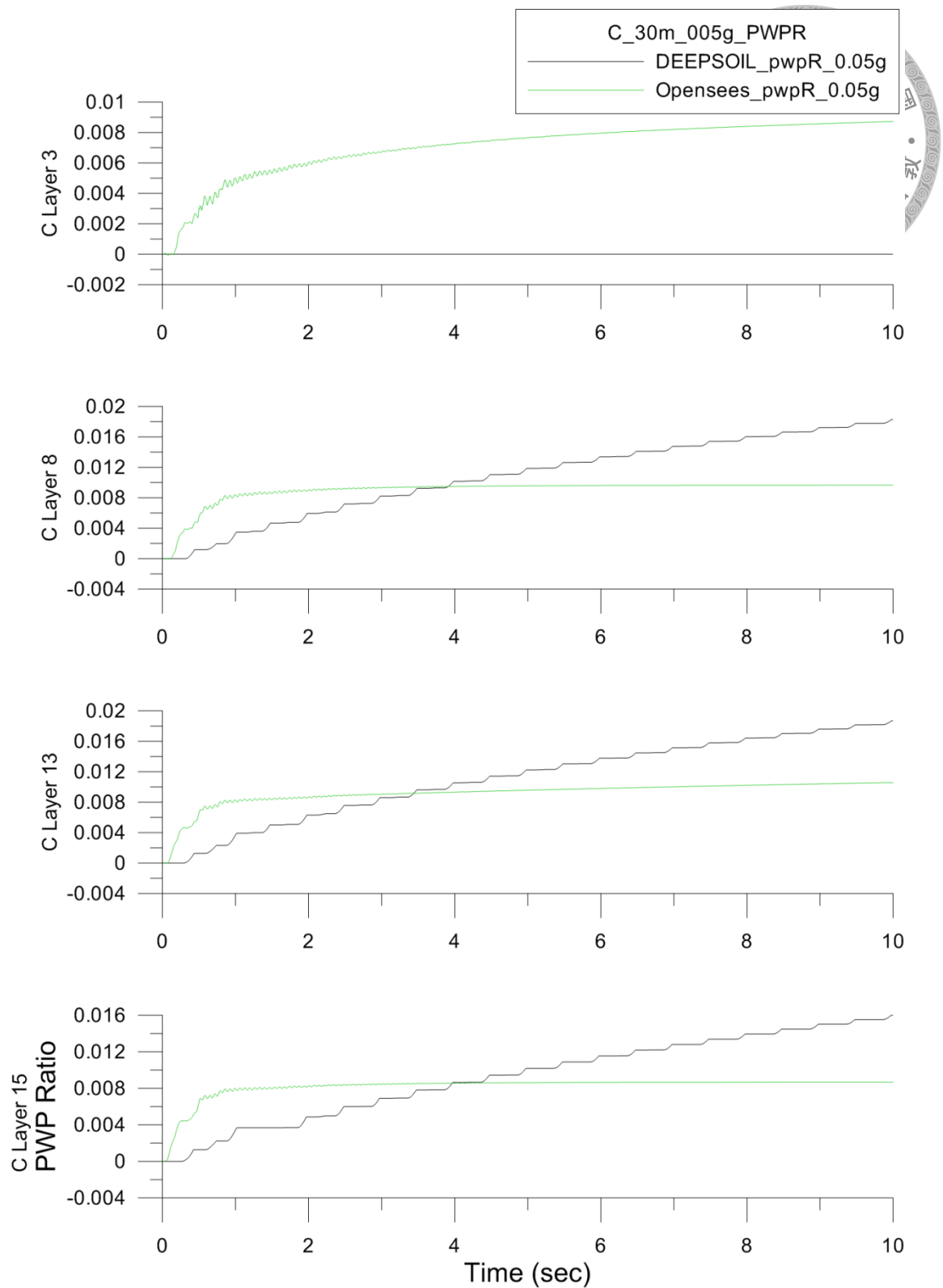


Figure 3-12 Pore water pressure ratio of case (b) with weak input motion.

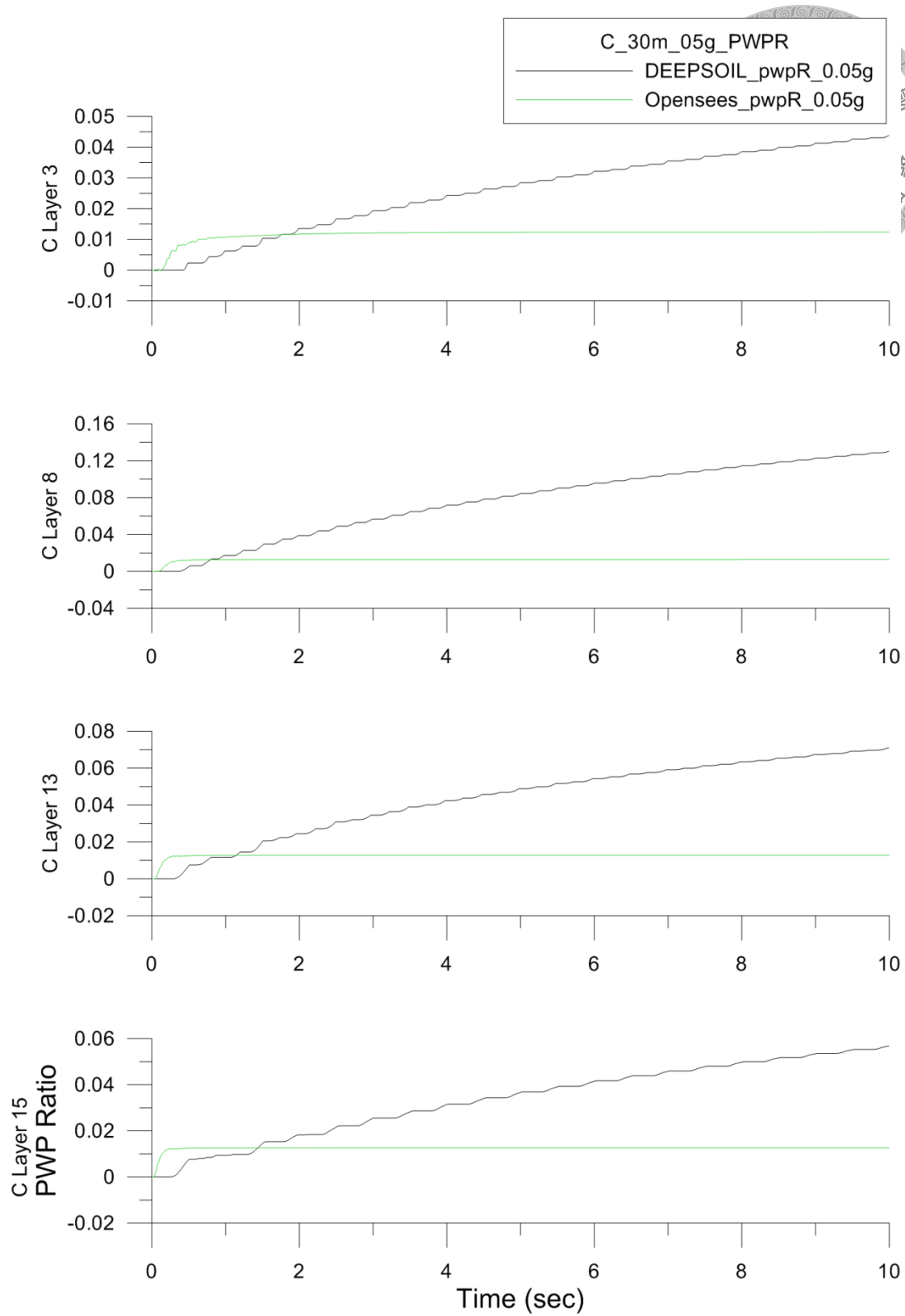


Figure 3-13 Pore water pressure ratio of case (b) with strong input motion.

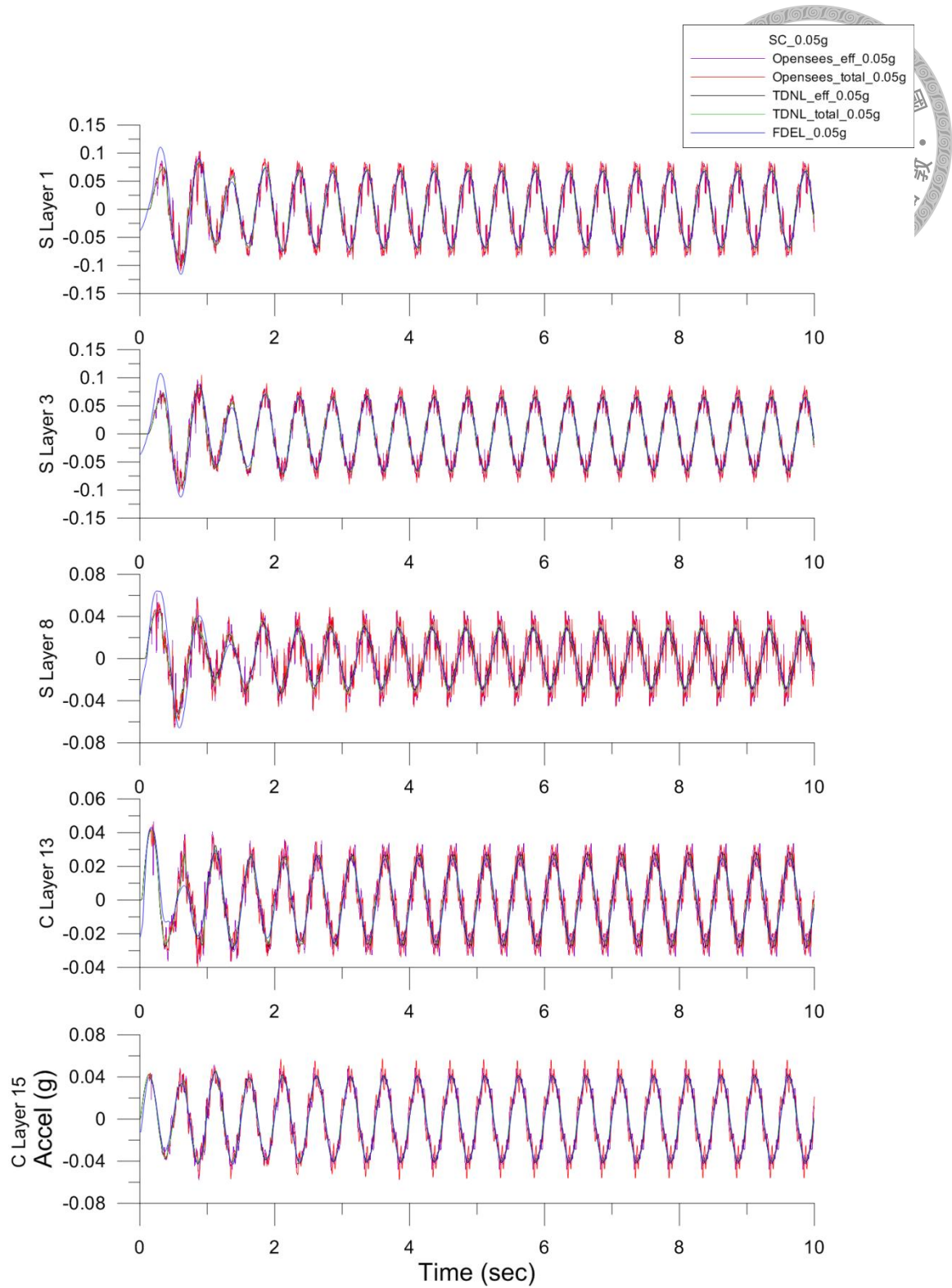


Figure 3-14 Acceleration history of case (c) with weak input motion.

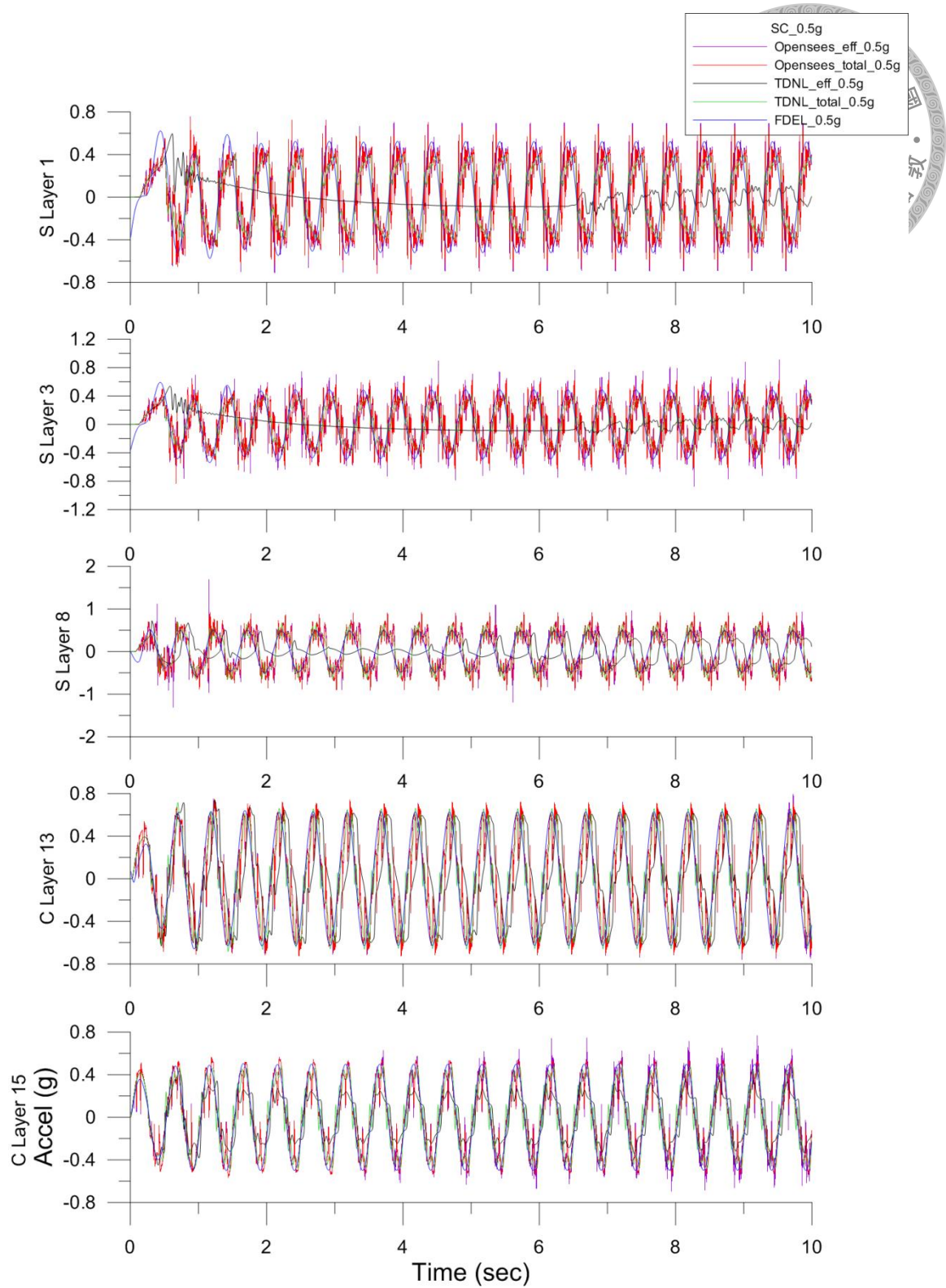


Figure 3-15 Acceleration history of case (c) with strong input motion.

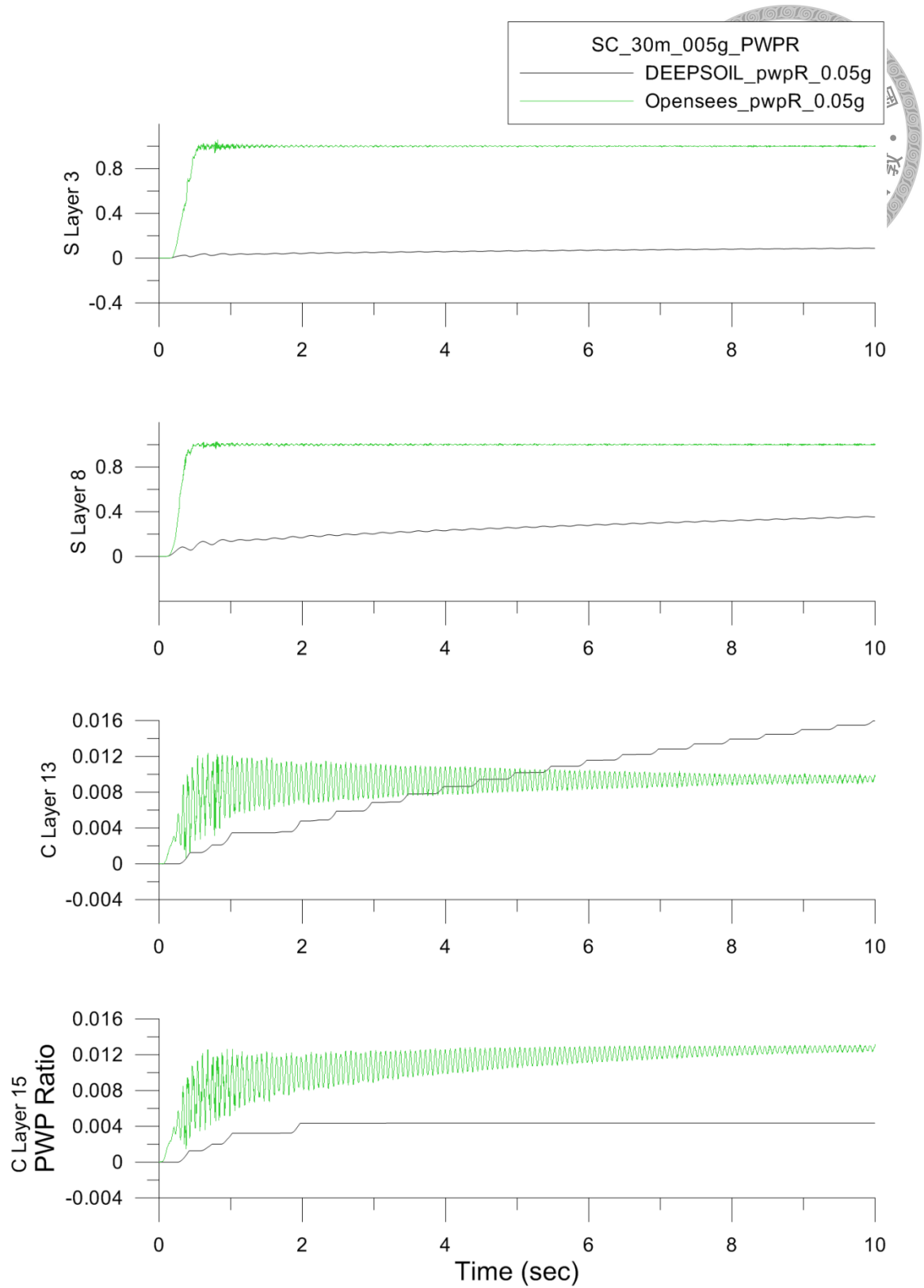


Figure 3-16 Pore water pressure ratio of case (c) with weak input motion.

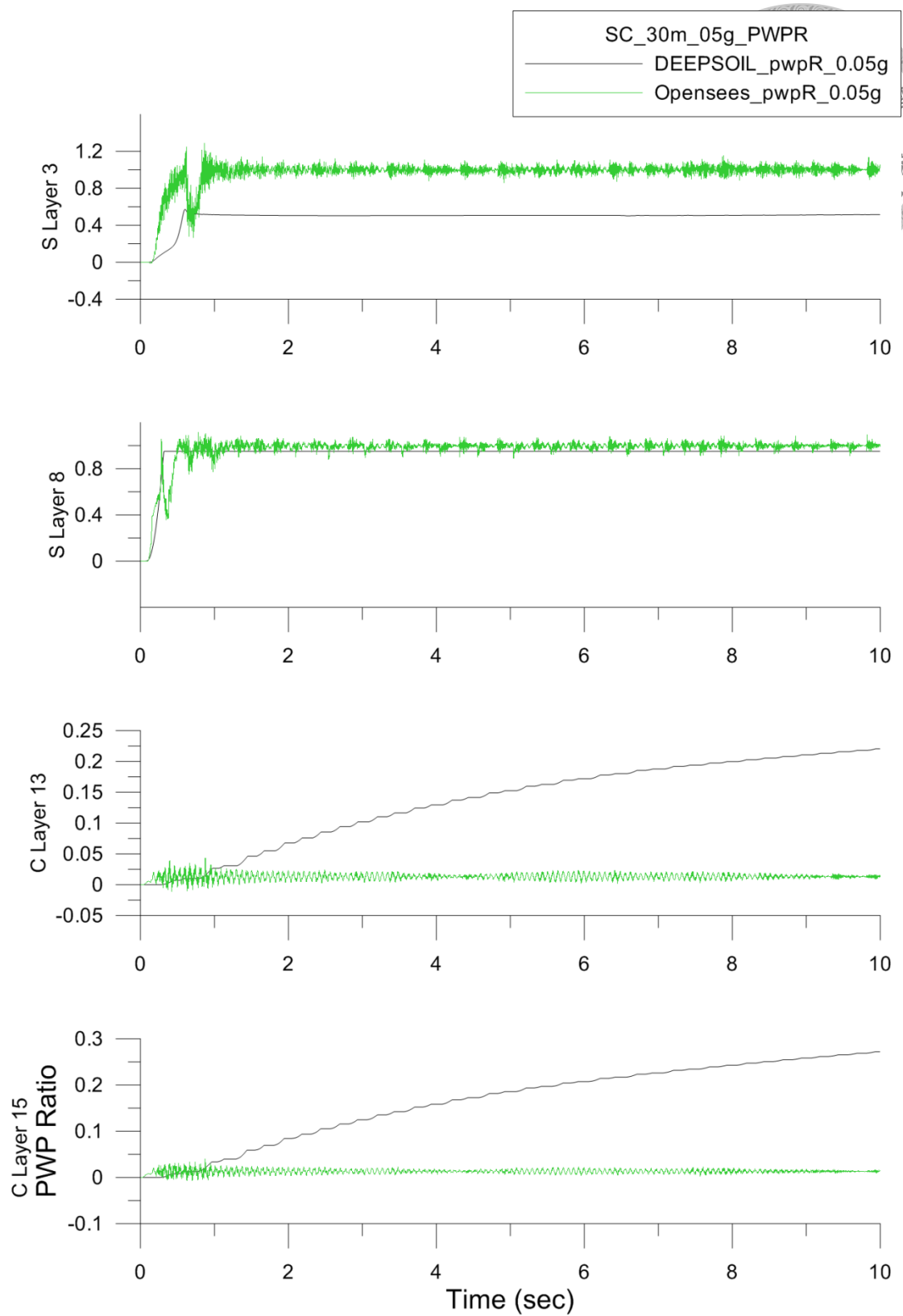


Figure 3-17 Pore water pressure ratio of case (c) with strong input motion.

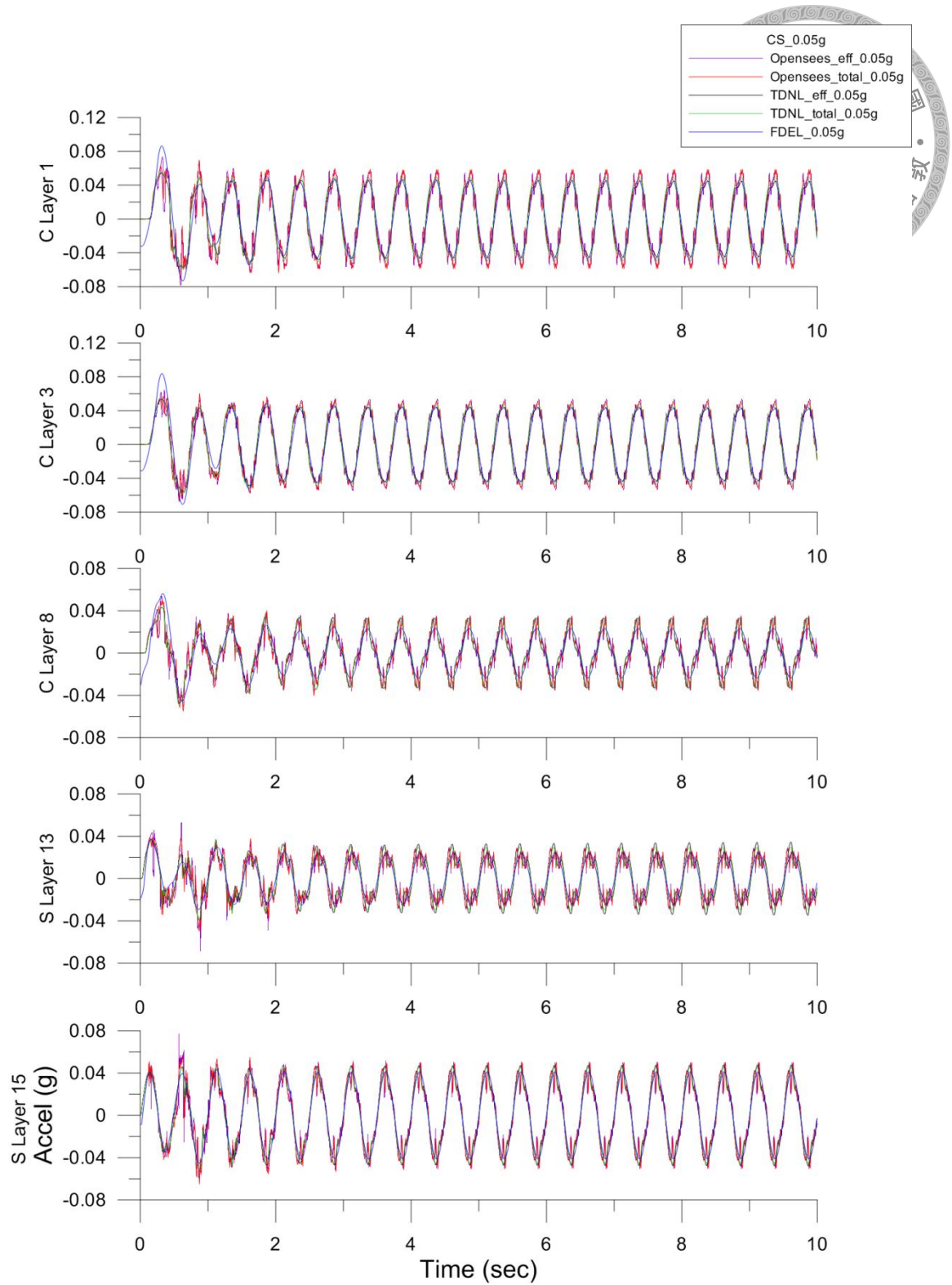


Figure 3-18 Acceleration history of case (d) with weak input motion.

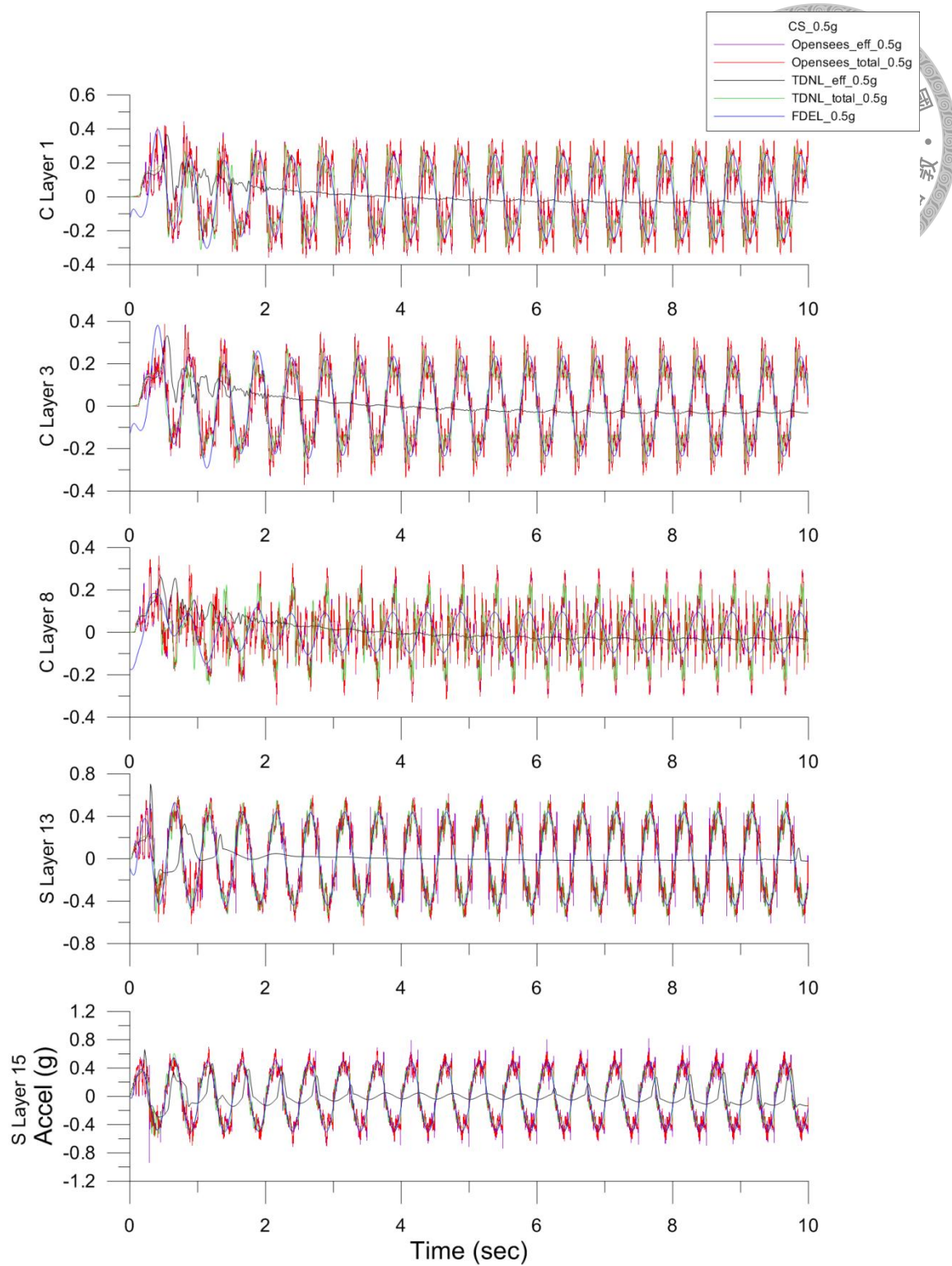


Figure 3-19 Acceleration history of case (d) with strong input motion.

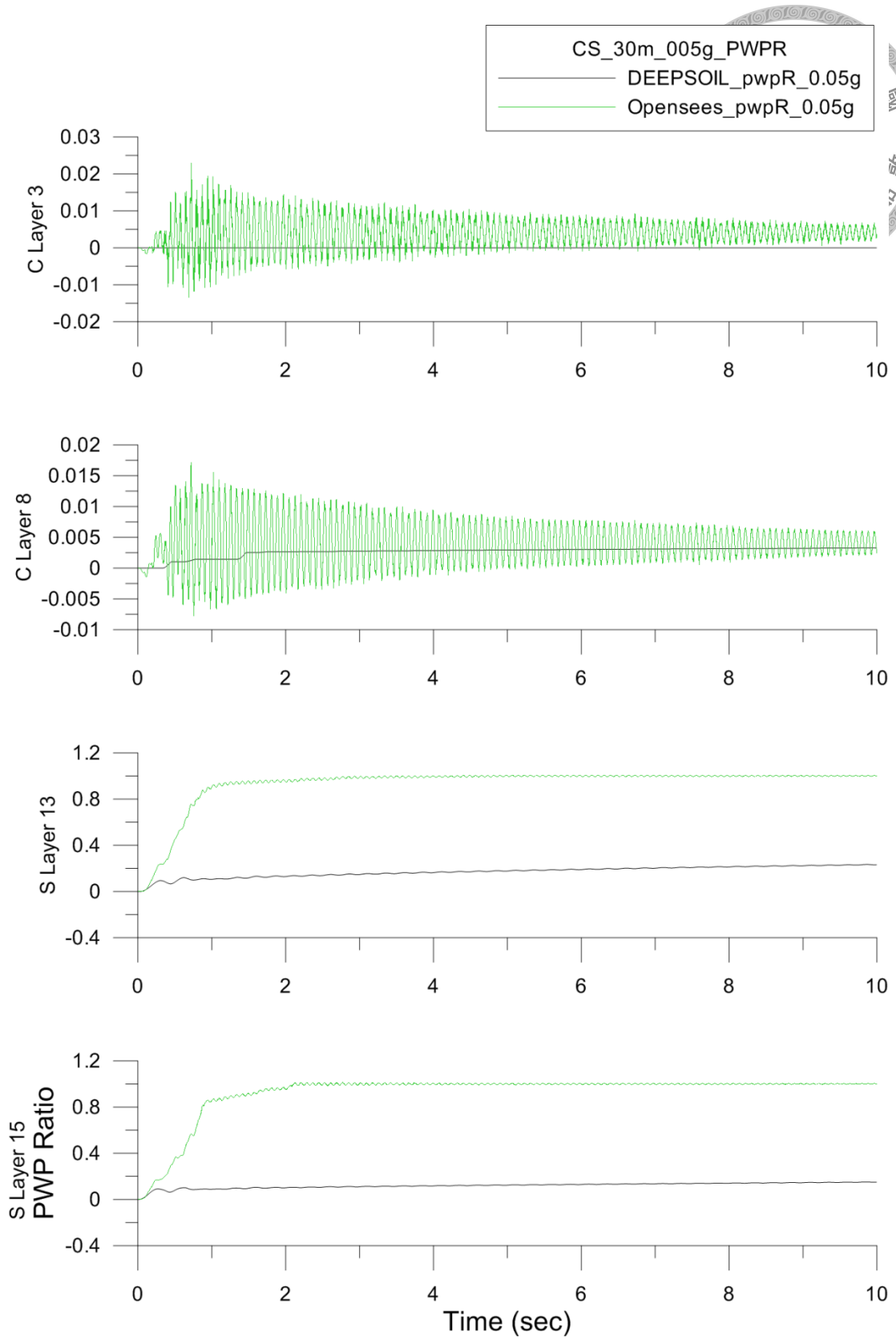


Figure 3-20 Pore water pressure ratio of case (d) with weak input motion.

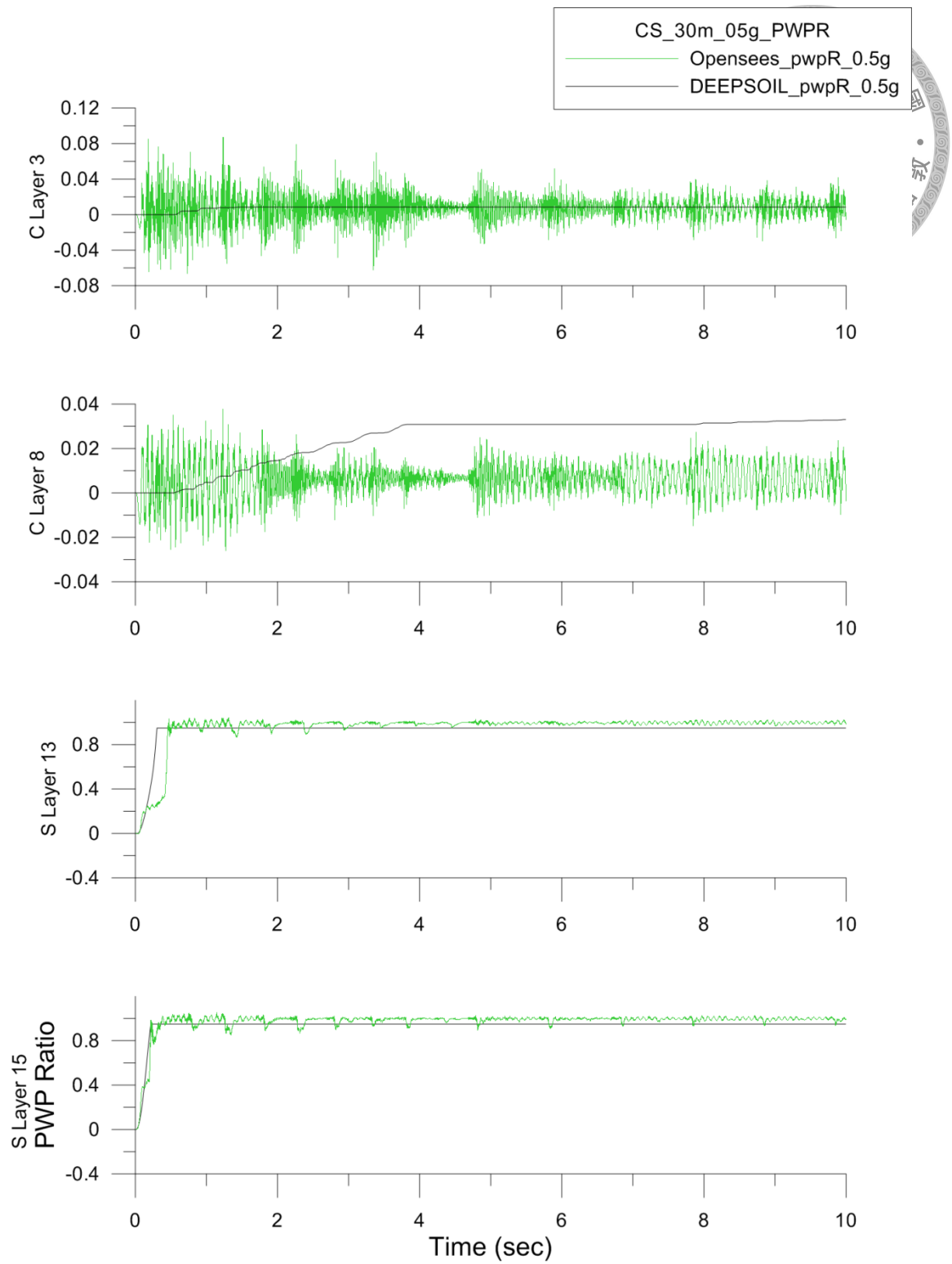


Figure 3-21 Pore water pressure ratio of case (d) with strong input motion.

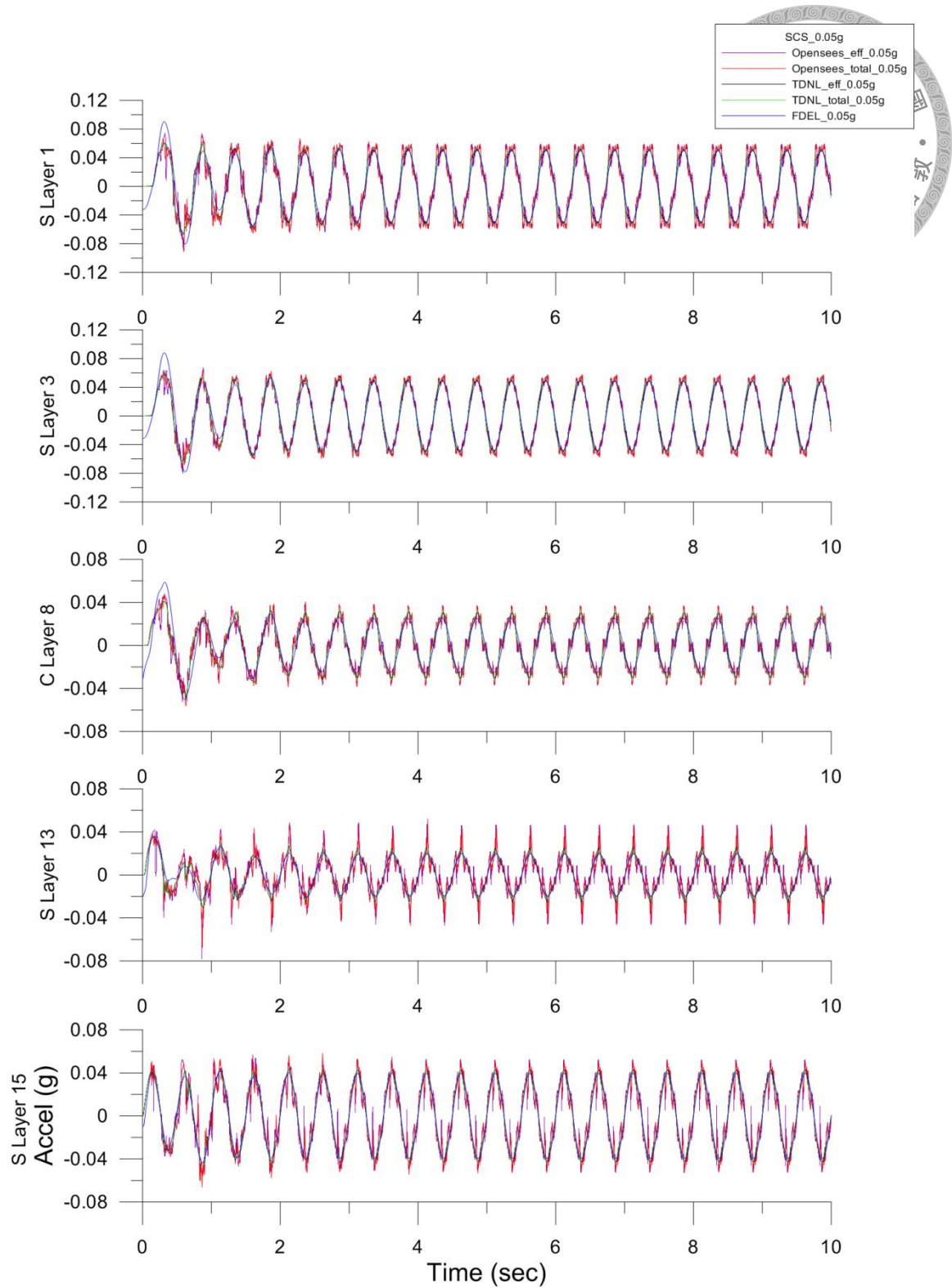


Figure 3-22 Acceleration history of case (e) with weak input motion.

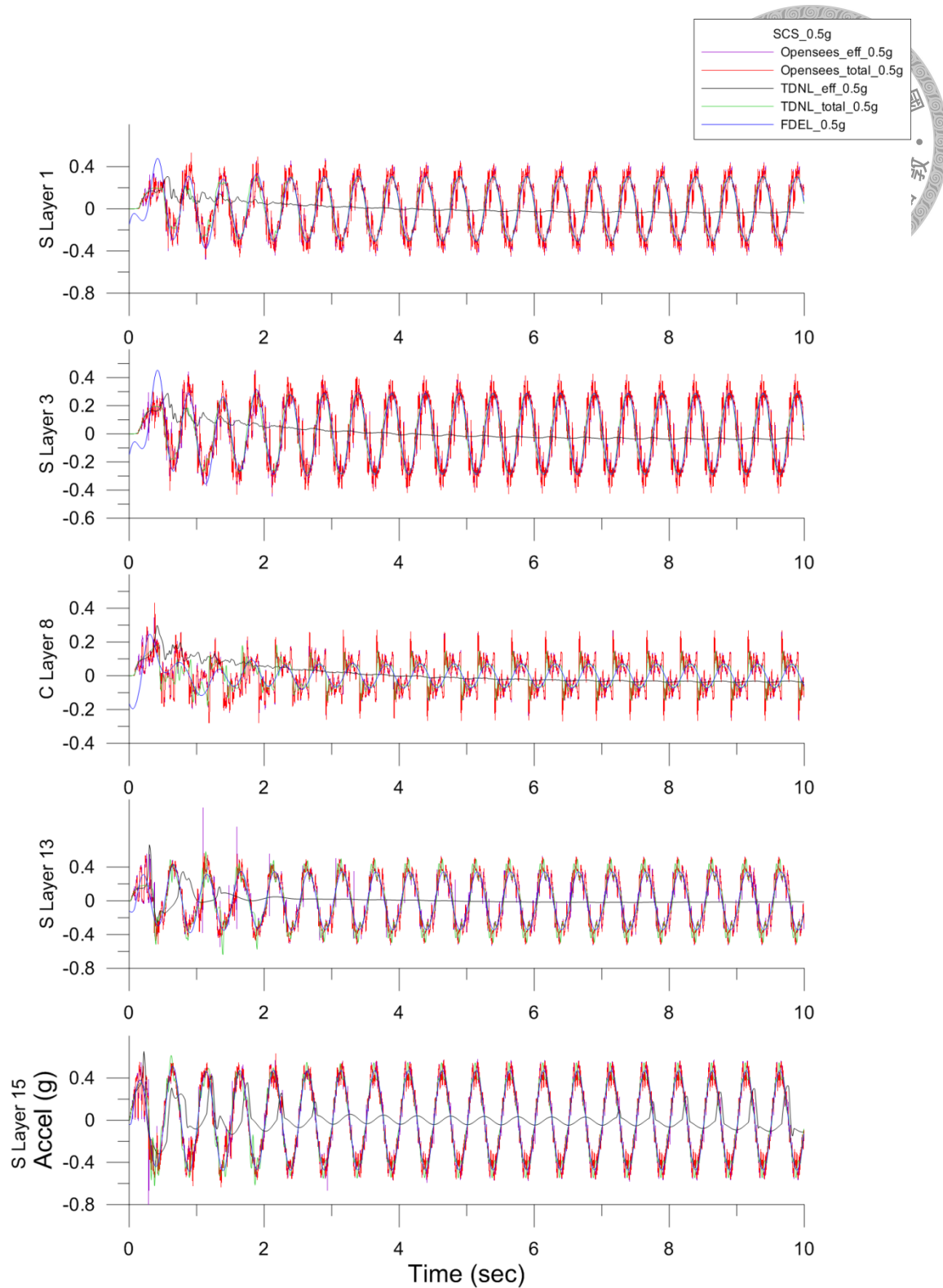


Figure 3-23 Acceleration history of case (e) with strong input motion.

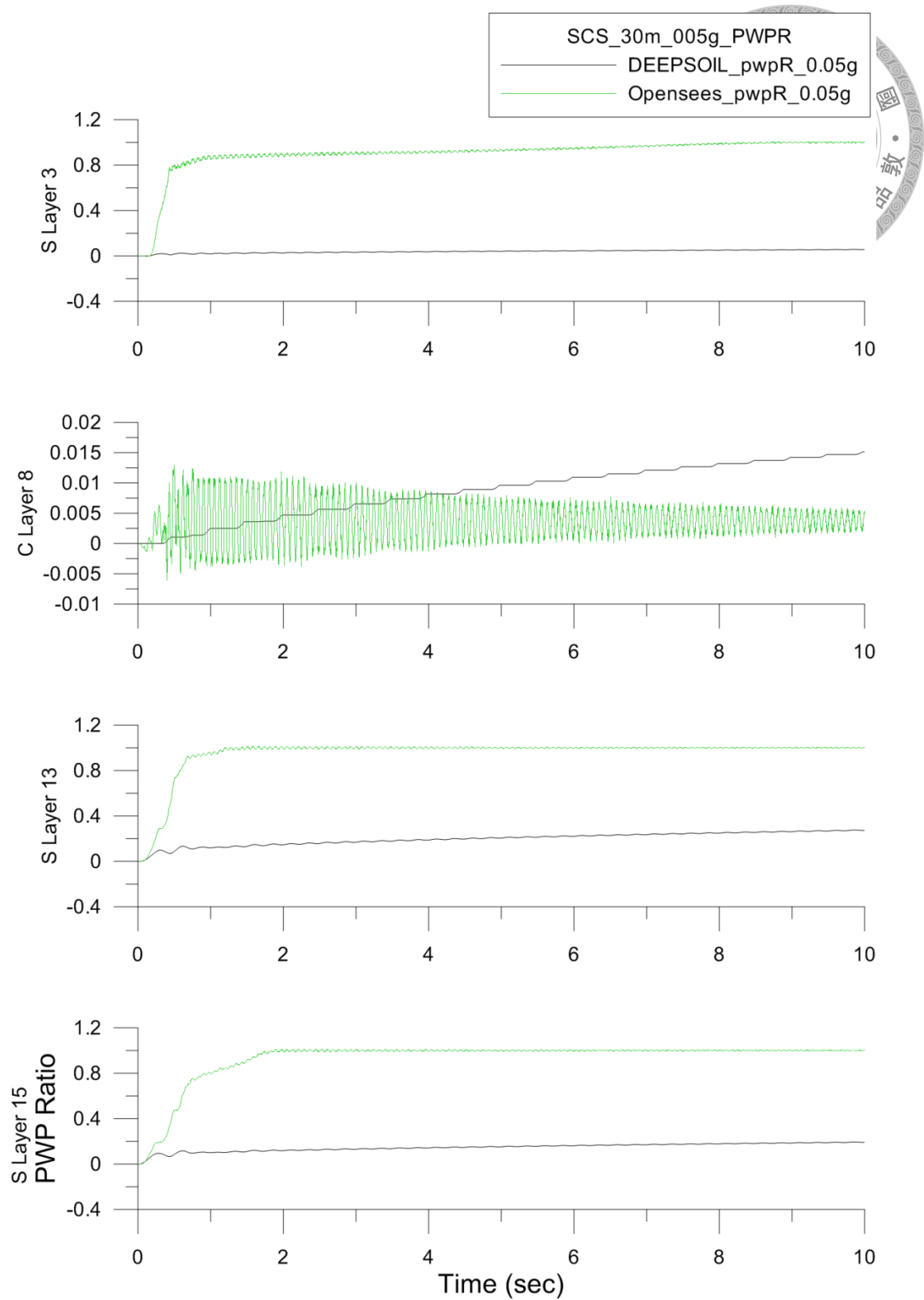


Figure 3-24 Pore water pressure ratio of case (e) with weak input motion.

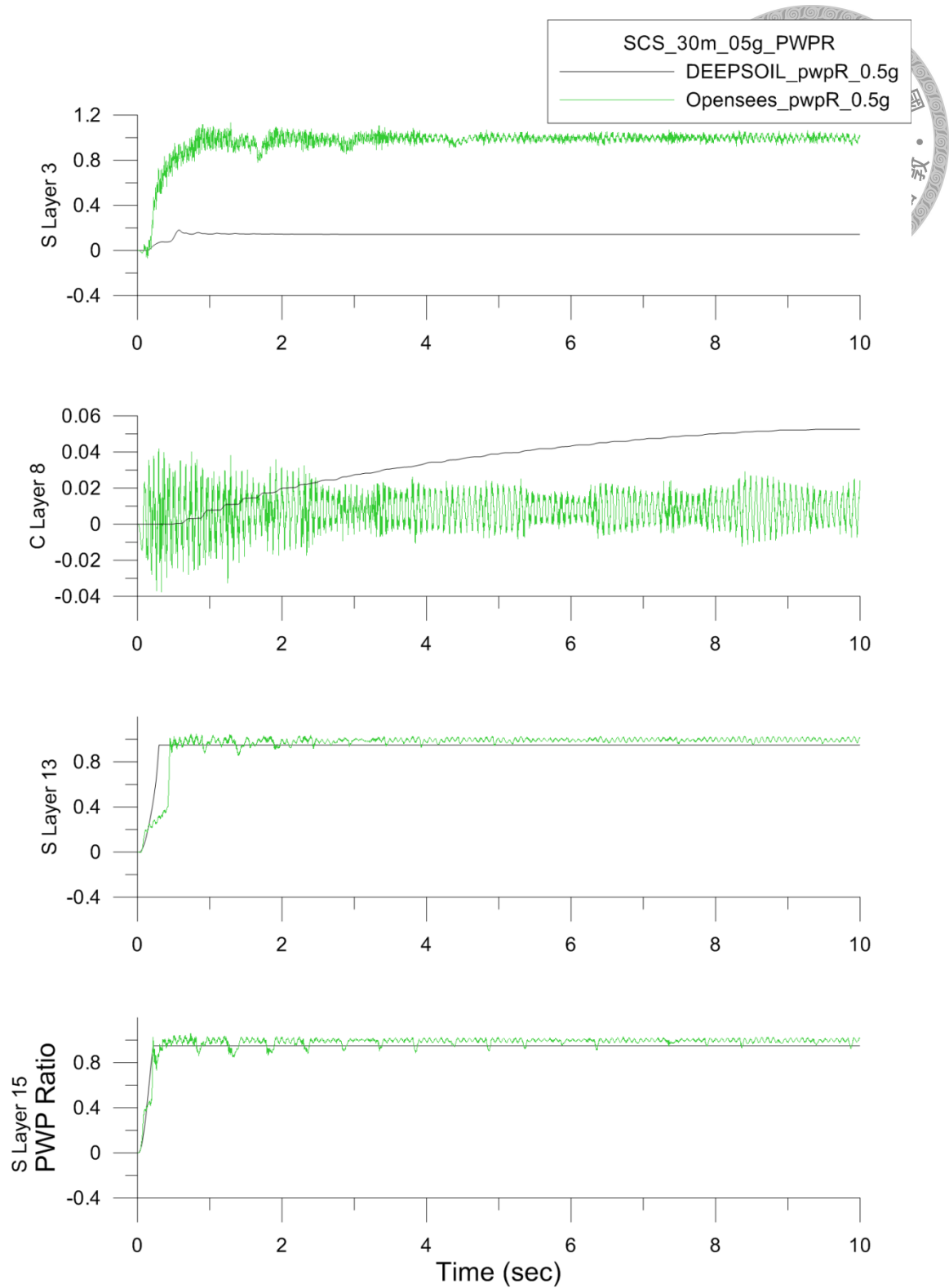


Figure 3-25 Pore water pressure ratio of case (e) with strong input motion.

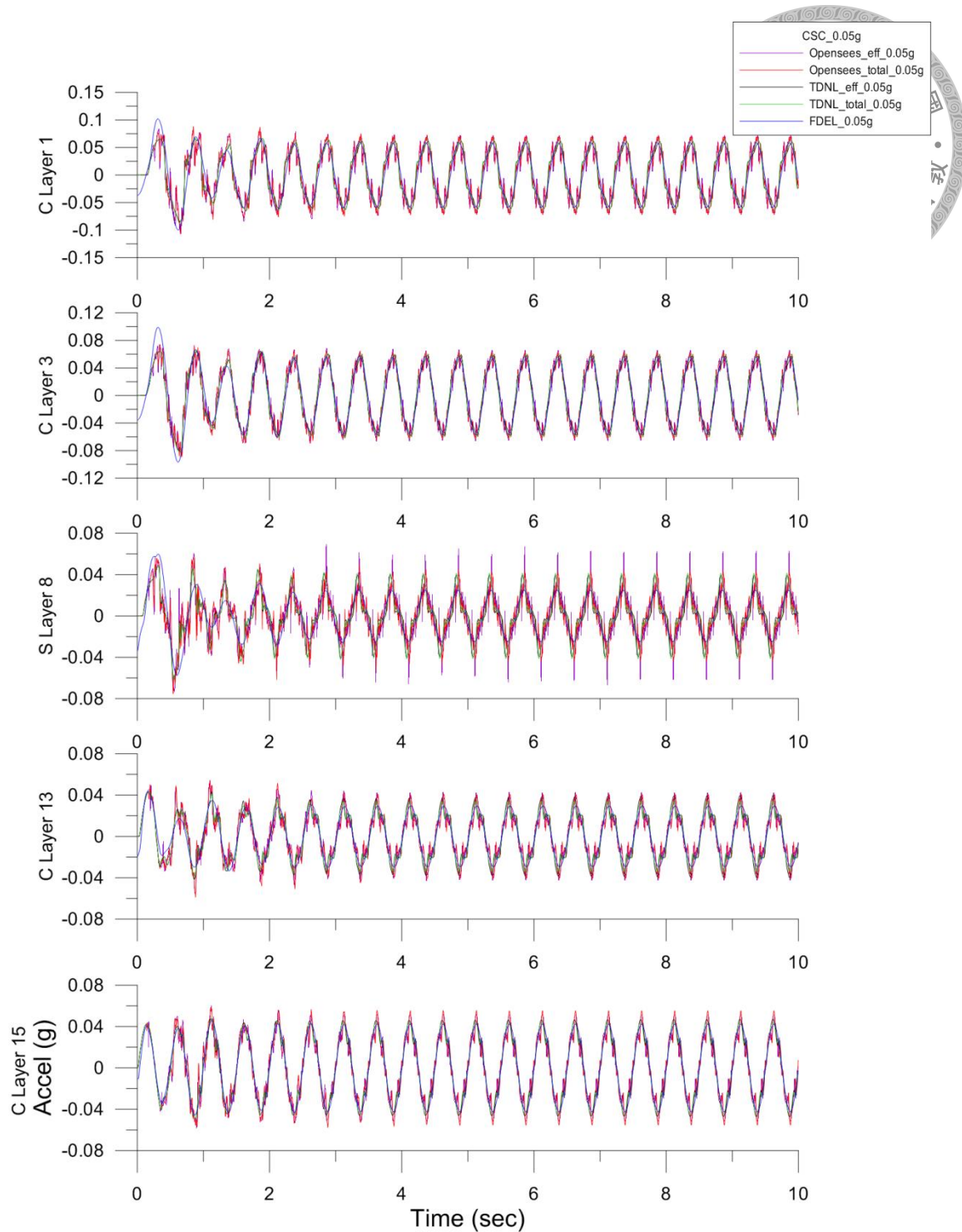


Figure 3-26 Acceleration history of case (f) with weak input motion.

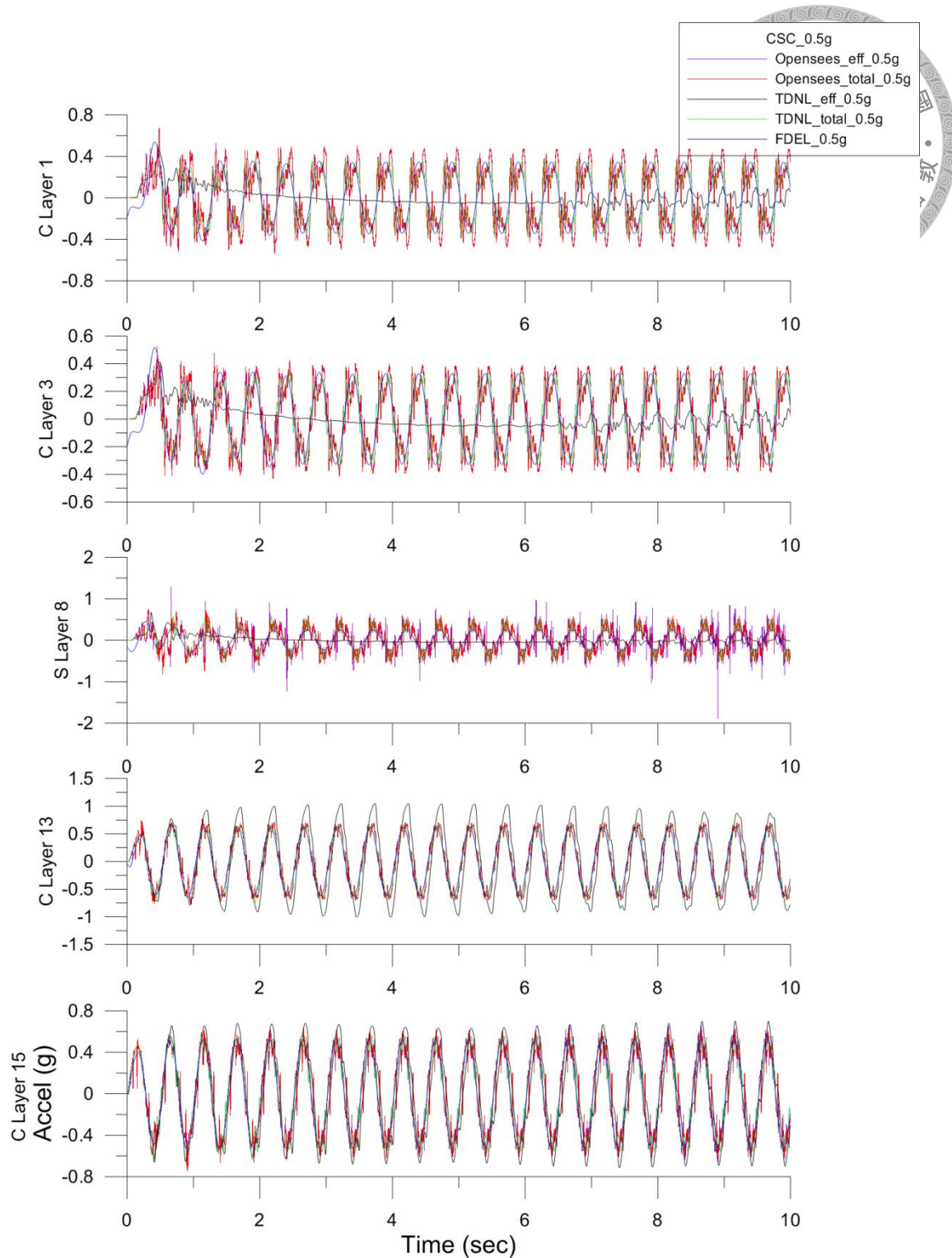


Figure 3-27 Acceleration history of case (f) with strong input motion.

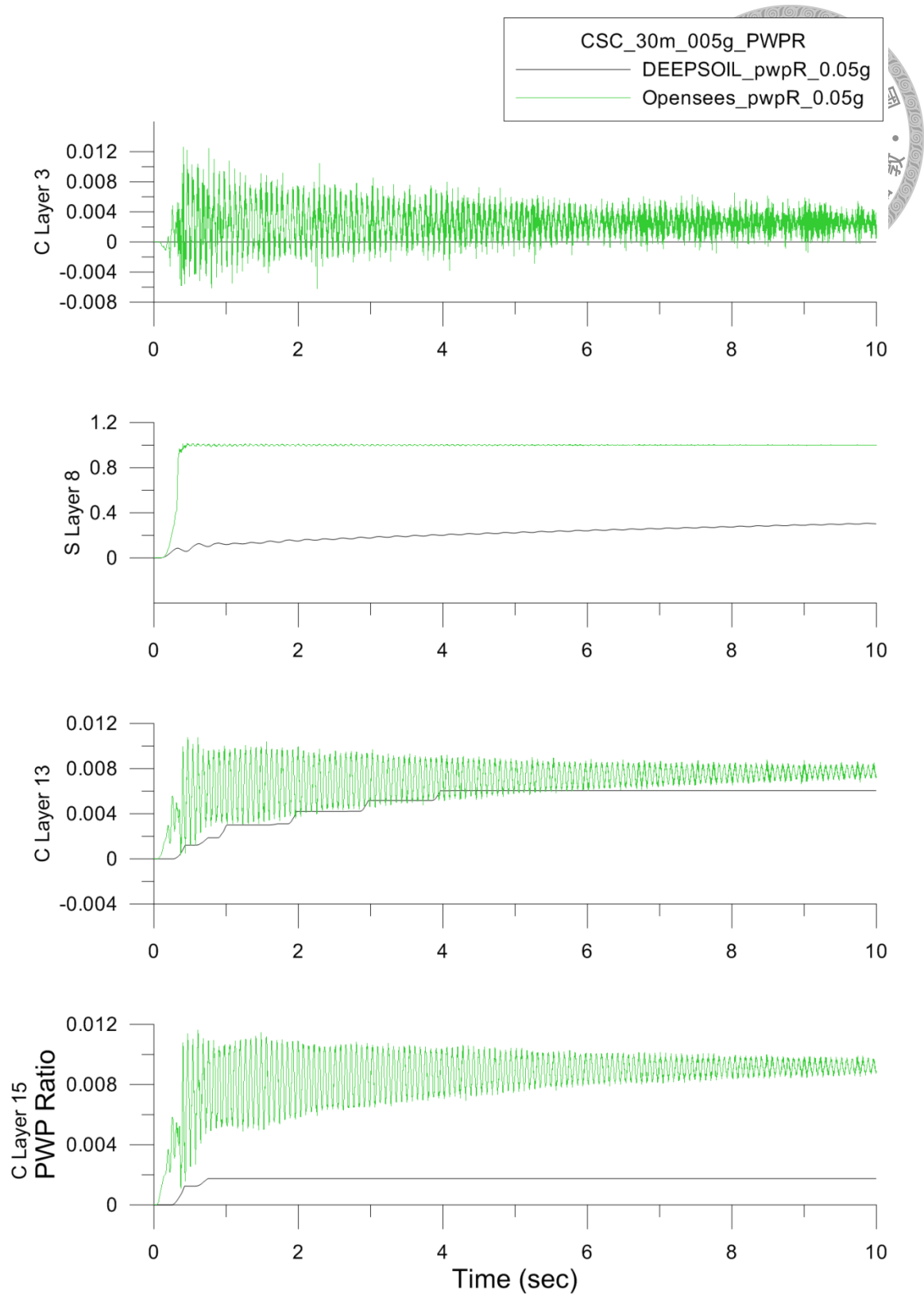


Figure 3-28 Pore water pressure ratio of case (f) with weak input motion.

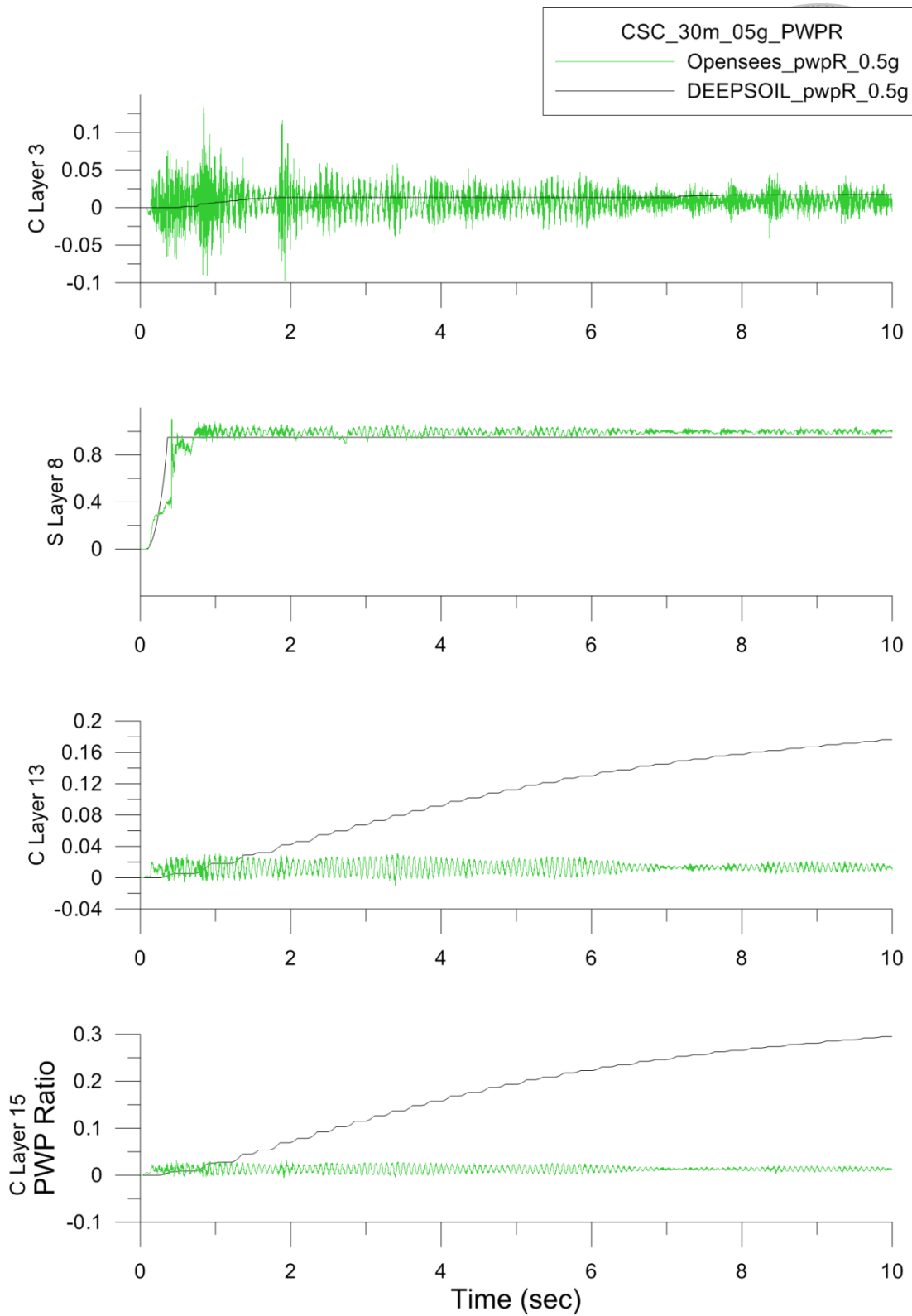


Figure 3-29 Pore water pressure ratio of case (f) with strong input motion.

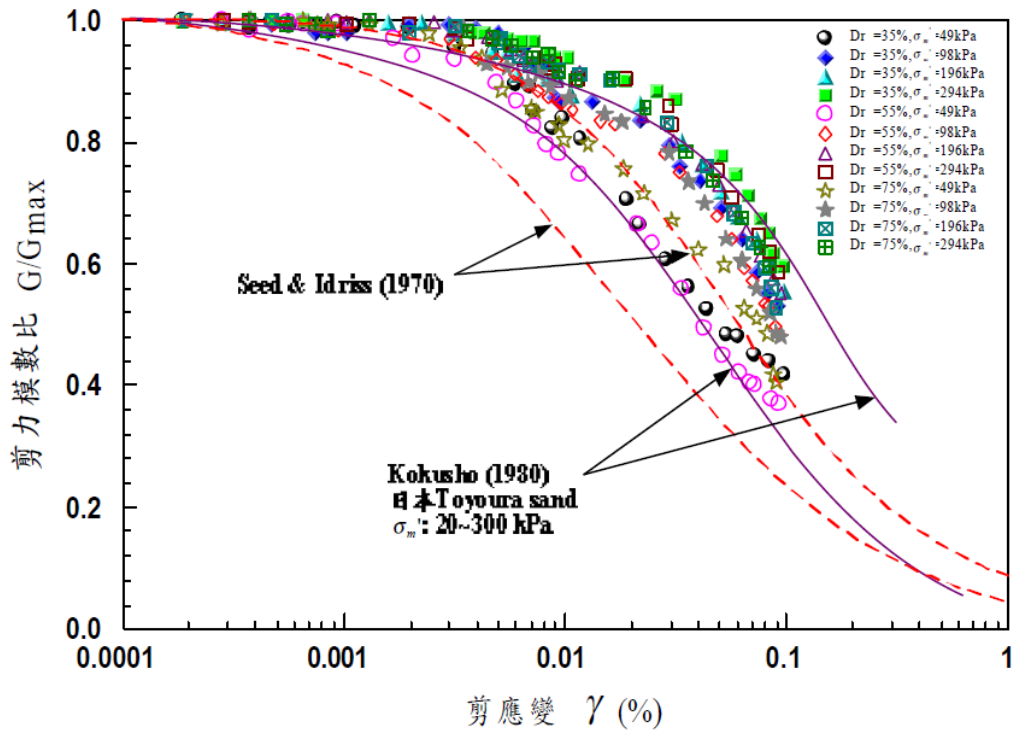


Figure 3-30 Normalized shear modulus data for Vietnam sand (Wang, 2004).

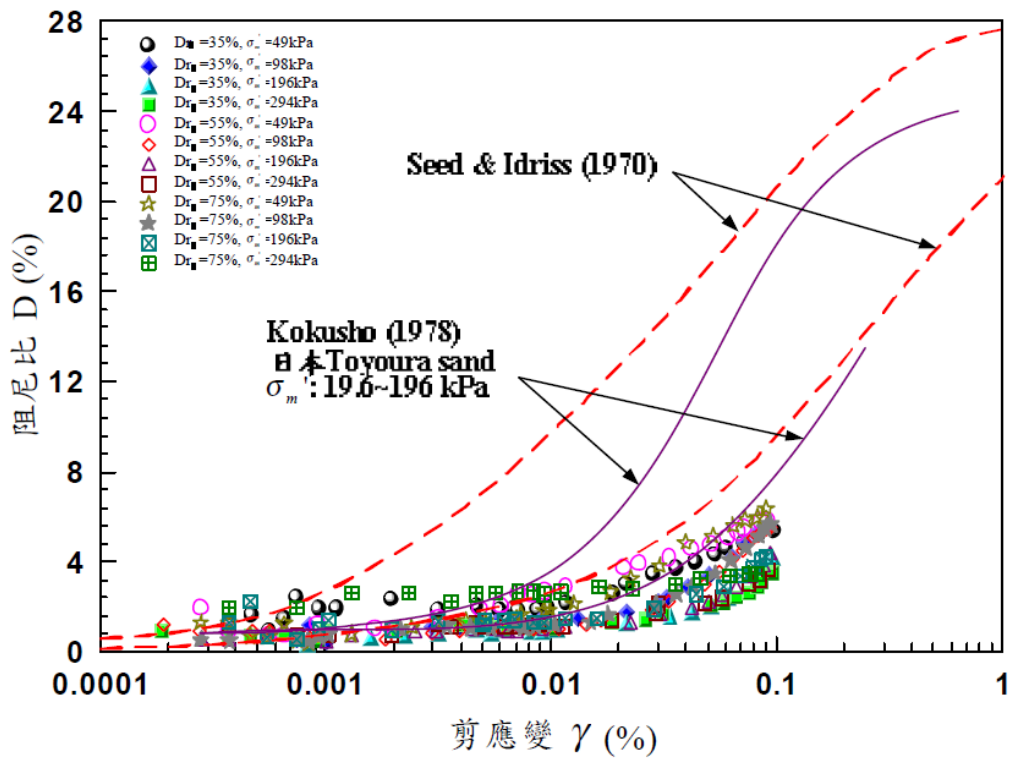


Figure 3-31 Damping ratio curve of Vietnam sand (Wang, 2004).

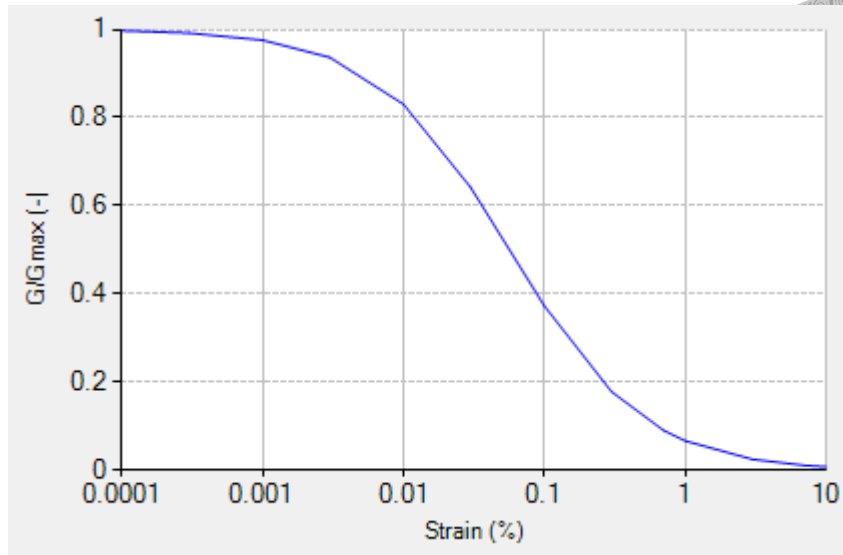


Figure 3-32 Shear modulus curve of Vietnam sand in numerical analysis.

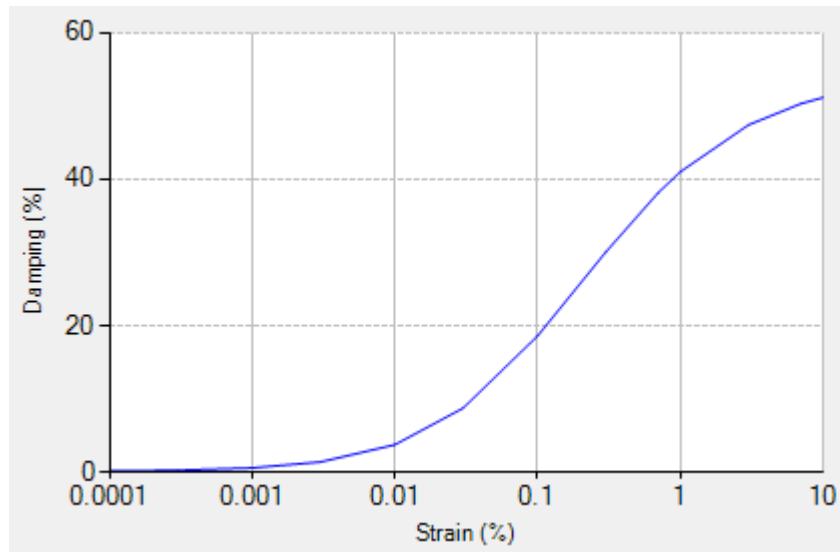


Figure 3-33 Damping ratio curve of Vietnam sand in numerical analysis.

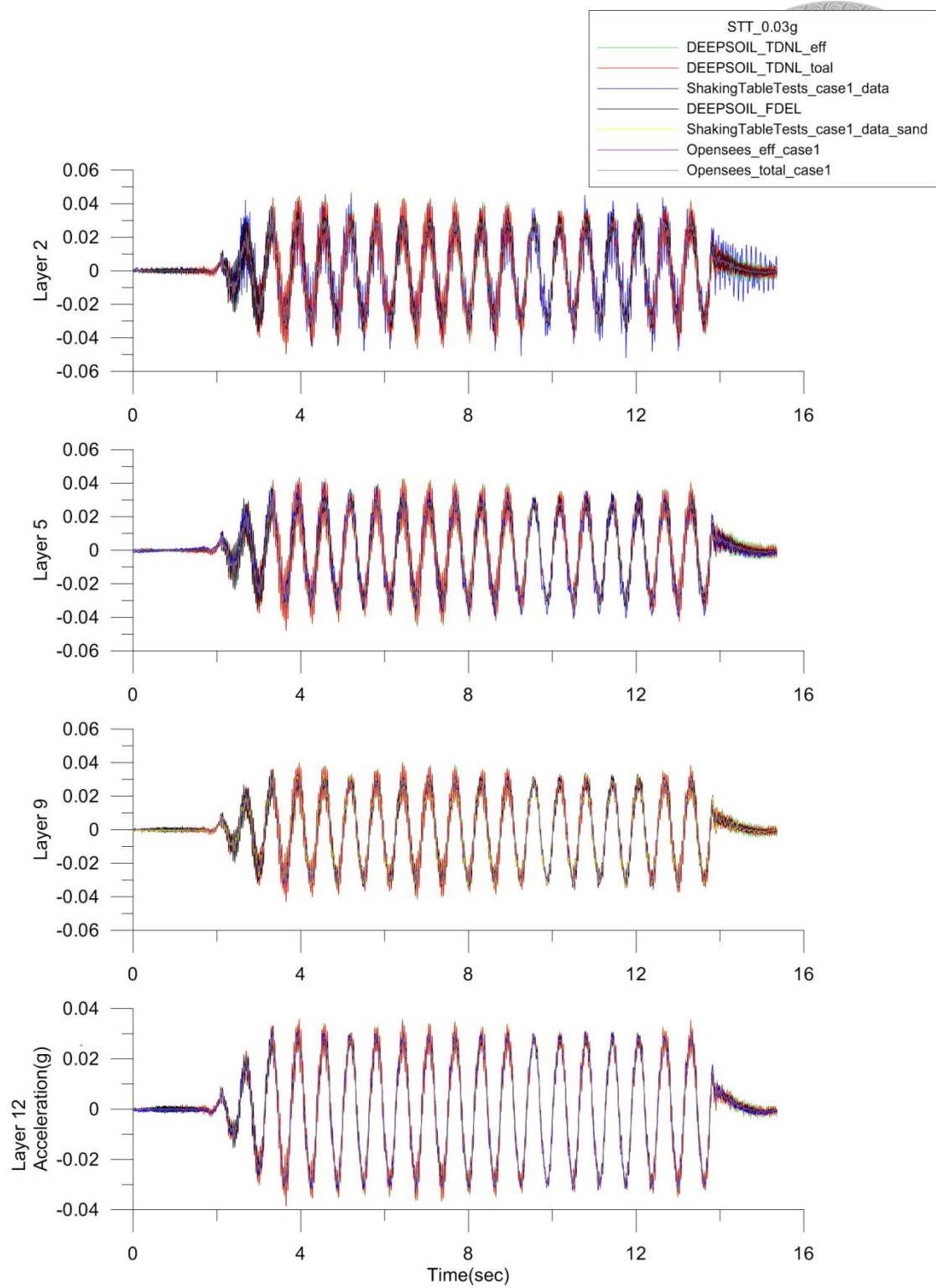


Figure 3-34 Acceleration history of shaking table test case 1 (weak motion).

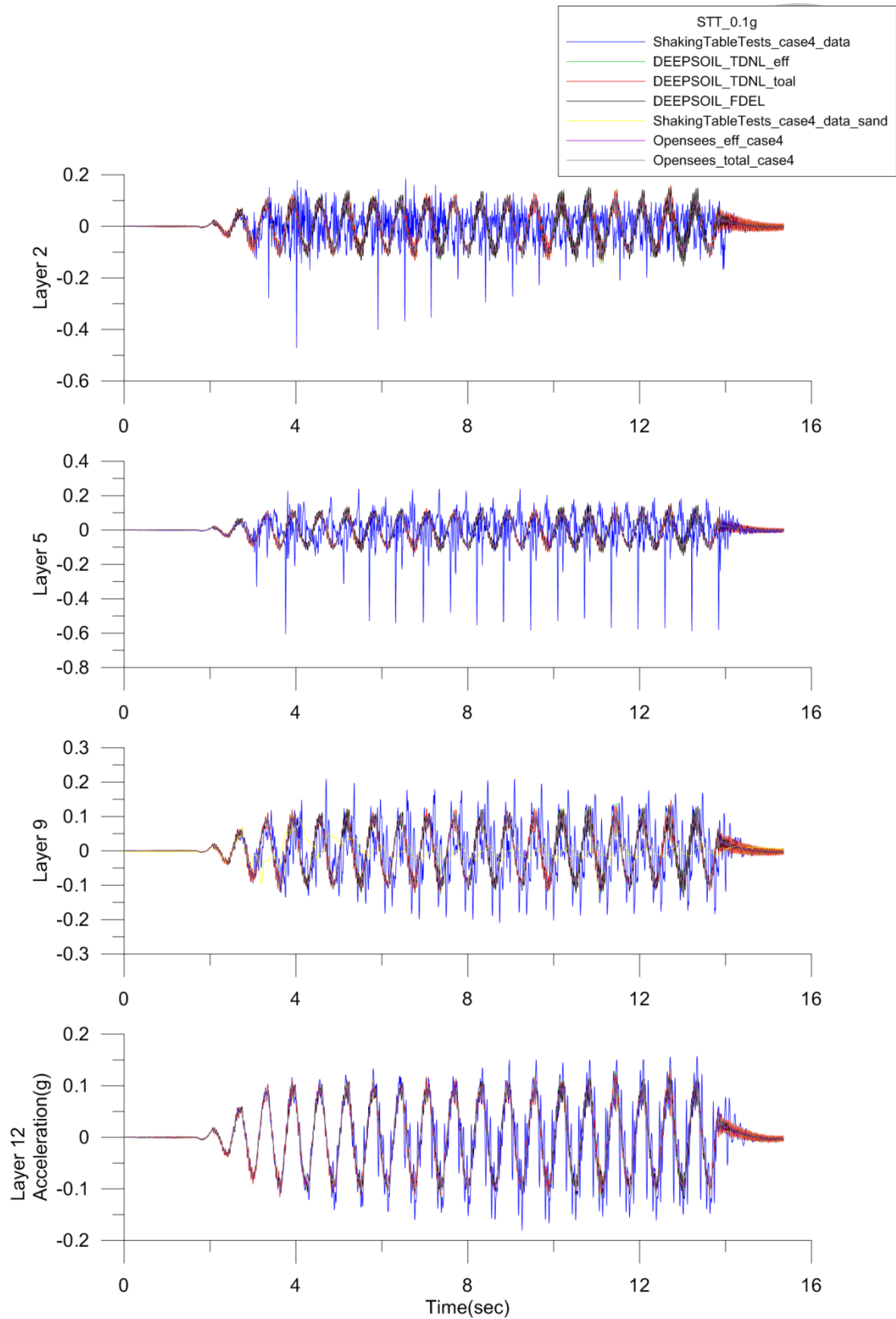


Figure 3-35 Acceleration history of shaking table test case 4 (strong motion).

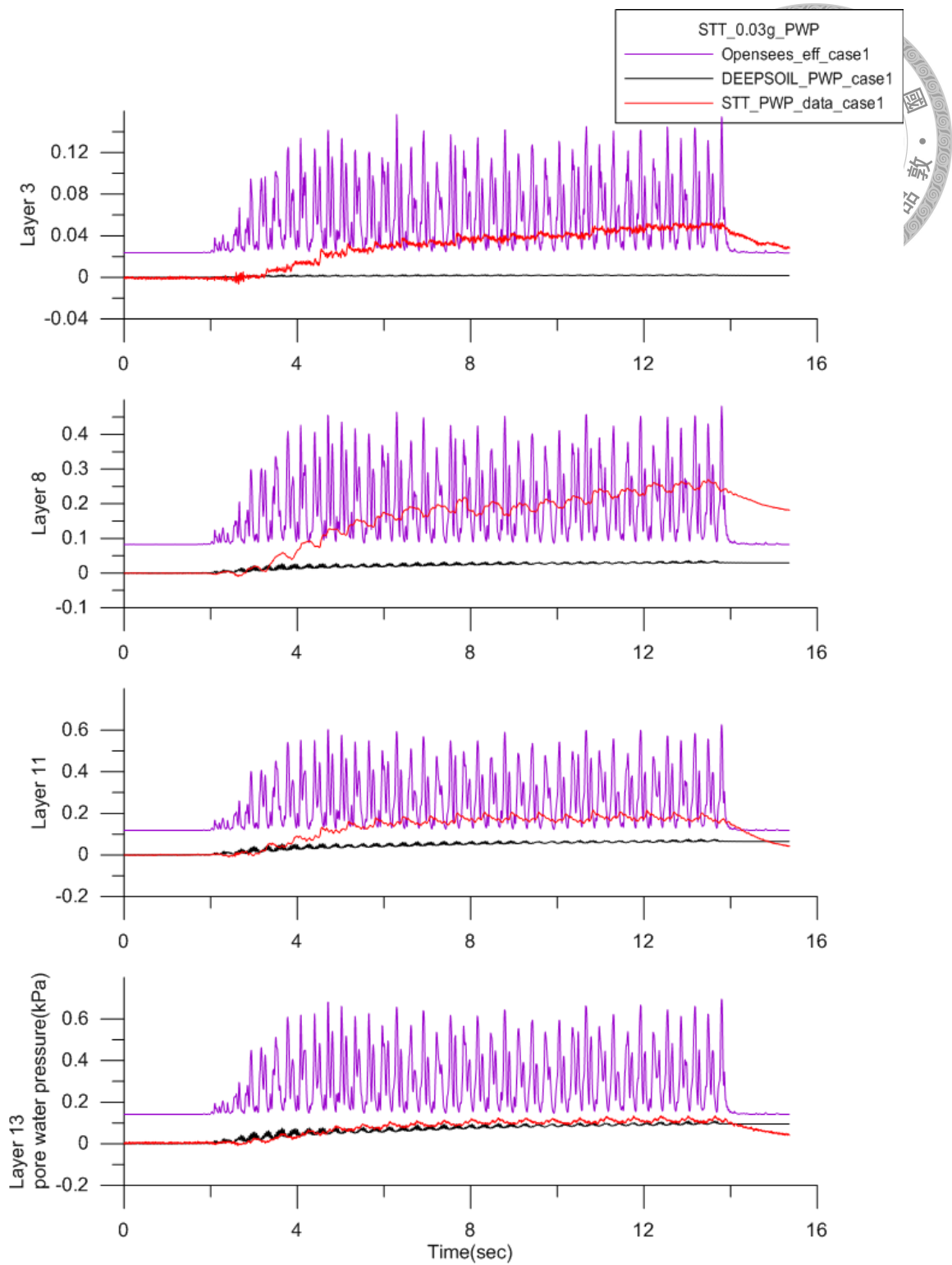


Figure 3-36 Pore water pressure ratio of shaking table test case 1 (weak motion).

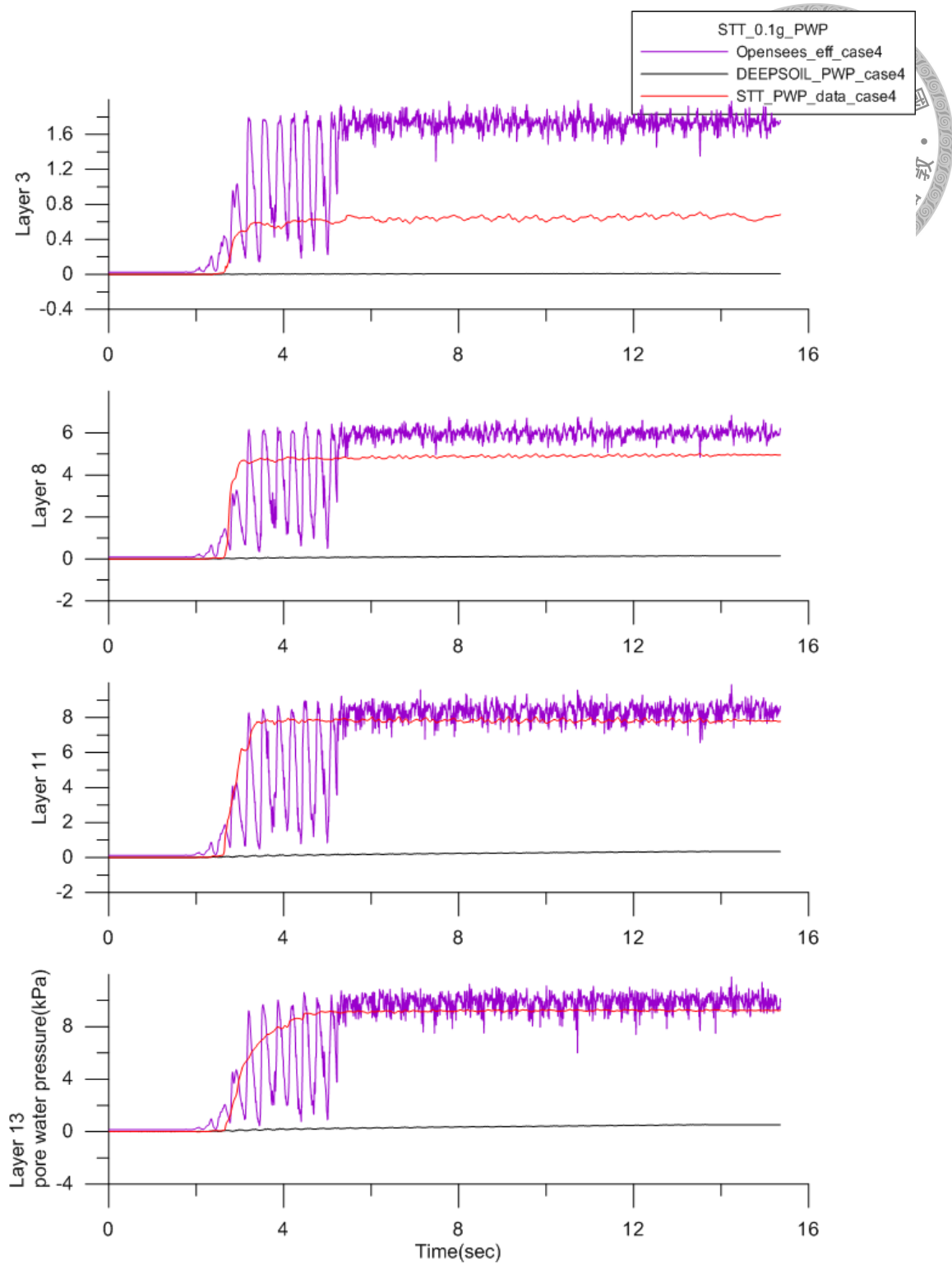


Figure 3-37 Pore water pressure ratio of shaking table test case 4 (strong motion).

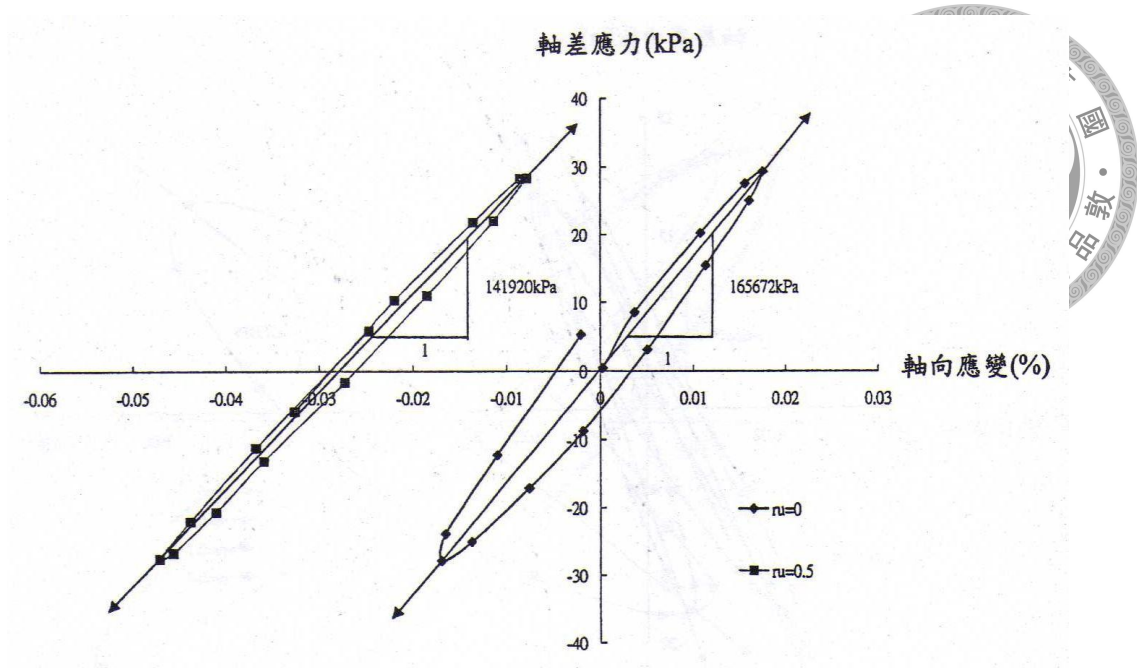


Figure 3-38 Deviator stress and axial strain of triaxial test, $\sigma'_v = 196kPa$, $Dr = 39\%$ (Jiang, 2000).

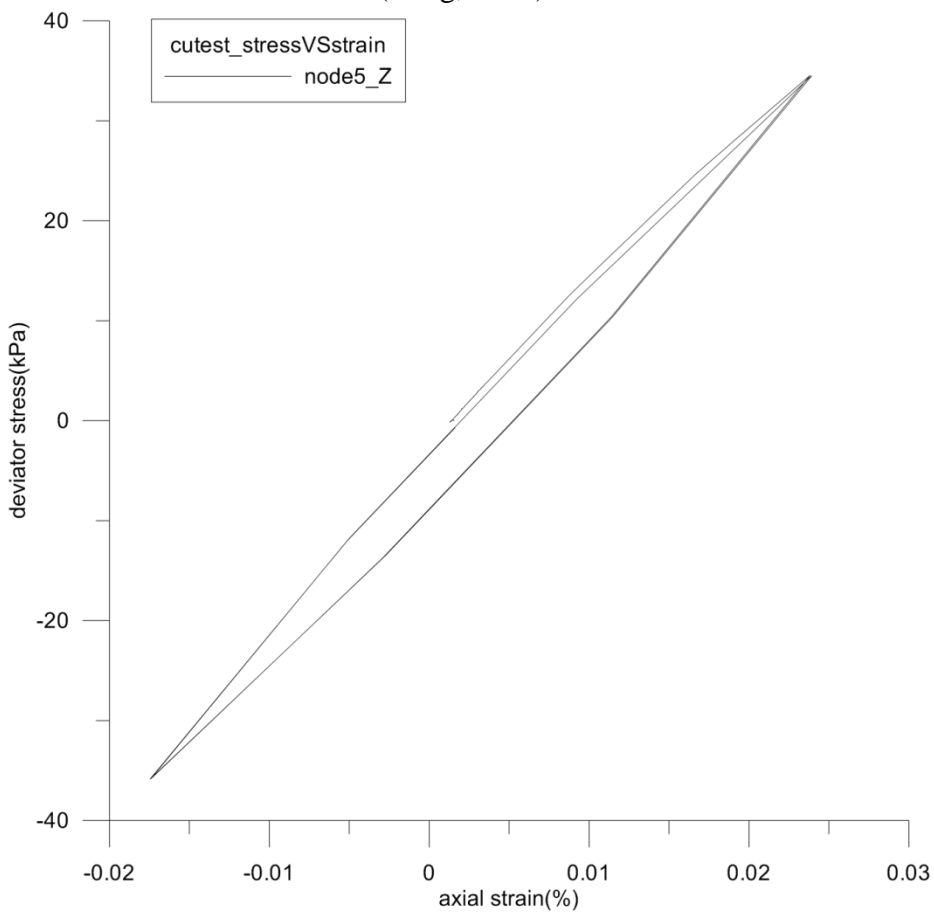


Figure 3-39 Deviator stress and axial strain of Opensees simulation.

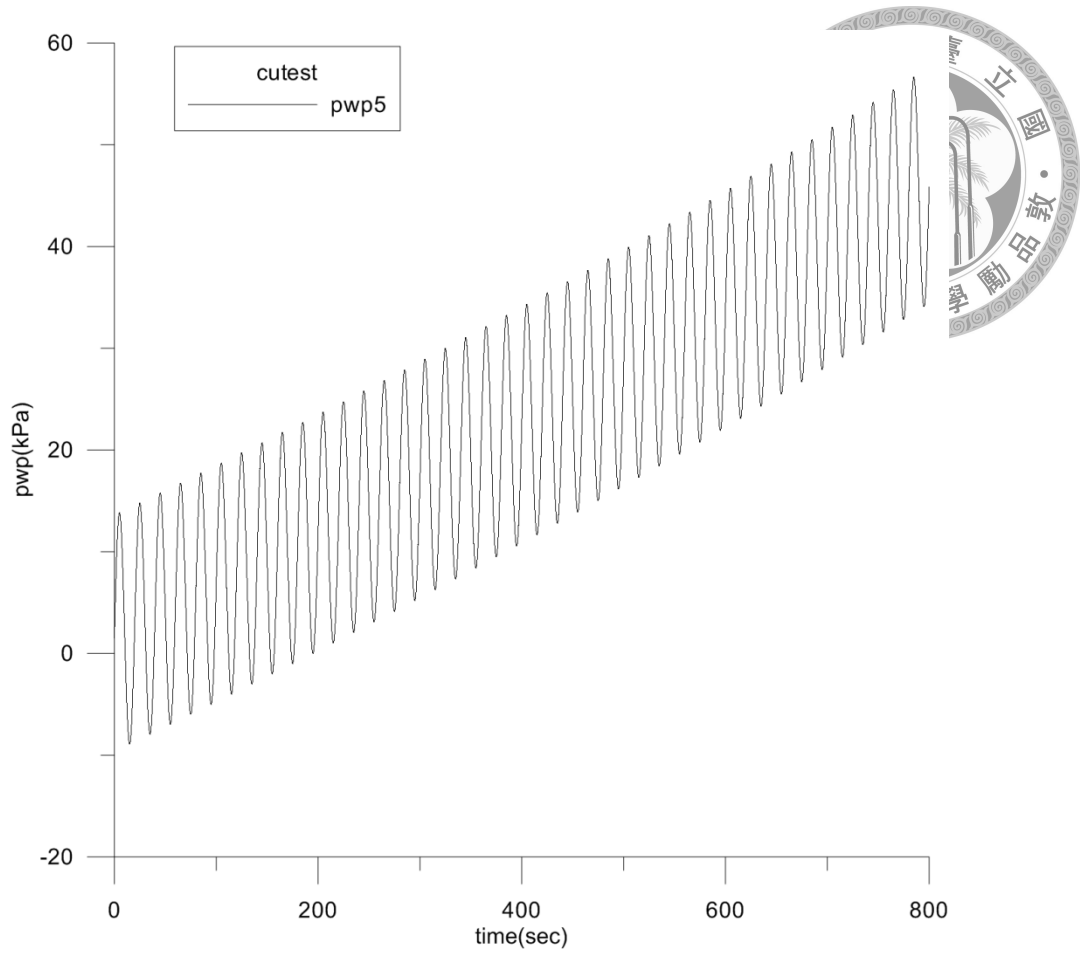


Figure 3-40 Pore water pressure of OpenSsees simulation.

Table 3-1 Soil properties of simple hypothetical cases

Soil type	Sand	Clay
Soil unit weight(kg/m³)	18	19
Shear wave velocity(m/s)	200	180
G/G_{max}	Seed and Idriss 1991	Vucetic and Dorby 1991
Damping curve	Seed and Idriss 1991	Vucetic and Dorby 1991
Relative density (%)	50	-
Plasticity index	-	40

Table 3-2 Soil properties of shaking table tests

Soil type	Vietnam sand
Soil unit weight(kg/m³)	18.433
Shear wave velocity(m/s)	150
G_s	2.65
D₁₀(mm)	0.18
D₆₀(mm)	0.31
e_{max}	0.797~0.912
e_{min}	0.569~0.62
Cu	1.75

Table 3-3 Soil properties of cyclic triaxial test

Soil type	Vietnam sand
Soil unit weight(kg/m³)	19.33
Shear wave velocity(m/s)	205
Friction angel	31.161
G_s	2.65
D₁₀(mm)	0.17
D₅₀(mm)	0.26
e_{max}	0.879
e_{min}	0.596
Cu	1.59
Dr(%)	39

Chapter 4 Conclusion and Recommendation for Future Research



4.1 Conclusions

In this study, effective-stress dynamic analyses are performed for several simple hypothetical sites, cyclic triaxial test and shaking table tests. The following summarizes the observations from the simulation results.

1. When the amplitude of the input motion is relatively small (below 0.1g), the predicted ground motions from different analysis types (frequency-domain analysis, time-domain total-stress and effective-stress analyses) are generally similar. Moreover, the predicted pore water pressure response from different pore water pressure generation schemes may be similar in magnitude (on average); however, the shape of the excess water pressure history from different schemes can be very different from each other.
2. When the amplitude of the input motion is relatively large (above 0.1g), the predicted ground motions from effective-stress dynamic analysis may start to deviate from those obtained using total-stress dynamic analysis.
3. The predicted pore water pressures in clay are in general smaller than that in sand, even with the same input motion level.
4. When simulation is performed to model the soil behavior at an element level (e.g. cyclic triaxial test), the simulation results generally agree well with the laboratory results.
5. At small input motion level, shaking table tests (in terms of acceleration history

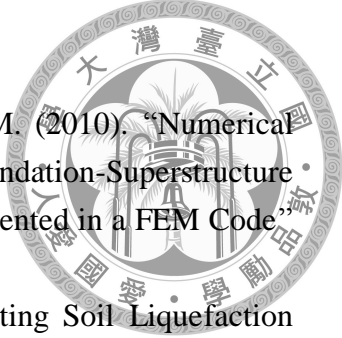
and excess pore pressure history) can be successfully modeled using any type of site response analysis.

6. At large input motion level, the acceleration histories predicted by different analysis types are generally similar and consistent with the shaking table data. However, only the pore pressure response predicted by OpenSees is consistent with the shaking table data. There may be some bias associated with the pore pressure generation model in DEEPSOIL.

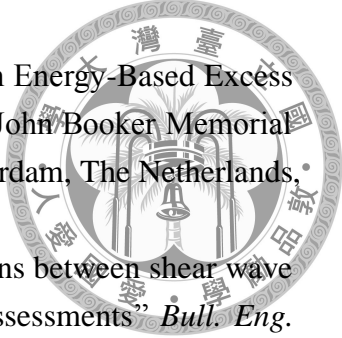
4.2 Recommendations for Future Research


1. In this research, effective-stress dynamic analyses are only performed for several hypothetical sites, cyclic triaxial test and shaking table tests. In the future, the effective stress dynamic analyses can be applied to real sites with excess pore water pressure measurements.
2. Only cyclic triaxial test on sand was simulated in this study. In future study, simulation should be performed on dynamic tests on clays.
3. Effective stress analysis from OpenSees should use very small time step (0.001~0.0005) to avoid huge fluctuations from the results.
4. Parametric study should be performed in the future to examine the effect of uncertainty in input parameters on ground motion and pore water pressure prediction.
5. By comparing the total stress and effective stress site response analyses for a series of vertical array sites (for different earthquake input motions), it may be possible to identify the conditions when it is advantageous to perform effective stress site response analyses.


Reference

- 
- [1]. Abate G., Massimino M.R., Maugeri M. and Wood D.M. (2010). “Numerical Modelling of a Shaking Table Test for Soil-Foundation-Superstructure Interaction by Means of a Soil Constitutive Model Implemented in a FEM Code” *Geotech Geol Eng* (2010) 28:37-59.
- [2]. Ahmad J.M. and Radu P. (2004). “Solutions for Mitigating Soil Liquefaction Effects a Numerical Study” *13th World Conference on Earthquake Engineering Vancouver, B.C., Canada, August 1-6, 2004, Paper No. 3016.*
- [3]. Bartlett S.F. (2011), “1D Ground Response Analysis” *Introduction to Earthquake Engineering and Soil Dynamics, lecture 8 – Ground Response analyses, page 3.*
- [4]. Baydaa, H.M., Ling, X.Z. and Xu, P. (2011) “3D FEM Numerical Simulation of Seismic Pile-supported Bridge Structure Reaction in Liquefying Ground” *Research Journal of Applied Sciences, Engineering and Technology* 3(4): 344-355.
- [5]. Bernard R. W., Jason T. D., and Thomas S. (2012). “Guidelines for Estimation of Shear Wave Velocity Profiles” *Pacific Earthquake Engineering Research Center.*
- [6]. Byrne P.M., Park S.S., Beaty M., Sharp M., Gonzalez L. and Abdoun T. (2004). “Numerical Modeling of Dynamic Centrifuge Tests” *13th World Conference on Earthquake Engineering, Paper No. 3387.*
- [7]. Chang D., Travararou T. and Chacko J. (2008). “Numerical Evaluation of Liquefaction-Induced Uplift for An Immersed Tunnel” *The 14th World Conference on Earthquake Engineering October 12-17, 2008.*
- [8]. Cheng Z. (2003). “Implement the Rounded Mohr-Coulomb Model to Opensees” *Term Project, ECI 284 Theoretical Geomechanics, Winter 2003.*
- [9]. Ebrahimian, B. (2013). “Numerical Modelling of the Seismic Behaviour of Gravity-Type Quay Walls” *Engineering Seismology, Geotechnical and Structural Earthquake Engineering, Chapter 11.*
- [10]. Elgamal A., Yang Z., Parra E. and Ragheb A. (2002). “Computational modeling of cyclic mobility and post-liquefaction site response” *Soil Dynamics and Earthquake Engineering* 22 (2002) 259-271.
- [11]. Elgamal A., Yang Z., Parra E. and Ragheb A. (2002). “Modeling of cyclic mobility in saturated cohesionless soils” *International Journal of Plasticity* 19 (2003) 883-905.
- [12]. Evelyne F. and Hormoz M. (2007). “Nonlinear numerical method for earthquake site response analysis II— case studies” *Bull Earthquake Eng* (2007) 5:325-345.
- [13]. Fattah, M. Y., Abbas, S. F. and Karim, H. H. (2012). “A Model for Coupled Dynamic Elasto-Plastic Analysis of Soils” *Journal of GeoEngineering, Vol.7 No.*

3, pp. 089-096, December 2012.

- 
- [14]. Green, R. A., Mitchell, J. K., and Polito, C. P. (2000). "An Energy-Based Excess Pore Pressure Generation Model for Cohesionless Soils" John Booker Memorial Symp.-Developments in Theoretical Geomechanics, Rotterdam, The Netherlands, 383-390.
- [15]. Hasancebi, N, and R Ulusay (2007). "Empirical correlations between shear wave velocity and penetration resistance for ground shaking assessments" *Bull. Eng. Geology and the Environment*, 66:203-213.
- [16]. Hashash. (2012) "DEEPSOIL V5.1 user manual and tutorial" Department of Civil and Environmental Engineering University of Illinois at Urbana-Champaign.
- [17]. Hashash, Y.M.A., Phillips, C., and Groholski, D.R. (2010). "Recent advances in non-linear site response analysis" *Recent Advances in Geotechnical Earthquake Engineering and Soil Dynamics*, 5th .
- [18]. Idriss, I.M., and Sun, J. (1992). "User's Manual for SHAKE91: a computer program for conducting equivalent linear seismic response analyses of horizontally layered soil deposits," Department of Civil & Environmental Engineering, University of California, Davis, California
- [19]. Jafarzadeh F., Faghihi D. and Ehsani M. (2008). "Numerical Simulation of Shaking Table Tests on Dynamic Response of Dry Sand" *The 14th World Conference on Earthquake Engineering October 12-17. 2008*.
- [20]. Jishnu R.B., Naik S.P., Patra N.R. and Malik J.N. (2013). "Ground response analysis of Kanpur soil along Indo-Gangetic Plains" *Soil Dynamics and Earthquake Engineering* 51 (2013) 47-57.
- [21]. Lai T., Elgamal A., Yang Z., Wilson D.W. and Kutter B.L. (2004). "Numerical Modeling of Dynamic Centrifuge Experiments On A Saturated Dense Sand Stratum" *11th Int. Conf. on Soil Dynamics & Earthquake Engineering and 3rd Int. Conf. on Earthquake Geotechnical Engineering, 7th - 9th January 2004, University of California, Berkeley*.
- [22]. Matasovic, N., and Vucetic, M. (1993). "Cyclic Characterization of Liquefiable Sands" *Journal of Geotechnical Engineering*. 119, 1805-1822.
- [23]. Matasovic, N., and Vucetic, M. (1995). "Generalized cyclic-degradation-pore-pressure generation model for clays" *Journal of geotechnical engineering*, 1995.121:33-42.
- [24]. McGann, C., and Arduino, P. "Site Response Analysis of a Layered Soil Column (Total Stress Analysis)" *OpenSees examples page*, Retrieved from [http://opensees.berkeley.edu/wiki/index.php/Site_Response_Analysis_of_a_Layered_Soil_Column_\(Total_Stress_Analysis\)](http://opensees.berkeley.edu/wiki/index.php/Site_Response_Analysis_of_a_Layered_Soil_Column_(Total_Stress_Analysis))

- 
- [25]. McGann, C., and Arduino, P.. “Effective Stress Site Response Analysis of a Layered Soil Column” *OpenSees examples page*, Retrieved from http://opensees.berkeley.edu/wiki/index.php/Effective_Stress_Site_Response_Analysis_of_a_Layered_Soil_Column
- [26]. McKenna, F. and Fenves G.L. (2014). “The OpenSees command language manual, version 1.2.” Pacific Earthquake Engrg. Research Center, Univ. of Calif., Berkeley. (<http://opensees.berkeley.edu>).
- [27]. Phillips, C., and Hashash, Y.M.A. (2009). “Damping formulation for nonlinear 1D site response analyses” *Soil Dynamics and Earthquake Engineering*, 29(7), 1143-1158.
- [28]. Ptilakis K., Kirtas E., Sextos A., Bolton M., Madabhushi G. and Brennan A. (2004). “Validation by Centrifuge Testing of Numerical Simulations for Soil Foundation Structure Systems” *13th World Conference on Earthquake Engineering 2004, Paper No.2772*.
- [29]. Puzrin, A.M. (2012). “Constitutive Modelling in Geomechanics” *Springer-Verlag Berlin Heidelberg*, Chapter 13.
- [30]. Rayhani T. and Naggar E. (2009). “Numerical Modeling of Seismic Response of Rigid Foundation on Soft Soil” *International journal of geomechanics, ASCE 2008, 336-346*.
- [31]. Rober A., Peter H., and James W. (1999). “Progress Toward a Safer Future Since the 1989 Loma Prieta Earthquake” *U.S. Geological Survey Fact Sheet 151-99*, Retrieved from <http://pubs.usgs.gov/fs/1999/fs151-99/>
- [32]. Stewart, J. (1997). “Key Geotechnical Aspects of the 1989 Loma Prieta Earthquake” *nisee, National Information Service for Earthquake Engineering, University of California, Berkeley*. Retrieved from http://nisee.berkeley.edu/loma_prieta/stewart.html
- [33]. Stewart J. P., A.O.L Kwok, Y. M.A. Hashash, N. Matasovic, R. Pyke, Z. Wang and Z. Yang (2008). Benchmarking of Nonlinear Geotechnical Ground Response Analysis Procedures, PEER Report 2008/04, Pacific Earthquake Engineering Research Center, University of California, Berkeley.
- [34]. Yang Z., Elgamal A., Adalier K. and Sharp M. K. (2004). “Earth Dam on Liquefiable Foundation and Remediation: Numerical Simulation of Centrifuge Experiments” *Journal of engineering mechanics, 2004.130:1168-1176*.
- [35]. Yang Z. (2010) “OpenSees Geotechnical Simulation Capabilities” *U. C. Sand Diego*, Retrieved from <http://www.soilquake.net/opensees/>
- [36]. 李哲安, (2012). 「一維與二維振動對砂土液化行為之影響」, 國立台灣大學工學院土木工程學系碩士論文

- 
- [37].黃正佑, (2005). 「含細粒料砂土之盤剪實驗研究」, 私立中原大學土木工程學系碩士學位論文
- [38].江國良 ,(2000).「飽和砂土受反覆荷重作用後之不排水受剪行為」,國立台灣大學土木工程學研究所碩士論文
- [39].張文忠, 陳志芳, 林德洪, 謝明志, 盧又彥, (2013) 「沉箱式碼頭動態模型試驗之數值模擬」第 35 屆海洋工程研討會論文集 國立中山大學 2013 年 11 月
- [40].任芬頤, (2006). 「盤剪方式影響疏鬆砂土相對密度之研究」, 私立中原大學土木工程學系碩士學位論文
- [41].王金山 ,(2004). 「共振柱試驗之土壤動力性質」, 國立中央大學土木工程學系碩士論文
- [42].翁作新, 陳家漢, 彭立先, 李偉誠, (2003). 「大型振動台剪力盒土壤液化試驗(II)—大型砂試體之準備與振動台初期試驗」, 國家地震工程研究中心報告, 報告編號:NCREE-03-042
- [43].翁作新, 陳家漢, 程漢瑋, 吳繼偉, (2006). 「大型振動台剪力盒土壤液化試驗(III)—飽和越南砂試體受振沉陷之探討」, 國家地震工程研究中心報告, 報告編號:NCREE-06-019